

DISSERTATION

Ultrafast Electron Dynamics in Laser-Driven Atoms and Molecules

Ausgeführt am

Institut für Photonik der Technischen Universität Wien

und am

Physics Department der University of Ottawa, Canada

zum Zwecke der Erlangung des akademischen Grades
eines Doktors der technischen Wissenschaften

unter der Anleitung von

A.o. Univ.-Prof. Dipl.-Ing. Dr. techn. Thomas Brabec

Eingereicht an der Technischen Universität Wien
Fakultät für Elektrotechnik und Informationstechnik

von

Dipl.-Ing. Markus Kitzler

Matrikelnummer 9525362

Burggasse 20/1/12, 1070 Wien, Österreich

und

430 Daly Avenue, K1N 6H4, Ottawa, Ontario, Canada

Wien und Ottawa, im August 2003

Abstract

Laser light is able to produce field strengths capable of ionizing atoms, molecules and other complex multi-electron systems like clusters of atoms. Whilst ionization of atoms is understood relatively well, understanding the electron dynamics determining ionization of spatially extended systems remains a challenge.

This dynamics takes place on the timescale of the half cycle of the light oscillation period, which is about 1 femtosecond (10^{-15} s) for common lasers in the infrared frequency regime. Inner-shell relaxation processes in atoms are even faster and take place in the attosecond (10^{-18} s) regime. In order to resolve such time-scales with pump-probe experiments, pulses in the extreme ultraviolet (xuv) spectral range with durations of a few hundred attoseconds are necessary. Recently the first measurements of single attosecond pulses using laser dressed single photon xuv ionization of gas atoms were reported. The determination of the xuv pulse duration from the electron spectrum was carried out with a classical theory. Although classical models are known to give a qualitatively correct description of strong laser atom interaction, the range of validity for accurate determination of sub-fs pulses must be scrutinized by a quantum mechanical analysis. In this thesis a theoretical framework for the accurate temporal characterization of attosecond xuv pulses, using a Fourier Bessel expansion of the xuv electron spectrum under the strong field approximation and a semi-classical derivation is established, putting earlier results on a rigorous theoretical footing. The analysis reveals an improved scheme that is by more than an order of magnitude more efficient than the one used so far and allows – for the first time – for direct experimental discrimination between single and multiple attosecond pulses.

To study the laser induced electron dynamics in molecules it has turned out that it is indispensable to abandon the single active electron approximation, where only the weakest bound electron of a system is considered to interact with the laserfield in an average potential of all other electrons and which has proven to give good results for atoms. Because for the interaction of matter with strong laser fields the Schrödinger equation must be solved in a non-perturbative way and since there are no analytical methods available for molecules, numerical methods must be used. A full numerical solution of the time-dependent Schrödinger equation is, with the computer power available at the moment, only possible for at maximum two electrons in a strong field. Therefore efficient numerical methods capable of treating multiple electrons and taking into account the correlated electron-response must be developed. A promising approach based on Hartree-Fock theory but extended to several configurations for considering electron-correlation and able to deal with time dependent problems (Multi-configuration Time-dependent Hartree-Fock, MCTDHF), limited to one spatial dimension, will be introduced.

With the help of the developed MCTDHF method, laser induced electron dynamics in spatially far extending systems like extremely big molecules, quantum dots and other structures in semiconductors is studied. The results of these investigations can be summarized as follows. If a system is excited with a photon frequency smaller

than a characteristic frequency of the system, as it is usually the case for infrared lasers applied to atoms and molecules, the electrons follow the laser-tilted potential and are pushed towards the lowered potential barrier. Completely the opposite happens in systems which are excited with a frequency larger than the characteristic frequency. There the electron dynamics is comparable to the one of free a electron: The electrons are pulled away from the lowered potential barrier and tunneling ionization is suppressed. The characteristic frequency for this special dynamics is the difference between the first excited state and the ground state in the one-electron case. For the behaviour of a cloud of electrons it is the plasma frequency. By systematically calculating the ionization probability of one- and multi-electron systems as a function of the system size, the ionization potential, the photon energy and the laser intensity and -duration it was possible to prove that the electron dynamics can be modelled by classical mechanics and to identify the ionization mechanism in this special frequency range. That is, the electrons pick up energy from the field when they are decelerated by the potential barriers and thereby dephased from the laser field. A parameter range, where the quantum mechanical electron dynamics can be described by classical mechanics, is identified.

As a last point of this thesis tunneling ionization in molecules in the quasistatic frequency regime is investigated. Recent experiments show that ionization of molecules cannot be described by the quasistatic tunneling theory of Ammosov-Delone-Krainov (ADK) but exhibits a factor of 5-10 higher saturation intensities than predicted by this theory. The electron dynamics taking place during tunneling ionization is investigated with the MCTDHF method. It will be shown that the laser induced polarization of the molecule is responsible for the differences between experiment and theory. That is, the laser induced excursion of the remaining electron cloud adds to the effective potential felt by the tunneling electron. This boost of the Coulomb barrier decreases the tunneling probability and thus increases the saturation intensity. In atoms, where due to their much smaller polarizability the remaining electrons do not move, this boost is not present and consequently there is no increased Coulomb barrier.

Zusammenfassung

In jenen extrem hohen Feldstärken, die moderne Laser zu produzieren imstande sind, wirken auf die Elektronen in Atomen, Molekülen und anderer komplexer Multielektronen-Materie wie Cluster von Atomen Kräfte, welche die Bindungskräfte um ein Vielfaches übersteigen, sodaß die Atome, Moleküle, etc. ionisiert werden. Während Ionisation in Atomen schon sehr gut verstanden ist, ist das Wissen über die Elektronendynamik, welcher der Ionisation in großen Systemen zugrunde liegt, noch relativ gering.

Diese Dynamik passiert auf einer Zeitskala vergleichbar mit der halben Oszillationsperiode des Lichts, das ist im infraroten Frequenzbereich ungefähr eine Femtosekunde (10^{-15} s). Relaxationsprozesse im Inneren von Atomen passieren noch viel schneller, nämlich auf der Zeitskala von Attosekunden (10^{-18} s). Will man solch kurze Zeiten mit Hilfe von Pump-Probe Experimenten auflösen, muß man Lichtpulse im extremen Ultraviolett (xuv) Frequenzbereich mit Pulsdauern von nur wenigen Hundert Attosekunden verwenden. Kürzlich gelang die erste Messung eines einzelnen derartigen Attosekundenpulses. Die verwendete Meßmethode zur Bestimmung der Pulsdauer basierte auf einem klassischen Modell. Obwohl klassische Mechanik normalerweise gute Dienste für die qualitative Erklärung von Prozessen in der Physik starker Felder liefert, ist eine quantitative Übereinstimmung zwischen klassischer Mechanik und Quantenmechanik nur selten der Fall. In dieser Dissertation wird daher eine quantenmechanische Methode zur genauen Bestimmung der Dauer von Attosekundenpulsen im xuv-Wellenlängenbereich vorgestellt. Die quantenmechanische Analyse ergibt ein um mehr als eine Größenordnung effizienteres Meßsetup als das bisherige und ermöglicht die direkte experimentelle Unterscheidung eines einzelnen Attosekundenpulses von mehreren, was für den praktischen Einsatz sehr wichtig ist.

Es hat sich herausgestellt, daß es in Molekülen unbedingt notwendig ist, von der in Atomen sehr erfolgreichen Einelektronen-Approximation, wo nur ein einzelnes Elektron in einem effektiven Potential aller anderen betrachtet wird, abzugehen, wenn man laserinduzierte Elektronendynamik in solchen Systemen studieren möchte. Weil für die Wechselwirkung von intensiven Laserpulsen mit Materie die Schrödingergleichung nichtperturbativ gelöst werden muß, sind numerische Methoden unablässlich. Eine voll numerische Lösung der Schrödinger Gleichung für mehr als zwei Elektronen in einem starken Laserfeld ist jedoch mit heutiger Computertechnologie nicht möglich. Deshalb müssen numerische Verfahren, welche der voll korrelierten Elektronendynamik gerecht werden, entwickelt werden. Eine vielversprechende Methode, basierend auf Hartree-Fock Theorie aber ausgeweitet auf mehrere Konfigurationen und beschränkt auf eine räumliche Dimension (genannt Multi-configuration Time-dependent Hartree-Fock, MCTDHF), welche es erlaubt Elektronenkorrelation zu studieren, wird in dieser Arbeit vorgestellt.

Die entwickelte MCTDHF-Methode wird dann verwendet, um laserinduzierte Elektronendynamik in großen Systemen wie Quantendots und Strukturen in Halbleitern zu studieren. Das Ergebnis dieser Studie kann wie folgt beschrieben wer-

den. Wenn das betrachtete System mit einer Photonenfrequenz kleiner als eine bestimmte systemcharakteristische Frequenz angeregt wird, wie das für Atome und Moleküle in infraroten Laserfeldern üblicherweise der Fall ist, folgen die Elektronen dem durch das Laserfeld geneigten Potential. Das Verhalten kehrt sich ins Gegenteil, wenn das System mit einer Photonenfrequenz größer als die charakteristische Frequenz erregt wird. Die Elektronen verhalten sich dann wie freie Elektronen und werden von der niedrigeren Potentialbarriere weg gezogen, sodaß Tunnelionisation unterdrückt wird. Die bestimmende Frequenz für diese 'überresonante' Dynamik ist die Differenz zwischen Grundzustand und erstem angeregten Zustand in Systemen mit nur einem Elektron. Für Multielektronensysteme ist diese charakteristische Frequenz die Plasmafrequenz des Systems. Indem die Ionisationswahrscheinlichkeit von Ein- und Mehrelektronensystemen in Abhängigkeit der Größe des Systems, des Ionisationspotentials, der Photonenenergie und der Laserintensität und -pulsdauer studiert wurde, war es möglich zu beweisen, daß die Elektronendynamik in diesem 'überresonanten' Bereich mit klassischer Mechanik modelliert werden kann. Weiters konnte der Ionisationsmechanismus erforscht werden. Die Elektronen nehmen Energie aus dem Laserfeld auf, wenn sie durch die Potentialbarriere gegenüber dem Feld verlangsamt werden und außer Phase geraten. Weiters wird ein Parameterbereich, in dem die Elektronendynamik mit klassischer Mechanik beschrieben werden kann, angegeben.

Als letzten Punkt dieser Arbeit untersuchen wir Tunnelionisation in Molekülen im quasistatischen Frequenzregime. Kürzlich ausgeführte Experimente zeigten, daß die Ionisationswahrscheinlichkeit in diesen komplexen Systemen nicht durch die Tunneltheorie von Ammosov-Delone-Krainov (ADK) beschrieben werden kann, sondern daß Moleküle eine um 5-10 mal höhere Sättigungsintensität aufweisen als von ADK vorhergesagt. Es wird gezeigt, daß die laserinduzierte Polarisierung des Moleküls für diese Differenzen zwischen Theorie und Experiment verantwortlich ist. Die Auslenkung der nicht ionisierten Elektronen aus ihrer Ruhelage erhöht für das tunnelnde Elektron die effektive Coulomb-Potentialbarriere des Moleküls, sodaß die Tunnelwahrscheinlichkeit sinkt und die Sättigungsintensität steigt. In Atomen existiert diese Beweglichkeit der verbleibenden Elektronen nicht, daher gibt es dort auch nicht diese erhöhte Coulomb-Barriere.

**One femtosecond relates to one
minute as one minute to the age of
the Universe.**

This thesis deals with processes taking place within
time spans even shorter than one femtosecond.

**The Schrödinger equation describes
the behaviour of all known forms of
matter.**

P. W. ATKINS

**The Schrödinger equation in its full
beauty is useless.**

V. P. KRAINOV

Acknowledgements

I would like to thank my supervisor Prof. Dr. Thomas Brabec (PHYSICS DEPARTMENT, UNIVERSITY OF OTTAWA) for giving me the possibility to work in this fascinating field and for all the experiences I was allowed to gather throughout my work with him. I am also deeply indebted to Dr. Armin Scrinzi (PHOTONICS INSTITUTE, VIENNA UNIVERSITY OF TECHNOLOGY) for all he taught me about numerical physics as well as for interesting discussions about literature, cinema and the world in general.

Special thanks go to my colleagues and friends at the ROMY SCHNEIDER CENTER FOR THEORETICAL INVESTIGATION OF LASER-MATTER INTERACTION AT THE UNIVERSITY OF OTTAWA, Jürgen Zanghellini, whom I have been working with for years with great joy, especially on the MCTDHF method of chapter 3, and Christian Jungreuthmayer, who has always tried to support my work as much as possible, as well as to my friend Marc Smits from the NATIONAL RESEARCH COUNCIL OF CANADA (NRC), OTTAWA, whose hints and results have been very useful for the work presented in chapter 5 of this thesis and whom I could always count on when I needed some distraction.

It is a pleasure to further acknowledge various interesting and fruitful discussions with Dr. Nenad Milosevic (PHOTONICS INSTITUTE, VIENNA UNIVERSITY OF TECHNOLOGY), Dr. Albert Stolow, Dr. Paul Corkum and Dr. Dave Rayner (all NRC), Prof. Dr. Vladimir Krainov (MOSCOW INSTITUTE OF PHYSICS AND TECHNOLOGY), whom I was allowed to work with on the analytical theory of chapter 5 and Prof. Dr. Ferenc Krausz (PHOTONICS INSTITUTE, VIENNA UNIVERSITY OF TECHNOLOGY), whom I had the delight to work with on the attosecond measurement method of chapter 2.

These acknowledgements would be incomplete without thanking Inga for her understanding and patience throughout my work on 'shooting with lasers on matter', as she puts it, and especially for going to Canada with me.

Contents

| | | |
|----------|-------------------------------------------------------------------------------------------------|-----------|
| 1 | Introduction | 1 |
| 1.1 | Theoretical Methods | 2 |
| 1.2 | Motivation and Overview | 12 |
| 2 | Attosecond Pulse Measurement | 15 |
| 2.1 | Theory | 16 |
| 2.1.1 | SFA Solution of the Schrödinger Equation | 16 |
| 2.1.2 | The Multiphoton Picture | 18 |
| 2.1.3 | The Semiclassical Picture | 19 |
| 2.2 | Results | 22 |
| 2.2.1 | Classical Mechanics vs. Quantum Mechanics | 22 |
| 2.2.2 | Increasing Measurement Efficiency | 24 |
| 2.2.3 | Single vs. Multiple XUV Pulses | 25 |
| 2.3 | Concluding Remarks | 26 |
| 3 | Numerical Treatment of Laser driven Multielectron Systems | 27 |
| 3.1 | The Hartree-Fock Approach | 28 |
| 3.2 | MCTDHF | 30 |
| 3.2.1 | Derivation of the Working Equations | 32 |
| 3.2.2 | Computational Details | 36 |
| 3.2.3 | The Single-Electron Case | 40 |
| 4 | Elimination of Tunneling and Classical Ionization | 43 |
| 4.1 | Overresonant Potential Wells | 44 |
| 4.1.1 | Ionization Probability over Well Length | 45 |
| 4.1.2 | Ionization through Classical Mechanics | 47 |
| 4.2 | Overresonant Multi-Electron Dynamics | 51 |
| 4.2.1 | MCTDHF Simulations | 53 |
| 4.2.2 | Initial Conditions and Classical Wavepacket Propagation in the Multi-Electron Case | 54 |
| 5 | Tunneling Suppression through Laser Induced Polarization | 60 |
| 5.1 | The Quasistatic Limit | 61 |
| 5.2 | The Effective One-Electron Potential | 62 |
| 5.3 | Tunneling Dynamics | 64 |

| | | |
|----------|----------------------------------------------------------------|-----------|
| 5.4 | The Effects of the Laser-Induced Polarization | 66 |
| 5.5 | Comparison with ADK | 68 |
| 5.6 | Interpretations | 73 |
| | Conclusion and Outlook | 75 |
| A | Derivation of the Multi-Electron Ionization Probability | 77 |
| B | Derivation of Electron Densities | 78 |
| C | Conversion between Atomic Units and SI | 79 |
| D | Common Abbreviations | 80 |
| | List of Figures | 81 |
| | Bibliography | 82 |
| | Curriculum Vitae | 90 |

Chapter 1

Introduction

Laserlight is a unique type of energy. It is light with a well defined wavelength which propagates as a ray. This ray can be focused to very small spots, and the energy can be applied within very short times. Since the first description of the Laser-principle [1] in 1958 by A. L. Schawlow and C. H. Townes and the works of A. M. Prokhorov and N. G. Basov¹ a lot of progress has been made. Nowadays, laser pulses can be as short as a few femtoseconds (10^{-15} s). The pulsation of the energy leads to enormous peak powers of some Terawatt (10^{12} W) and together with the small focal spots to intensities of 10^{20} W/cm² and more. The electric field equivalent to such high intensities exposes the electrons in matter to forces which exceed the atomic binding forces by orders of magnitude. This leads to the removal of the electrons from the atomic nuclei, the atoms are ionized. Ionization of atoms in strong electric fields was theoretically studied first by L. V. Keldysh in 1965 [2]. In that work analytical expressions for the ionization probability of atoms in strong fields were derived. According to this theory two main ionization mechanisms are responsible for the ionization of the atom. For "weakly" bound electrons, "strong" fields and "small" light frequencies tunneling ionization is dominant. This is possible because in the presence of a strong laserfield the Coulomb barrier is tilted such that the electron can tunnel through the potential barrier of the atom. In the opposite parameter regime the electron is ionized by a multiphoton mechanism where the electron absorbs several laser photons to overcome the binding energy. In a more strict way the so called *Keldysh parameter* must be calculated in order to decide whether ionization happens in the one way or the other.

In the last decades, besides from simple tunneling or multiphoton ionization, a wealth of interesting phenomena, which occur when high power laser pulses interact with atoms, were investigated. In 1979 it was found that an electron can absorb more than the minimum number of photons required for ionization [3]. This was

¹In 1964 C. H. Townes, N. G. Basov and A. M. Prokhorov recieved the Nobel Prize for their work about the theory of Lasers. A. L. Schawlow was given the Nobel Prize (together with N. Bloembergen and Kai M. Siegbahn) in 1981 for his work on the development of Laser spectroscopy.

surprising since a free electron cannot absorb energy due to momentum conservation. But in a Coulomb field of an atom the conditions are matched such that the electron experiences energy transfer from the laserfield. This phenomenon was called above-threshold ionization (ATI). Another interesting effect is multiple ionization [4] where not only the weakest bound electron but also stronger bound electrons are ionized in a strict sequential manner. A special form of multiple ionization was discovered a bit later: non-sequential double (or multi) ionization [5, 6, 7]. This topic continues to be one of the very hot ones in today's research. Basically, non sequential double ionization can be understood by a recollision mechanism within the so called three-step-model, first introduced by Corkum [8] and Kulander [9]. But there are still unresolved issues when it comes to the question which role correlation plays [10]. A real revolution in strong field atom ionization was the investigation of high harmonic generation (HHG). When an ionized atom returns back to the nucleus it can recombine with the ion and the excessive energy of the electron is emitted in the form of a photon in the extreme ultraviolet (xuv) or soft x-ray regime. This process can once again be understood by the three-step-model [8, 9]. Very recently HHG has led to the generation of single photonic pulses in the sub-femtosecond (or attosecond, 10^{-18} s) range [11, 12, 13] and thus laid the foundations to a new field in laser-matter interaction which was dubbed *Attophysics* [14, 15]. Recently increasing interest was being paid to the investigation of the interaction of complex systems like molecules and clusters of gas- or metal-atoms with laserlight. This has led to the discovery of laser triggered explosion of clusters [16] resulting in neutron production [17], time-resolved Coulomb explosion imaging [18], strong field control of chemical processes [19, 20, 21] as well as to the observation of decreased ionization [22, 23] in molecules as compared to atoms, and non-adiabatic multi-electron effects in molecules [24, 25, 26].

1.1 Theoretical Methods

Perturbative Interaction — Nonlinear Optics

The response of matter to intense radiation (e.g. laser fields) manifests itself in a nonlinear dependence of the induced polarization (atomic dipole moment times density of atoms) on the electric (and possibly magnetic) field of the incident radiation. The nonlinearity can originate from distinctly different processes, depending on the intensity. At low and moderate intensities the external laser field is much weaker than the static atomic Coulomb field. As a consequence, the laser field perturbs only slightly the atomic quantum states under non-resonant excitation conditions [27]. The energy levels suffer only a faint shift proportional to the intensity $I_L \propto E_L^2$ of the laser field E_L , which is referred to as the AC Stark shift [28]. The atoms remain, with a high probability, in their ground state. Nonlinear interactions taking place under these conditions can be well described by a perturbative approach. Hence we refer to this parameter range as the regime of *perturbative nonlinear optics*.

To derive the nonlinear response of an atomic ensemble we consider the Schrödinger equation for the simplest atom consisting of only one electron and one proton (Hydrogen atom) in the dipole approximation and in the length gauge²

$$i\partial_t\Psi(\mathbf{r};t) = H(\mathbf{r};t)\Psi(\mathbf{r};t), \quad (1.1)$$

where the Hamiltonian, H , is of the form

$$H = -\frac{1}{2}\nabla^2 + U(\mathbf{r}) - \mathbf{r} \cdot \mathbf{E}_L(t), \quad (1.2)$$

with $U(\mathbf{r})$ the atomic Coulomb potential, $U(\mathbf{r}) = -1/|\mathbf{r}|$, and the interaction term with the field $-\mathbf{r} \cdot \mathbf{E}_L(t)$. For low field strengths, as we want to consider here, this interaction term can be considered as a perturbation to the Hamiltonian, such that

$$H = H^{(0)} + \lambda H^{(1)}, \quad (1.3)$$

with a parameter λ , which can be set to unity in the end. The unperturbed Hamiltonian is

$$H^{(0)} = -\frac{1}{2}\nabla^2 - V(\mathbf{r}) \quad (1.4)$$

and the perturbation reads³

$$H^{(1)} = -\mathbf{r} \cdot \mathbf{E}_L(t) = -zE_L(t), \quad (1.5)$$

For the further derivation it is assumed, that the atomic polarization follows the change of the field instantly, which is a good approximation even at a timescale of femtoseconds [27], because the induced atomic dipole moment is of purely electronic origin. Hence, time-independent perturbation theory [29, 30, 31] can be used to calculate the atom's energy E . In order to do this we expand the wavefunction and the atom's energy into Taylor series with respect to the parameter λ . This yields

$$|\Psi\rangle = |\Psi^{(0)}\rangle + \lambda|\Psi^{(1)}\rangle + \lambda^2|\Psi^{(2)}\rangle + \dots \quad (1.6)$$

for the wavefunction and

$$E = E^{(0)} + \lambda E^{(1)} + \lambda^2 E^{(2)} + \dots \quad (1.7)$$

for the atom's energy, where $E^{(0)}$ is the unperturbed energy in the absence of the field. If we introduce these two expressions into the (time-independent) Schrödinger equation

$$H|\Psi\rangle = E|\Psi\rangle \quad (1.8)$$

²Throughout this thesis, with only one exception in this subsection, indicated below, the system of atomic units, which is utilized almost exclusively in atomic physics, is used. This system is obtained from the Gaussian System of Units by formally setting $\hbar = m_e = e^2 = 1$, where \hbar is the Planck's constant, m_e is the electron mass and e is the elementary charge. Conversion factors between atomic units and SI are given in appendix C on page 79.

³For the sake of simplicity, an isotropic medium is considered. Then the electric field and the polarizability are parallel. Furthermore the electric field shall be polarized in z-direction.

we obtain equations for the energies $E^{(m)}$ and wavefunctions $|\Psi^{(m)}\rangle$, for every order $m = 0, 1, 2, \dots$ of the above Taylor series. Carrying out the procedure of perturbation theory leads to

$$E = E^{(0)} - \langle \Psi^{(0)} | H^{(1)} | \Psi^{(0)} \rangle + \sum_{n \neq 0} \frac{\langle \Psi^{(0)} | H^{(1)} | n \rangle \langle n | H^{(1)} | \Psi^{(0)} \rangle}{E^{(0)} - E_n} + \dots, \quad (1.9)$$

where the orthonormal states $|n\rangle$ are determined by

$$H^{(0)} |n\rangle = E_n |n\rangle. \quad (1.10)$$

Reinserting the expression $-zE_L$ for $H^{(1)}$ leads to

$$E = E^{(0)} + \langle \Psi^{(0)} | z | \Psi^{(0)} \rangle E_L + \sum_{n \neq 0} \frac{\langle \Psi^{(0)} | z | n \rangle \langle n | z | \Psi^{(0)} \rangle}{E^{(0)} - E_n} E_L^2 + \dots \quad (1.11)$$

The Hellmann-Feynman theorem [31],

$$\frac{dE}{dT} = \left\langle \frac{\partial H}{\partial T} \right\rangle, \quad (1.12)$$

when using the laser field E_L instead of the general parameter T , leads to an expression

$$\left\langle \frac{\partial H}{\partial E_L} \right\rangle = \left\langle \frac{\partial H^{(1)}}{\partial E_L} \right\rangle = -\langle z \rangle = -\alpha, \quad (1.13)$$

where α is the electric polarizability. Inserting this result into the Hellmann-Feynman theorem yields

$$\frac{dE}{dE_L} = -\alpha. \quad (1.14)$$

This means, that calculating the derivative of the atom's energy equ. (1.11) with respect to the laser field, E_L , leads to an expression for the electric polarizability α . This expression, as can be seen in equ. (1.11), is a Taylor series with respect to powers of E_L . The polarization, P , of an N -atomic ensemble can be calculated from the polarizability by

$$P = N \alpha E_L. \quad (1.15)$$

Inserting the Taylor series for α with respect to the electric field into this equation we arrive at the famous nonlinear expression for the polarization [27, 32], which builds the basis of nonlinear optics. This expression reads⁴

$$P = \varepsilon_0 \chi^{(1)} E_L + P_{nl}, \quad (1.16)$$

where

$$P_{nl} = \varepsilon_0 \chi^{(2)} E_L^2 + \varepsilon_0 \chi^{(3)} E_L^3 + \varepsilon_0 \chi^{(4)} E_L^4 + \dots \quad (1.17)$$

⁴For the rest of this subsection, in order to be conform with the notation commonly used in electrical engineering, exceptionally the international system of units, SI, is used.

is the nonlinear part of the polarization. Here $\chi^{(k)}$ is the k th-order susceptibility. Since optics deals with the propagation of light in a non-linear medium, the polarization equ. (1.17) must be introduced into the Maxwell theory. This is done via the relation

$$D = \varepsilon_0 E_L + P, \quad (1.18)$$

with D the electric flux density. Inserting this relation into the wave equation for the electric field leads to

$$\partial_z^2 E_L - \frac{1}{c_0^2} \partial_t^2 E_L = \mu_0 \partial_t^2 P, \quad (1.19)$$

with c_0 the vacuum speed of light and μ_0 the vacuum magnetic permeability. Thus, the source term on the right hand side with the second derivative of the polarization takes into account the reaction of the matter on the laserfield. However, in nonlinear optics it is usual to express the reaction of the matter in terms of the susceptibility χ or the optical refractive index $n = \sqrt{1 + \chi}$ [33]. The light induced changes of n give rise to a wealth of interesting effects [32, 27, 33], like for example frequency doubling and triplication, frequency conversion and the optical Kerr effect, which is routinely used for the generation of femtosecond laser pulses (*Kerr-lens mode locking*; also called *passive mode locking*).

The Non-Perturbative Regime

Unfortunately this self consistent description of light-matter interaction given in the previous subsection cannot be extended to the range of strong fields, which we will exclusively consider in this thesis. This is because as the electric field strength increases, outer-shell electrons are detached from the atoms by either a multi-photon process or, for even higher intensities, by tunneling or above-barrier ionization. The interaction-term due to the laser field, $-\mathbf{r} \cdot \mathbf{E}_L(t)$, in the Hamiltonian equ. (1.2) can no longer be considered a perturbation since it is (at least) of the same order of magnitude as the Coulomb potential. Thus, a perturbative description of the form equ. (1.17) is no longer possible. Very high orders in the expansion would be necessary, which is not feasible any more. Hence, this parameter range is called *non-perturbative regime*. In order to properly describe the processes taking place in this parameter regime the Schrödinger equation (1.1) must be solved with methods different from the perturbation approach equ. (1.6) in order to correctly describe the interaction of the laser field $E_L(t)$ with the considered system. One approach would be to solve the Schrödinger equation numerically on a grid. Unfortunately with the computer power available at the moment this is only feasible for the Hamiltonian equ. (1.2) of the Hydrogen atom or at maximum for a "Helium"-Hamiltonian (2 electrons and 2 nuclei, denoted by indices 1 and 2) given here in Born-Oppenheimer

approximation⁵ [29, 31]

$$H = -\frac{1}{2} (\nabla_1^2 + \nabla_2^2) - \frac{2}{|\mathbf{r}_1|} - \frac{2}{|\mathbf{r}_2|} + \frac{1}{|\mathbf{r}_1 - \mathbf{r}_2|} - (\mathbf{r}_1 + \mathbf{r}_2) \cdot \mathbf{E}_L(t). \quad (1.20)$$

This limitation is due to the fact that because of the laser field time dependent methods have to be used and due to the large spatial extension of the Coulomb potential, which calls for large grid boxes. The limitation on the number of electrons arises from the electron-electron potential $\frac{1}{|\mathbf{r}_1 - \mathbf{r}_2|}$, which inhibits a separation into two one-electron Schrödinger equations. Even for the two-electron problem, equ. (1.20), the code must be parallelized on supercomputers [34].

Therefore, in order to calculate the response of more complicated systems than the Hydrogen or the Helium atom, certain approximations are necessary. The most common ones are the single-active-electron-approximation (SAEA) and the strong-field-approximation (SFA). Both approximations have been used to model atoms [2, 35, 36, 37] and molecules [38] in strong laserfields. In the SAEA-picture only the weakest bound electron in an effective (atomic) potential and in the laserfield is considered [39]. The SFA relies on the assumption that the evolution of continuum electrons is dominated by the intense laser field and that the influence of the Coulomb potential is negligible by comparison [2]. This means that an electron in positive energy (continuum) states can be treated like a free particle.

The Three-Step Model

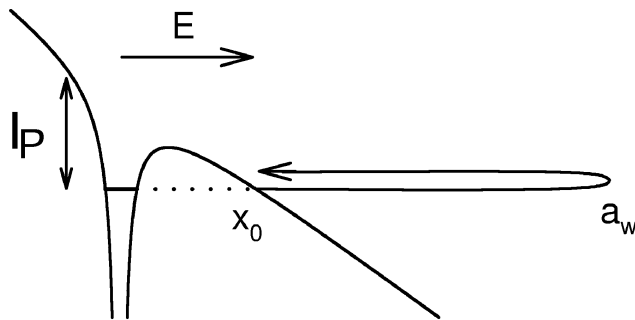


Figure 1.1: Schematic illustration of the continuum evolution of an electron in a strong laser field. In the first step the electron is ionized by tunneling ionization and is born in the continuum at position x_0 with some drift velocity [40]. Subsequently it follows the periodic motion of the laser field. The maximum amplitude during the first excursion is denoted by a_w .

⁵In Born-Oppenheimer approximation the nuclei are considered to be fixed in position during the laser pulse. This is justified by the fact that the nuclei are much heavier than the electrons and therefore do not react to the field as compared to the electrons, which react almost instantaneously.

The already mentioned three-step-model makes use of the SFA [8, 9]. For an illustration of the continuum evolution of an electron according to the SFA see fig. 1.1. In the quasistatic ionization regime (see next subsection) an electron can escape from the atom's Coulomb potential by tunneling through the tilted potential barrier and is born sufficiently far away from the nucleus such that the Coulomb potential can be neglected. This is the first step. Then, in the second step, the electron is accelerated by the strong laser field and its motion is only governed by classical mechanics (free particle). The influence of the Coulomb potential is not considered in the SFA, since it is weak as compared to the laser field. In a linearly polarized laser field the electron's motion is parallel to the polarization direction⁶. Therefore, the electron will change its direction and return to the parent ion, when the laser field changes its sign in the next half cycle. At this point the electron's amplitude is maximum, denoted by a_w in fig. 1.1. The third step describes the interaction of the electron with the parent ion. For example HHG can be seen as such a three step process, see fig. 1.2. There the accelerated electron returns to the parent atom and recombines to its original ground state. Such a recombined electron emits one single photon with an energy equal to the sum of the kinetic energy acquired along its orbit and the binding energy of the parent atom [27]. The returning electron does not necessarily recombine with the ion but can also hit the ion and can "knock out" another electron [6, 8, 9, 7]. This process is called *non-sequential double ionization* or, if more than one electron is knocked out, *non-sequential multi ionization*, and is one of the major research topics in laser-atom interaction [42].

The Quasistatic Approximation

As we have seen above, the dependency of the Hamiltonian on the time, which is caused by the alternating laser field, is one of the severe difficulties in the numerical but as well as in the analytical treatment of laser-matter interaction. Therefore it is obvious to get rid of this time dependency. This can be done in the so called *quasistatic limit*. In this parameter regime the electronic wavefunction reaches a quasistatic state before the electric field changes significantly [43] and the ionization probability can be calculated using the static field ionization rate. To decide if the ionization takes place in the quasistatic limit the so called Keldysh parameter is used. The Keldysh theory [2] considers one electron in an atomic potential. The laser electric field tilts the potential and the bound states are coupled to the continuum states. For high field strengths the electron can tunnel through the Coulomb barrier. The time that this process takes must be compared to the frequency of the electric field. If the tunneling time is short as compared to the laser frequency such that the electric field does not change during the tunneling process ionization takes place in the quasistatic limit. Then the Keldysh parameter is small as compared to unity.

⁶This is true as long as the magnetic part of the laser field can be neglected, which in the visible and near-infrared spectral range is the case for moderate intensities below $\approx 10^{18}$ W/cm² [41]. In this thesis we will always deal with intensities where only the electric field is of importance.

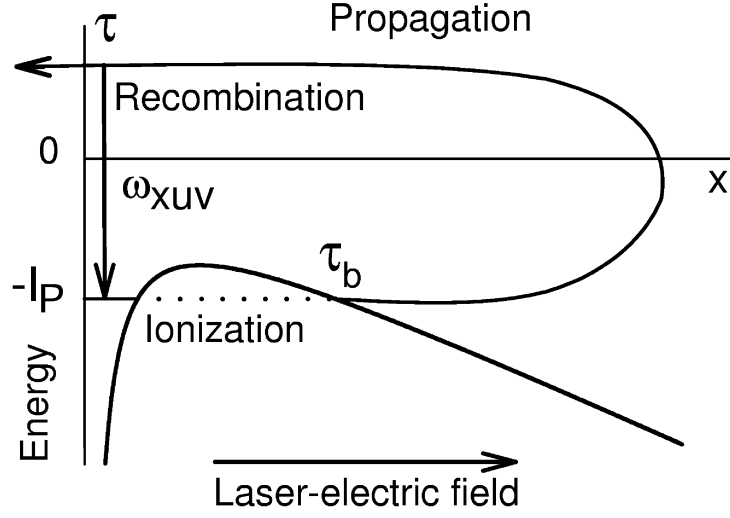


Figure 1.2: Schematic illustration of the elementary processes responsible for high harmonic generation. A free electron is born at instant τ_b by tunnel ionization, is subsequently accelerated in the laser field, returns to the nucleus, and emits a high-energy xuv photon upon recombination to the ground state at the instant τ .

If the Keldysh parameter is large as compared to unity ionization takes place via a multiphoton process.

The Keldysh Parameter

To calculate the Keldysh parameter one has to consider the length l the electron has to tunnel through the Coulomb barrier given by

$$l = \frac{I_P}{E_L}, \quad (1.21)$$

where I_P is the ionization potential of the electron under consideration and E_L is the maximum/momentary field strength. The electron's equivalent classical velocity is given by

$$v = \sqrt{2I_P}. \quad (1.22)$$

Thus the characteristic tunneling time is

$$t = \frac{l}{v}, \quad (1.23)$$

and the equivalent tunneling frequency is

$$\omega_t = \frac{1}{t} = \sqrt{\frac{2}{I_P}} E_L. \quad (1.24)$$

Quasistatic tunneling occurs if the tunneling time is much shorter than the laser half cycle. Therefore the tunneling frequency ω_t must be compared to twice the laser frequency which leads to the definition of the Keldysh parameter

$$\gamma = \frac{2\omega_L}{\omega_t} = \frac{\omega_L\sqrt{2I_P}}{E_L}. \quad (1.25)$$

For $\gamma \ll 1$ ionization occurs through quasistatic tunneling – also called (*optical*) *field ionization* – and for $\gamma \gg 1$ the atom is ionized via a multiphoton mechanism, where the electron absorbs several laser photons to overcome its binding energy I_P . This process can be described perturbatively [44]. As already described, it is possible that the electron absorbs more than the minimum number of photons required to overcome I_P (ATI). Furthermore, if the electric field is so strong, that the Coulomb barrier is suppressed below the binding energy I_P of the electron, ionization happens through *above barrier ionization* (ABI) [45]. For an illustration of tunneling- and multi-photon ionization as well as for ATI and ABI see fig. 1.3. The original Keldysh theory was improved by Faisal [46] and Reiss [47] and is therefore sometimes called KFR theory (Keldysh-Faisal-Reiss).

WKB, (T)DFT, (TD)HF, PIC, MCTDHF and other Commonly Used Methods

In the quasistatic limit (or strong field limit), $\gamma \ll 1$, another useful approximation can be made: the quasiclassical- or WKB-approximation [28, 29] (named after Wentzel-Kramer-Brillouin). A very successful theory based on the WKB approximation is the so called ADK theory (after Ammosov-Delone-Krainov) [48, 37]. This tunneling theory gives the quasistatic tunneling rate for arbitrary atoms. When compared with experimental results it fits best for noble gas atoms.

Applying some or all of the mentioned approximations it was possible to describing the detailed behaviour of atoms in strong infrared laser fields [49, 50, 51, 52]. However, as the comparison of theoretical results with experiments shows it is often necessary to consider more than one electron [7] or, since neither the ADK- nor the KFR-theory account for bound state dynamics, to include excited states into the theoretical description. Furthermore, if one wants to consider the interaction of strong laser fields with more complex systems than atoms, e.g. molecules or clusters of atoms, it is indispensable to account for possibly important effects like bound state wave packet dynamics, effects induced by polarization, occupation of excited states and other non-adiabatic effects, multi-electron effects like charge shielding, Coulomb blocking and correlation between the electrons, as well as for plasma-like effects in very big systems with many electrons like clusters. Recently several experiments with such complex systems were carried out [23, 25, 24, 22, 53, 54, 26] and it was shown that the SAE picture as well as the quasistatic description fail to describe the observations. This calls for a more elaborated theoretical treatment than provided by the KFR or ADK theory. However, it is awfully difficult to analytically calculate ionization rates and bound state occupation even in the case of

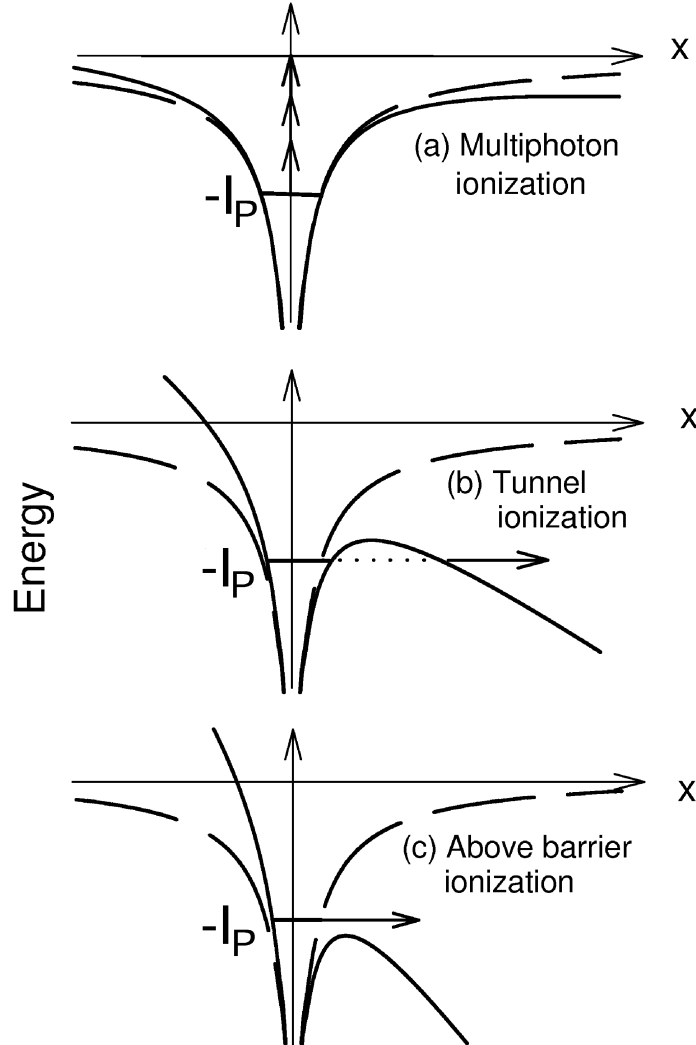


Figure 1.3: Regimes of atomic ionization. Exposing an atom to an intense laser field will result in a modified potential (solid line) composed of the Coulomb potential (dashed line) and the time dependent effective potential of the optical pulse. At moderate intensities the resulting potential is close to the unperturbed Coulomb potential and an electron can be liberated only upon simultaneous absorption of N photons, resulting in (perturbative) multiphoton ionization (a). The multiphoton ionization rate scales with the N th power of the intensity of the optical pulse. It is possible that more than N photons are absorbed which is called above threshold ionization (ATI). At sufficiently high field strengths the Coulomb barrier becomes narrow, allowing optical tunneling ionization (b) to take over and resulting in a tunneling current that follows adiabatically the variation of the resultant potential. At very high field strengths, the electric field amplitude reaches values sufficient to suppress the Coulomb barrier below the energy level of the ground state, opening the way to above-barrier ionization (ABI) (c).

an atom [55, 52], let alone those mentioned complex systems. Thus, once again one has to rely on numerical techniques (in addition with analytical estimations). But as said above, solving the Schrödinger equation for more than two electrons is only possible if special approximations are made. Sometimes only one spatial dimension is treated. This simplifies the solution a lot and is a reasonable approximation when the system under consideration has a certain favoured spatial extension. Especially in linearly polarized laserfields such favoured directions can be found. A numerical method developed for many-electron systems is *Density Functional Theory* [56]. But although this method works fine for stationary (time in-dependent) problems, time-dependent Density functional Theory (TDFt) [57, 58] is still plagued by fundamental problems [59]. Other approaches like *Time dependent Hartree-Fock* techniques do not perform well in describing non-perturbative multi-electron dynamics since they do not take into account electron-correlation [60, 61, 62, 63, 64, 65]. Therefore methods for the correct numerical description of multi-electron dynamics must be developed. For big clusters and plasmas, where hydrodynamic-like effects dominate the behaviour, the PIC (Particle in Cell) approach, which solves Maxwell's equations numerically on a 3-dimensional grid, together with a proper microscopic model to account for the quantum mechanical nature of ionization, is a promising route [66]. For molecular-systems, where the full quantum mechanical dynamics must be considered, multi-configurational time-dependent Hartree approaches were developed [67, 68, 69, 70]. In electronic systems such an approach must be extended in order to account for the total antisymmetry of the wavefunction. Multi-configurational approaches are capable of fully taking into account correlation [71]. Such methods are being developed at the moment [72].

1.2 Motivation and Overview

The discovery of high harmonic generation (HHG) [73, 74, 75] resulted in intensive experimental [76, 77, 78] and theoretical [27, 79, 8, 9] work to further improve this method which is capable of producing xuv- and x-ray photons. The shortest optical pulses available at that moment were about 4 fs FWHM (full width at half maximum)⁷ [82] carried at a wavelength of 780 nm. The laser cycle duration for that wavelength is roughly 2.7 fs, which means that the electric field exhibits only ≈ 1.5 oscillations within FWHM. Consequently such pulses are called *few-cycle pulses*. This pulse duration is obviously the natural limit for pulses in the infrared and visible spectral range and shorter pulses have to be carried on much shorter wavelengths. In 1992 Farkas and Toth proposed a method for using HHG to produce pulses in the attosecond regime [83]. This method is based on the fact that in the time domain harmonic emission is, within a laser oscillation period, confined to a small fraction of half the laser cycle duration $T_0/2$ (within a limited frequency band near the cutoff of the harmonic spectrum). This temporal structure gives rise to a train of subfemtosecond or even attosecond bursts. If only one pulse of this train could be cut out single photonic attosecond xuv-pulses would be possible. Indeed, there are possibilities to do this [27]. The most promising way is to use a few-cycle pulse. There, only one electron trajectory created at the pulse peak has the chance to return to the ion resulting in recombination and creation of an xuv photon only once within the time span of the driving infrared laser pulse [79, 27].

But even if single attosecond pulses can be produced there is still the problem of how their temporal structure can be measured, since for measurement of events such fast there need to be processes at least as fast as to be compared to and there needs to be a proper method for their temporal characterization. In 1995 Ivanov and co-workers suggested such a method [84]. With slight modifications this method was used to measure a roughly 2 fs short xuv pulse [11] (shorter than the light oscillation period !). Shortly after that the first pulse in the attosecond regime was created and measured [12]. The theory underlying these measurements is based on classical mechanics. Although classical models in strong laser field physics are known to give a qualitative correct description, a quantitative agreement between a classical model and full quantum mechanical descriptions is rarely the case. Quantum mechanical effects, like interference and quantum diffusion, play a significant role in strong laser field physics. Therefore, a reliable determination of sub-femtosecond pulse durations cannot be done without a thorough quantum mechanical analysis. In **chapter 2** on page 15 such an analysis will be presented.

Recent development of experimental techniques, like laser control of the motion

⁷Femtosecond pulses have led to a whole new field of research, called *Femtochemistry*. Molecules and atoms move (e.g. during chemical reactions) on the time scale of up to a few hundred femtoseconds [80, 81]. Therefore it is possible to trace the motion of atoms and molecules during chemical reactions with pump-probe experiments carried out with femtosecond pulses. For the development of time resolved spectroscopy the Nobel Prize for Chemistry was given to Ahmed H. Zewail in 1999.

of small molecules [85] and the availability of attosecond pulses [12] or ultrashort electron bunches [86], have increased the interest in the dynamics of the electronic hull of atoms, molecules and other multi-electron systems in strong laser fields. Theoretical calculations lag behind experimental possibilities in that the dynamics of at most two interacting electrons can be described with any degree of certainty, as already mentioned in section 1.1. Within the framework of the time-dependent Schrödinger equation, any additional degree of freedom like a third electron or nuclear motion can only be described using models or making severe approximations that are difficult to verify. Thus, for the time being, we are left out with a proper method to describe effects of collective excitation, correlation, screening, or the impact of the external field on internal dynamics. Time-dependent Density Functional Theory would be a suitable method. It takes into account the average influence of the multi-electron cloud in a so called "mean field". Thus, it is essentially designed for considering many electrons. Although it works well for time-independent cases it is still plagued by fundamental problems [59] in the time-dependent case, as already stated in section 1.1. Also the incapability of Time-dependent Hartree-Fock methods to take into account electron-correlation was mentioned. This motivates the development of a Time-dependent Multi-Configuration Hartree-Fock (MCTDHF) method, capable of treating multi-electron behaviour in complex systems like molecules, clusters of atoms, solids and doped structures in semi-conductors. Thanks to the multi-configurational approach it is possible to systematically include correlation and superposition- or excited states. The MCTDHF method will be presented in **chapter 3** on page 27.

With the help of the MCTDHF method it is, for the first time, possible to study the multi-electron response to strong laser fields. This is the content of the last two chapters of this work. In **chapter 4** an investigation of the electron dynamics in "big" systems (e.g., man-made structures in semi-conductors like quantum dots, ions of large organic molecules and the like) is presented. This study was motivated by the attempt of experimentalists to study ionization in metals within the last decades [87, 88, 89] and to distinguish between the multiphoton and the tunneling picture. I will address this question and explain how the electron dynamics in big systems is influenced by various laser parameters and by the size of the system. An explanation of the mechanism causing ionization in such systems will be given. The results of these investigations can be found on pages 43ff.

Another application of the MCTDHF-method is presented in **chapter 5**. Recent experiments showed that molecules [23, 22, 24, 25] but also metal-clusters [53] are harder to ionize than suggested by tunneling theories. It was believed that this is due to the polarizability of such multi-electron systems [22]. Furthermore there is evidence for non-adiabatic effects taking place in the interaction of laserfields with molecules [24, 25, 26]. As a first step to investigate the physics underlying these observations, a detailed study of the multi-electron response to strong laser fields in the long wavelength range was carried out. As explained in section 1.2, for low frequencies the Keldysh parameter yields values much smaller than unity and thus

the dynamics can be described quasi-statically. Therefore, non-adiabatic effects like population of higher (excited) states are negligible and only the pure tunneling behaviour can be observed and compared with theories valid in this regime. The outcome of this investigations is presented starting at page 60.

The thesis will be concluded by a summary and an outlook to future issues of the investigation of the interaction of matter with strong laser fields, see **chapter Conclusion and Outlook** on page 75.

I would like to take the opportunity to point out that this thesis deals exclusively with processes in matter which happen on the time scale of about 1 femtosecond or below. Although all processes are induced by strong femtosecond pulses, the electron dynamics in the irradiated matter for these processes follows exclusively the electric field of the laser rather than the envelope. The envelope of nowadays laser pulses is of the order of $\approx 5 - 20$ fs whilst the field changes (for wavelengths of $\approx 700 - 1500$ nm) on the order of some few femtoseconds. This limits the interaction of the electrons with the potential barriers in well potentials to about 1 fs, as can be seen in chapter 4. Tunneling in Coulombic potentials, as it is the case in atoms and molecules, happens only within a small fraction of the laser half cycle at the maxima of the laser electric field. The laser induced electron dynamics changes the tunneling behaviour on roughly the same time scale. Therefore those processes, studied in chapter 5, happen on a sub-femtosecond time scale. With even shorter time scales deals the process introduced in chapter 2, where a measurement method for pulses as short as ≈ 100 attoseconds is presented. Usually, for laser pulses the term "ultrashort" is used for femtosecond pulses [27]. All of the here considered physical processes are faster than those pulses. This justifies and explains the use of the term "ultrafast" in the title of this thesis.

Chapter 2

Attosecond Pulse Measurement

If one wants to measure a very short optical pulse there must be a direct measurable reference process at least as fast as the pulse. Xuv pulse durations are usually determined [90, 91, 92, 93] by laser dressed xuv photoionization. The time resolution of this method is limited to the order of the temporal duration of the pulse envelope and therefore, cannot be used in the attosecond time domain. To measure attosecond xuv pulses the reference process must be sensitive to the electric field rather than the pulse envelope. The electric field changes on the order of approximately 1 femtosecond and therefore optical pulses as short as roughly 100 attoseconds can be measured when using the electric field as a time reference [94]. Recently several cross-correlation methods [95, 96, 11, 97] sensitive to the electric field were proposed that have the potential to resolve attosecond-pulse durations. The most promising concept is based on the laser induced shift of the photoelectron spectrum that is produced by laser-dressed single-photon ionization of gas atoms by an xuv attosecond pulse. This method was originally proposed by Ivanov and co-workers [84] and first introduced for xuv-pulses by Toma and co-workers [98]. Two modifications of this method were used to measure an attosecond-pulse train [97] and single xuv-pulses with durations of around 2 fs [11] and 650 as [12]. Our investigation focuses on the configuration first realized in ref. [11], which has the advantage that single attosecond-pulses can be measured in contrast to the method used in ref. [97]. In difference to earlier experiments [90, 91, 92, 93, 98] the sub-laser cycle resolution in refs. [11, 12] is achieved by measuring the electron spectrum only over a limited solid angle [11]. The xuv-pulse duration is determined by using a *classical* model that relates the shift and the broadening of the electron spectrum to the xuv-duration. The classical model allows efficient numerical implementation making this method a particularly attractive method for attosecond-pulse measurement.

Although classical models in strong laser field physics are known to give a qualitative correct description, a quantitative agreement between classical model and full quantum mechanical description is rarely the case. Quantum mechanical effects, like interference and quantum diffusion, play a significant role in strong laser field

physics. Therefore, a reliable determination of sub-fs pulse durations cannot be done without a thorough quantum mechanical analysis.

Véniard et al. [99] have developed a quantum mechanical theory for the measurement of a train of attosecond pulses [97]. Here a theory for single attosecond pulse measurement based on laser dressed xuv photoionization [11, 12, 94, 100] is developed. We use exact integration of the Schrödinger equation and analytical integration under the strong field approximation (SFA), i.e. the influence of the atomic Coulomb potential on the free electrons is neglected. Based on the SFA we derive an expression for the SFA-spectrum of the xuv electron spectrum by means of an Fourier Bessel expansion and a semi-classical equation for the n -th moment of the electron spectrum that can be integrated orders of magnitude faster than the Schrödinger equation. The Fourier Bessel expansion is exact within the SFA, whereas the semi-classical theory underlies certain restrictions, but gives clear insight into the physics and presents a generalization of the classical model used in Refs. [11, 12] and, in special cases, becomes identical with the classical model. The validity of the semi-classical approach is verified by a comparison to exact results which yields good agreement for an intermediate laser intensity range. For higher and lower intensities additional quantum effects going beyond the semi-classical approximation must be taken into account and the Fourier Bessel expansion-formula has to be used. This formula also allows to make contact with the measurement model for attosecond pulse trains [99] used in ref. [97].

Finally, our model is used to identify an optimized experimental scheme. To achieve a certain signal to noise ratio in the measurement, an appropriate electron yield is necessary. This electron yield must be achieved by accumulating over a great number of incidents (attosecond pulses). Furthermore, the yield drops with increasing xuv-wavelength. Therefore, experiments are limited by the wavelength and by the long data collection times. The here presented optimized setup is by more than one order of magnitude more efficient than the one used so far [11, 12]. This reduces collection times considerably and allows the extension of this method to shorter wavelengths. Further on this setup allows, for the first time, for direct experimental discrimination between single and multiple attosecond pulses, which is of major importance for attosecond pump-probe experiments.

2.1 Theory

2.1.1 SFA Solution of the Schrödinger Equation

Our analysis makes use of the single active electron approximation (SAEA) and starts from the three-dimensional Schrödinger equation,

$$i\partial_t\Psi(\mathbf{r}) = \left[-\frac{1}{2}\nabla^2 - \frac{1}{|\mathbf{r}|} - \mathbf{r}\mathbf{E}(t) \right] \Psi(\mathbf{r}), \quad (2.1)$$

where the electron is coupled to the classical electromagnetic field in dipole approximation and in the length gauge. Here, $\mathbf{r} = (x, y, z)$ denotes the space coordinates, ∇ is the corresponding gradient operator, ∂_t is the time derivative, and Ψ represents the electron wavefunction. The electric field, $\mathbf{E}(t) = \mathbf{E}_L + \mathbf{E}_x$, comprises a laser, \mathbf{E}_L , and an xuv, \mathbf{E}_x , contribution. The laser component is of the form

$$\mathbf{E}_L = \hat{\mathbf{e}}_L F_L(t) \cos(\omega_L t) \quad (2.2)$$

and the xuv contribution has the form

$$\mathbf{E}_x = \hat{\mathbf{e}}_x F_x(t - t_x) \cos(\omega_x(t - t_x)), \quad (2.3)$$

where $\hat{\mathbf{e}}_L$ and $\hat{\mathbf{e}}_x$ denote the laser- and the xuv- polarization vectors of unity, respectively. $F_i(t)$ with $i = \{L, x\}$ denotes a smooth pulse envelope and ω_L and ω_x are the laser- and the xuv carrier frequency, respectively. The xuv pulse peak is delayed to the laser pulse peak by a time $t_x = t_d$.

In the following, equ. (2.1) is solved analytically by applying the SFA [2], i. e. the Coulomb potential is neglected as compared to the laser field. As a result, the Coulomb continuum eigenfunctions may be substituted by plane waves and equ. (2.1) is integrated by using the ansatz

$$\Psi = |0\rangle \exp(iI_P t) + \int d^3p b(\mathbf{p}, t) |\mathbf{p}\rangle. \quad (2.4)$$

Here, $|0\rangle$ denotes the ground state with ionization potential I_P , the plane wave is given by $|\mathbf{p}\rangle = \exp(i\mathbf{p}\mathbf{r})$ with \mathbf{p} the electron momentum, and $b(\mathbf{p}, t)$ is the momentum-space wave function of free electrons. Within the SFA we obtain the electron spectrum as [27]

$$b(\mathbf{p}) = i \int_{-\infty}^{\infty} \mathbf{E}(t') \mathbf{d}(\mathbf{p} - \mathbf{A}(t')) \exp \left[-i \int_{t'}^{\infty} \frac{1}{2} (\mathbf{p} - \mathbf{A}(t''))^2 dt'' + iI_P t' \right] dt'. \quad (2.5)$$

The vector potential, \mathbf{A} , and the electric field are related via $\mathbf{E} = -(1/c)\partial_t\mathbf{A}$, where c denotes the velocity of light. The dipole moment is determined by $\mathbf{d}(\mathbf{p}) = \langle \mathbf{p} | \mathbf{r} | 0 \rangle$. For the special case of continuum transitions from hydrogen bound s-states, $\mathbf{d} \propto \mathbf{p}/(\mathbf{p}^2 + 2I_P)^3$. For calculations in noble gases we have derived dipole moments from cross sections tabulated in ref. [101].

The integral in equ. (2.5) is calculated in two ways, a Fourier Bessel expansion of the exponential function in harmonics of the laser field [102] and by the stationary phase method [103].

2.1.2 The Multiphoton Picture

The Fourier Bessel formulas read [102]

$$e^{-iz \sin(\alpha)} = \sum_{n=-\infty}^{+\infty} e^{-in\alpha} J_n(z) \quad (2.6)$$

$$e^{-iz \cos(\alpha)} = \sum_{n=-\infty}^{+\infty} (-i)^n e^{-in\alpha} J_n(z), \quad (2.7)$$

with $J_n(z)$ the n -order Bessel functions. Since we are only interested in the xuv-part of the photoelectron spectrum we neglect the laser-part of the electric field in the preexponential factor of equ. (2.5). Additionally we do not consider the contributions of the xuv-field to the action integral in equ. (2.5). This is justified because the xuv-contribution is by orders of magnitude smaller than the one from the laser-field. Further on we take the laser vector potential $A_L(t)$ only at the instant of the xuv-pulse-peak, t_d . This does not alter the final result (the spectrum) as long as the xuv-pulse is much shorter than the laser half cycle, which is the case for the here considered sub-femtosecond pulses. With that the action integral can be readily integrated. Then we rewrite the resulting terms in the exponential function of equ. (2.5) into exponentials of trigonometric functions and insert the Bessel formulas equ. (2.6) and equ. (2.7). After some rearrangements and making use of the properties of the Bessel functions we arrive at the expression

$$|b(\mathbf{p})|^2 = \left| \sum_{n=-\infty}^{+\infty} i^n J_n(a, b) \mathcal{F}_n(p) \right|^2 \quad (2.8)$$

for the xuv-photoelectron spectrum, with

$$\mathcal{F}_n(p) = \int_{-\infty}^{+\infty} \mathbf{d} \cdot \mathbf{E}_x(t - t_d) \exp[i(p^2/2 + I_p + U_p(t_d) + n\omega_L)t] dt \quad (2.9)$$

and $U_p(t_d) = F_L^2(t_d)/(4\omega_L^2)$, which is the so called laser ponderomotive potential. The contributions \mathcal{F}_n from the n -th side-band in equ. (2.8) are weighted by the generalized Bessel functions

$$J_n(a, b) = \sum_{m=-\infty}^{+\infty} J_{n+2m}(a) J_{-m}(b) \quad (2.10)$$

with

$$a = \mathbf{p} \cdot \hat{\mathbf{e}}_L F_L(t_d) / \omega_L^2 \quad (2.11)$$

and

$$b = F_L^2(t_d) / (8\omega_L^3). \quad (2.12)$$

We have compared equ. (2.5) and equ. (2.8) numerically and they give identical results for xuv-pulse durations up to the order of the laser half cycle.

The solution in equ. (2.8) can essentially be understood as contributions of all sidebands of the xuv-photoelectron spectrum to the final momentum \mathbf{p} of the electron. In practice the infinite sum needs to be taken only over a few sidebands since the weighting of the sidebands with $J_n(a, b)$ ensures convergence. The term \mathcal{F}_n from equ. (2.9) is the Fourier transform of the time components determining the energy distribution of the electron, namely dipole moment and xuv-pulse envelope (i.e. duration). This Fourier transform contributes to the final momentum of the electron according to its index n . The Fourier transform is done with respect to the energy of the electron, $p^2/2$, increased by the ionization potential, I_P , and the laser ponderomotive potential at the instant of the xuv-pulse-peak, $U_p(t_d) = F_L^2(t)/(4\omega_L^2)$. The electron is additionally accelerated or decelerated by the laser field and consumes or emits n laser photons of energy ω_L . The function of the laser field as a reference manifests itself in this term and in the ponderomotive potential. With the help of equ. (2.8) contact to the theory of attosecond pulse-train measurement is made [99]. There the spectrum (due to the repetitive time pattern) stays discrete and can be modelled by sidebands. For a single pulse the sidebands broaden and overlap such that the spectrum becomes a continuous function.

2.1.3 The Semiclassical Picture

A simpler solution of the integral in equ. (2.5) can be obtained with the help of the stationary phase method. This solution requires several approximations, but gives plain and clear insight into the underlying physics. We are interested in the case where the electron is ionized by single photon ionization and the free electron is dressed by the laser electric field. As a result, we again neglect the laser electric field in the preexponential factor that accounts for laser induced ionization. This is valid as long as $\omega_0/U_p \gg 1$, where $\omega_0 = \omega_x - I_P$ is the initial energy of the electron at the time t_s of birth in the continuum. Further, the rotating wave approximation [32] is utilized with respect to \mathbf{E}_x in the preexponential factor, i.e. the term $\exp(-i(\omega_x + I_P)t)$ is neglected as compared to $\exp(i(\omega_x - I_P)t)$. Finally, the effect of the xuv-field on the free electron dynamics is neglected, i.e. $\mathbf{A} \approx \mathbf{A}_L$ in equ. (2.5). Applying the above approximations we obtain

$$b(\mathbf{p}) \approx \sum_{t_s} \sqrt{\frac{2\pi}{i\ddot{S}(t_s)}} F_x(t_s - t_d) \hat{\mathbf{e}}_x \mathbf{d}(\mathbf{p} - \mathbf{A}(t_s)) \exp(-iS(t_s)) \quad (2.13)$$

where

$$S(t_s) = (1/2) \int_{t_s}^{\infty} (\mathbf{p} - \mathbf{A}_L(t''))^2 dt'' + \omega_0 t_s \quad (2.14)$$

is the classical action, and

$$\ddot{S}(t_s) = -E_L(t_s)(p \cos \theta - A_L(t_s)) \quad (2.15)$$

is the second time derivative of the classical action. The stationary phase points t_s are determined by solution of the equation

$$(1/2)(\mathbf{p} - \mathbf{A}_L(t_s))^2 = \omega_0, \quad (2.16)$$

which expresses the conservation of energy during the laser dressed photoionization.

Next we assume that the laser field is polarized along the z -direction, $\hat{\mathbf{e}}_L = \hat{\mathbf{e}}_z$, and introduce spherical coordinates for \mathbf{p} , which are the final electron kinetic energy $\Omega = p^2/2$ and the angle θ between \mathbf{p} and the z -axis. Then, the stationary phase equation can be recasted into

$$\begin{aligned} \Omega \approx & \omega_0 + U_p(t_s)(\cos(2\omega_L t_s) - 1) + 4U_p(t_s) \sin^2(\omega_L t_s) \cos^2 \theta \\ & + \sqrt{8\omega_0 U_p(t_s)} \sin(\omega_L t_s) \cos \theta, \end{aligned} \quad (2.17)$$

which agrees exactly with the classical model used in refs. [11, 12]. The term $U_p(t_s)$ represents the ponderomotive shift following the laser pulse envelope. Variation of the birth time between $-\infty < t_s < \infty$ determines the real solutions of equ. (2.17) which lie in the energy range $\Omega_{min} \leq \Omega \leq \Omega_{max}$. Beyond this range, equ. (2.17) has complex (t_s) solutions. Classical mechanics and the semi-classical wavefunction obtained by stationary phase integration are limited to the energy range $\Omega_{min} \leq \Omega \leq \Omega_{max}$. In order to take account of the wavefunction outside the classical range, the complex solutions of equ. (2.17) must be taken into account by saddle point integration [102]. We confine our analysis here to the semi-classical limit. The relevance of the complex saddle points for attosecond-pulse measurement is investigated below. Note that, although the semiclassical wavefunction is incomplete, it contains two quantum mechanical effects that are neglected in the classical analysis: (i) interference effects covered by the sum over different trajectories contributing to the same final state, and (ii) wave packet spreading which is described by \ddot{S} .

For the further derivation it is convenient to re-express the second derivative of the classical action with the help of equ. (2.17) as

$$\ddot{S} = \frac{d\Omega}{dt_s} \left(1 - \frac{1}{1 + \sqrt{\frac{\omega_0}{2U_p \sin^2 \omega_L t_s \cos^2 \theta} - \tan^2 \theta}} \right) \approx \frac{d\Omega}{dt_s}. \quad (2.18)$$

The approximations made in the derivation of equ. (2.18) is justified by the condition $\omega_0/U_p \gg 1$ required above.

The Fourier-Bessel equation (2.8) and the semiclassical equation (2.13) reduce the computational effort for calculating the electron spectrum by four to five orders of magnitude as compared to the integration of equ. (2.1). This makes accurate determination of the xuv-pulse duration including quantum effects practically doable. It will be shown below that equ. (2.13) has a more limited validity range than equ. (2.8), however, has the advantage that contact can be made with the classically governed determination of the xuv-pulse duration of ref. [11].

The attosecond pulse measurement method in refs. [11, 12] relies on the fact that the electron spectrum is measured in a limited solid angle (θ, φ) . The xuv

pulse duration is determined by measuring the n -th moment of the electron energy spectrum as a function of the xuv pulse delay t_d , which is given by

$$\langle \Omega^n(t_d) \rangle = \frac{\int_{\theta_0}^{\theta_1} \int_0^\infty \Omega^n |b(\Omega, \theta)|^2 \sqrt{\Omega} d\Omega \sin\theta d\theta}{\int_{\theta_0}^{\theta_1} \int_0^\infty |b(\Omega, \theta)|^2 \sqrt{\Omega} d\Omega \sin\theta d\theta}. \quad (2.19)$$

The angle θ to the laser polarization axis is confined between θ_0 and θ_1 . We focus here on configurations with cylindrical symmetry, where the linear laser and xuv polarizations coincide, for which the integral over φ drops out of equ. (2.19). Usually, the center of gravity $\langle \Omega \rangle$ or the rms width of the electron spectrum $\Delta\Omega = \sqrt{\langle \Omega^2 \rangle - \langle \Omega \rangle^2}$ are used for attosecond pulse measurement [11, 12].

Equations (2.8) or (2.13) in combination with equ. (2.19) allow an efficient numerical evaluation of $\langle \Omega^n \rangle$. With the use of equ. (2.13) together with equ. (2.18), $\langle \Omega^n \rangle$ can be further simplified and yields a simple semi-classical formula. For that we insert equ. (2.13) into equ. (2.19) and transform from (Ω, θ) to (t_s, θ) , where $\Omega(t_s)$ is defined by the stationary phase equation equ. (2.17). This changes the differential volume element from $d\Omega \sin\theta d\theta$ to $(d\Omega/dt_s) dt_s \sin\theta d\theta$. By virtue of equ. (2.18), the additional factor $d\Omega/dt_s$ arising from the variable transformation cancels the factor $1/\ddot{S}$ in $|b|^2$ that accounts for quantum diffusion and wave packet spreading. For pulse durations comparable to the laser period interference between contributions from different stationary points t_s in equ. (2.13) modulate the electron spectrum on the scale of the laser photon energy, i.e. ≈ 1.5 eV for a wavelength of 800 nm. At laser intensities of $\approx 3 \times 10^{13}$ W/cm² the spectrum is much broader than the laser photon energy (see fig. 2.2) and therefore the modulations are averaged out in the integrals and contributions from different t_s can be summed independently. The physical reason for the irrelevance of interference effects is that parts of the electron wave packet produced at different t_s remain spatially well separated. Therefore the sum \sum_{t_s} over all stationary phase points in equ. (2.13) can be neglected for our further derivations. This all together yields

$$\langle \Omega^n(t_d) \rangle = \frac{\int_{\theta_0}^{\theta_1} \int_{-\infty}^{\infty} \Omega^{n+1/2}(t_s) F_x^2(t_s - t_d) (\hat{\mathbf{e}}_x \mathbf{d}(t_s))^2 dt_s \sin\theta d\theta}{\int_{\theta_0}^{\theta_1} \int_{-\infty}^{\infty} \Omega^{1/2}(t_s) F_x^2(t_s - t_d) (\hat{\mathbf{e}}_x \mathbf{d}(t_s))^2 dt_s \sin\theta d\theta}. \quad (2.20)$$

Equation (2.20) puts the classical derivation of ref. [11] on a more general and rigorous theoretical footing. In the special case of transitions to spherically symmetric s-continuum waves (angular momentum $l = 0$), the result of ref. [11] is exactly recovered. This is, because by virtue of the stationary phase condition, \mathbf{d} becomes independent of the integration variables and drops out of equ. (2.20). Calculating the n -th moment of the spectrum with the help of equ. (2.20) is extremely fast because only the xuv-pulse *envelope* has to be considered. The xuv-pulse duration is determined by fitting the calculated n -th moment with the pulse-duration as a free parameter to the n -th moment inferred from the measured electron spectra.

2.2 Results

2.2.1 Classical Mechanics vs. Quantum Mechanics

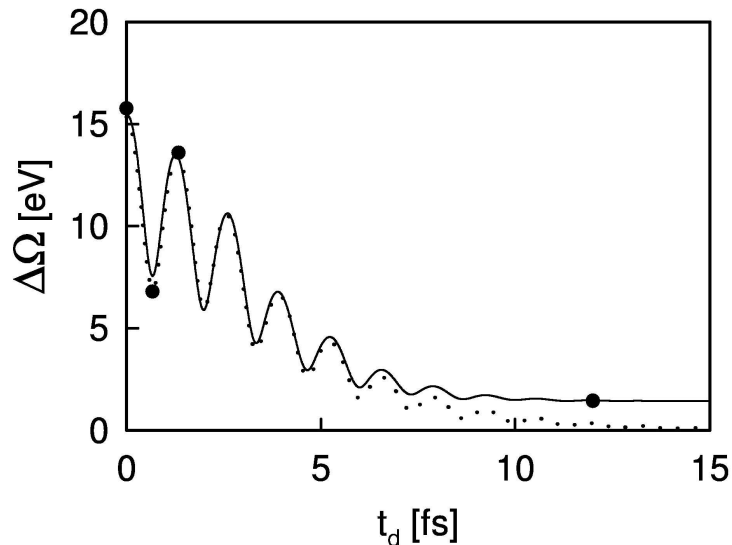


Figure 2.1: Rms width $\Delta\Omega$ of the electron spectrum for a hydrogen (1s) ground state as a function of delay time, t_d , between laser and xuv-pulse. The pulse parameters are: laser wave length $\lambda_L = 800$ nm, laser FWHM pulse duration 5 fs, sech laser pulse envelope, laser intensity $I_L = 3 \times 10^{13} \text{W/cm}^2$, $\omega_x = 90$ eV, xuv pulse duration 500 as, xuv pulse intensity $I_x = 10^{12} \text{W/cm}^2$. Laser and xuv polarization are chosen parallel to the direction of observation, $\hat{\mathbf{e}}_z = \hat{\mathbf{e}}_L \parallel \hat{\mathbf{e}}_x \parallel \mathbf{p}$, and $\theta_1 = 2^\circ$. $\Delta\Omega$ was calculated in various ways: exact numerical solution of equ. (2.1) (full circles), evaluation of the Fourier-Bessel equation (2.8) (solid line), and integration of the semiclassical equ. (2.20) (dotted line).

The quality of the approximations utilized in our derivation was tested by comparison to an exact numerical solution of equ. (2.1) based on a discretization of the Schrödinger equation in momentum space, as described in ref. [104]. For fig. 2.1 we have calculated the rms width $\Delta\Omega$ in various ways. The modulation of $\Delta\Omega$ appears for pulses shorter than one laser half cycle and gives a sensitive measure of the xuv pulse duration. The modulation increases with decreasing xuv-pulse duration. Full circles, solid line, and dotted line refer to the exact numerical solution of equ. (2.1) and to the Fourier-Bessel equation (2.8) in combination with equ. (2.19), and to the integration of equ. (2.20), respectively. The exact solution agrees well with the Fourier-Bessel solution, which demonstrates the validity of the SFA. The agreement with equ. (2.20) is best around the laser pulse center. The reason is that the semiclassical calculation of the electron spectrum based upon the stationary phase method fails for vanishing laser intensities. In this limit, the electron spectrum becomes a delta-peak at energy $\omega_x - I_P^1$. As a result $\Delta\Omega \rightarrow 0$ for large t_d , whereas in reality

¹In classical mechanics there is no spectral width.

the width never drops below the spectral width of the xuv pulse. The calculations in fig. 2.1 were repeated varying laser and xuv pulse parameters in the range relevant for attosecond pulse measurement (xuv/laser duration between 0.1/5 fs and 1/15 fs, xuv/laser peak intensity between 10^{12} and 10^{14} W/cm², sech and Gaussian pulse shape). The only parameter critical for the applicability of the semiclassical model is the laser peak intensity, for the reasons discussed above. For intensities well below 10^{13} W/cm² the semiclassical theory predicts wrong rms-widths, see fig. 2.1, and the Fourier-Bessel equation must be used. Finally, we did not plot the classical result, which is identical with the semiclassical calculation for the parameters chosen here. This is, because for $\theta \approx 0^\circ$ \mathbf{d} becomes again independent of the integration variables and drops out of equ. (2.20). For $\theta \approx 90^\circ$ the effect of \mathbf{d} is maximum and introduces a factor of 2 in the modulation depth of the rms width.

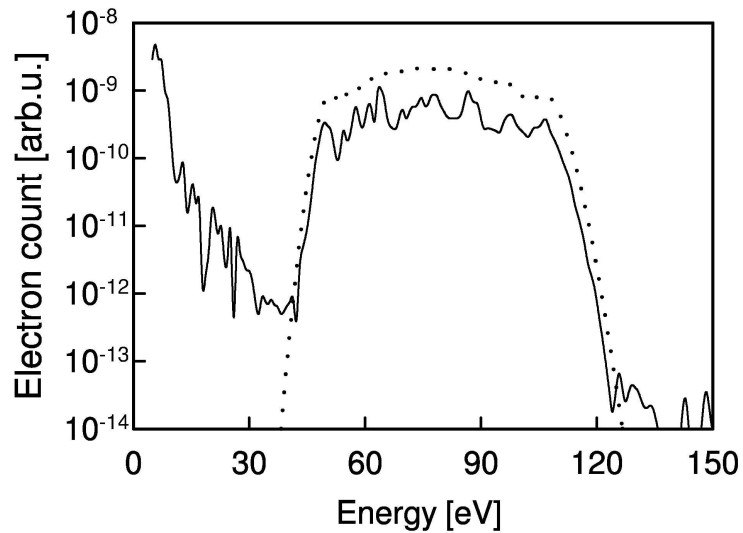


Figure 2.2: Photo electron spectrum for the parameters of fig. 2.1 and delay $t_d = 0$. The full and the dotted line denote the electron spectrum as determined by numerical integration of the Schrödinger equation (2.1) and the Fourier-Bessel equation (2.8), respectively. Note that in the derivation of equ. (2.8) laser induced ionization is not included, which is responsible for the low frequency part (<30 eV) in the exact calculation.

To further corroborate the applicability of the SFA, we have compared electron spectra in fig. 2.2, which were calculated by an exact solution of equ. (2.1) (full line) and by equ. (2.8) (dotted line). The agreement is excellent, justifying omission of the Coulomb potential in the derivation of equ. (2.8). Figure 2.2 reveals another important result. Except for the xuv-photoelectrons the spectrum at low energies contains a contribution of ATI (above threshold ionization) electrons generated by the laser directly. The experimental setup must be chosen in such a way that the two contributions fall into well separated spectral ranges. Otherwise the laser dressed photoionization signal, carrying the information on the attosecond pulse duration, is covered by the ATI electrons. So far, in order to minimize ATI, electrons were observed perpendicular to the laser polarization axis [11, 12]. The spectrum in fig. 2.2

shows that the level of ATI electrons is less than anticipated. Even for $\hat{\mathbf{e}}_L \parallel \mathbf{p}$, where ATI reaches the maximal energies, the laser induced part of the ionization spectrum is well separated from the x-ray photoionization spectrum. This can be understood from a simple estimate: The laser induced part of the ATI spectrum consists of a main part extending to $2U_p$ and of a smaller contribution coming from rescattering, with electron energies up to $10U_p$ [105]. Only the $2U_p$ contribution is strong enough to cover the xuv-induced electron signal. As a result, attosecond pulse measurement is feasible, as long as the lower cutoff of the xuv-photoelectron spectrum does not overlap with the $2U_p$ part of the laser induced ATI spectrum. Based on the stationary phase equation derived above the simple condition $8U_p \leq \omega_x - I_P$ is found, determining the parameter range in which the two spectral contributions remain separate. Only for laser peak intensities in excess of 10^{14}W/cm^2 , laser induced ionization becomes dominant and buries the single xuv-photoionization signal. This finding adds an additional degree of freedom to the realization of an optimum setup for attosecond pulse measurement, which will be the topic of the next section.

2.2.2 Increasing Measurement Efficiency

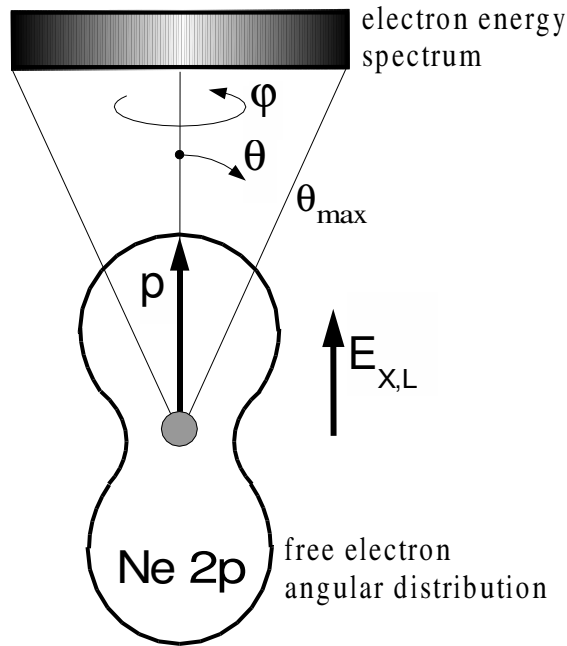


Figure 2.3: Schematic of the optimized experimental setup.

A major problem in attosecond pulse measurements is the low efficiency of harmonic sources and the resulting long data collection times and poor signal to noise ratio. So far attosecond measurement was performed with Kr 4p electrons, for which the single xuv-photon ionization is dominated by a transition to a spherically sym-

metric s-continuum wave [101]. We have compared various experimental setups with respect to efficiency in electron yield. We find an optimal setup when laser and x-ray polarization are chosen parallel to the direction of observation of the electron spectrum, i.e. $\hat{\mathbf{e}}_L \parallel \hat{\mathbf{e}}_x \parallel \mathbf{p}$, see fig. 2.3. Instead of Kr 4p we propose to use Ne 2p electrons. The overall gain in xuv electron yield as compared to the setup in refs. [11, 12] is a factor of 30 for the same opening angle of 40° . This enhancement can be attributed to two reasons. First, the Ne 2p transition is by an order of magnitude more efficient than the Kr 4p transition. Second, the xuv photoionization (90eV) of Ne 2p electrons is dominated by a transfer into a d-continuum wave, which extends into the direction of the x-ray polarization, see fig. 2.3. Therefore, a measurement along the x-ray polarization direction captures a larger part of the photoelectrons, which gives an enhancement by a factor of 3. The gain enhancement by more than one order of magnitude in our improved setup makes a more efficient measurement of attosecond pulses possible and allows an extension of the method towards shorter wavelengths.

2.2.3 Single vs. Multiple XUV Pulses

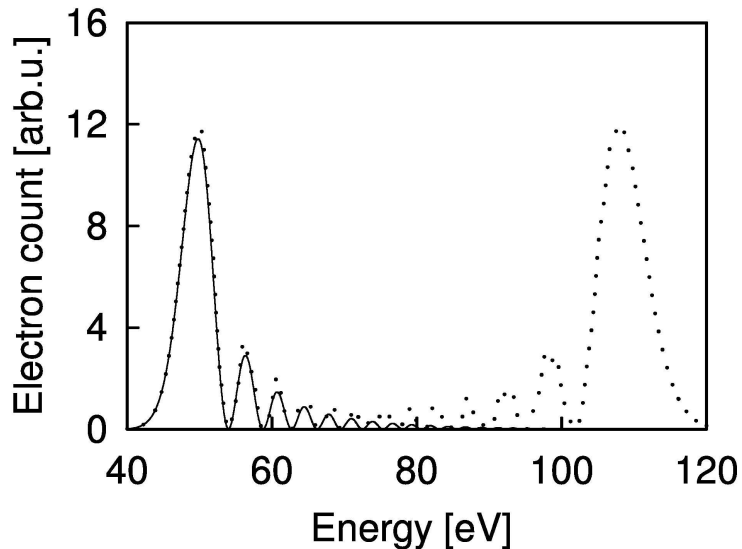


Figure 2.4: Signature of two attosecond pulses with delay times $t_d = \pm 1/4$ laser optical cycles compared to a single pulse with delay $t_d = 1/4$. The remaining pulse parameters are as in fig. 2.1. Electrons released at $t_d = \pm 1/4$ experience maximal acceleration and maximum deceleration by the laser, respectively, creating two well separated electron peaks (dotted line). A single pulse creates only a single peak (full line).

Higher harmonic generation with few cycle laser pulses tends to generate a single attosecond pulse with satellites at a repetition rate of twice the laser frequency. For practical applications it is essential to discriminate between a single attosecond pulse and a pulse train. Recently, indirect evidence of single attosecond pulses was ob-

tained by using the harmonic spectrum [12]. Measurement of the electron spectrum in laser polarization direction will allow for the first time to directly distinguish a single attosecond pulse from a pulse train, see fig. 2.4. This is because the shift of electron energies becomes sensitive to the sign of the laser vector potential at the time of xuv ionization. Depending on the sign, electrons are either accelerated or decelerated by the laser, leading to two well separated peaks in the electron spectrum. For one main and one or two smaller satellite pulses, the ratio of the peaks in the electron spectrum reflects the relative energy content carried in the satellites. Note that in a multi-shot experiment the absolute phase of the laser pulse must be stable from pulse to pulse.

2.3 Concluding Remarks

The here proposed setup has been used to experimentally energy-shift a photoelectron spectrum representing an attosecond-pulse with a duration of around 500 as² without significant distortion as compared to the spectrum without the infrared laser pulse [13]. This experiment beautifully demonstrates the simple functionality of our approach to distinguish between one and several attosecond pulses.

Recently the very first experiment on time-resolved atomic inner-shell spectroscopy was published [14]. In this pump-probe experiment the lifetime of M-shell vacancies in Krypton was measured by the use of roughly 900 as long x-ray pulses. The Auger measurement of the process taking place when the atom is excited with an xuv- or soft x-ray pulse can be modelled by a straightforward extension of the theory presented above [106]. The only difference to the measurement technique developed here, is that the generation of continuum electrons does not take place by a dipole transition induced by the field E_x , but by an Auger process [14]. This demonstrates the generality of the approach outlined in this chapter.

Concluding, a quantum mechanical model of laser dressed single xuv/x-ray photoionization was developed. It was shown that laser dressed photoionization can be quantitatively modelled by using the strong field approximation, i.e. by neglecting the Coulomb potential during the continuum evolution of the electron. Based on the strong field approximation a quantum mechanical and a semiclassical expression, that can be evaluated efficiently, were developed, making accurate determination of the attosecond pulse duration including quantum effects practicable. The validity range of the previously used classical model was established and an optimum setup for attosecond pulse measurement that is by a factor of 30 more efficient than existing schemes was identified. Finally, the proposed setup discriminates between single and multiple attosecond pulses. The results revealed by this quantum mechanical investigation open the way towards an accurate and more efficient measurement of attosecond pulses.

²This is up to date the shortest light pulse ever produced.

Chapter 3

Numerical Treatment of Laser driven Multielectron Systems

As mentioned in section 1.1, at the moment it is not possible to solve the Schrödinger equation for more than 2 electrons in a strong field numerically exact. Even for systems consisting of 2 electrons driven by strong laser pulses massively parallelized codes running on supercomputers must be applied. Therefore it is indispensable to make approximations when treating many-body problems, especially time-dependent ones, e.g. molecules and clusters in strong laser fields, which we would like to study here. The difficulties arise from the electron-electron Coulomb interaction and the interaction of the electrons with the nuclei but also from the interaction of the nuclei among each other. Fortunately the electrons are much lighter than the nuclei and thus respond almost instantaneously to strong field excitations as compared to the much heavier nuclei. Therefore it is possible to solve the many-body problem only for the electrons in the potential of the nuclei and consider the nuclei to be fixed in position. This procedure is known as *Born-Oppenheimer approximation* [29, 31].

Still, even within the Born-Oppenheimer approximation we are left with a time-dependent multi-dimensional, non-separable problem. If the number of electrons is denoted by f , the dimension of the wavefunction is $4f + 1$. This number consists of $3f$ spatial dimensions, f coordinates arising from the spin and one extra dimension for the time. Therefore the electronic wavefunction Ψ is of the form

$$\Psi = \Psi(\mathbf{q}_1, \dots, \mathbf{q}_f; t), \quad (3.1)$$

where \mathbf{q}_i denotes a coordinate consisting of a 3-dimensional spatial part \mathbf{x}_i and a spin part. The *Pauli exclusion principle* requires the wavefunction to be completely antisymmetric, i.e. it must change sign if the coordinates (spatial or spin) of any two electrons are interchanged. If the Hamiltonian is independent of the spin of the electrons the wavefunction can be separated into a spatial part and a spin part

$$\Psi(\mathbf{q}_1, \dots, \mathbf{q}_f; t) = \Psi(\mathbf{x}_1, \dots, \mathbf{x}_f; t)\chi(1, 2, \dots, f), \quad (3.2)$$

where the spatial part of the wavefunction must satisfy the Schrödinger equation

$$i\frac{\partial}{\partial t}\Psi(\mathbf{x}_1, \dots, \mathbf{x}_f; t) = \left[\sum_{m=1}^f \left(-\frac{1}{2}\nabla_m^2 + U(\mathbf{x}_m) - \mathbf{x}_m \cdot \mathbf{E}_L(t) \right) + \sum_{m<n}^f V(\mathbf{x}_m - \mathbf{x}_n) \right] \Psi(\mathbf{x}_1, \dots, \mathbf{x}_f; t). \quad (3.3)$$

In the here used Hamiltonian the molecular potential energy curve is taken into account by the potential U and the electron-electron Coulomb interaction by V . The laserfield, $\mathbf{E}_L(t)$, from which the time-dependency arises, couples to the system in dipole approximation. As mentioned, the Schrödinger equation (3.3) equation cannot be solved for $f > 2$ with presently available computer powers within reasonable time. Therefore, further approximations must be made. A very popular and successful one is the so called *central field approximation*, which was proposed by Hartree and Slater.

3.1 The Hartree-Fock Approach

The *central field approximation* is based on an independent particle model, in which each electron moves in an effective potential which represents the molecular potential energy curve (the nuclear potential) and the average effect of the repulsive interactions between this electron and the $(f-1)$ other electrons. As a result of this approximation the full wavefunction $\Psi(\mathbf{x}_1, \dots, \mathbf{x}_f; t)$ can be separated into electron orbitals,

$$\Psi(\mathbf{x}_1, \dots, \mathbf{x}_f; t) = u_1(\mathbf{x}_1)u_2(\mathbf{x}_2) \dots u_f(\mathbf{x}_f; t). \quad (3.4)$$

To reintroduce the spin into the wavefunction one has to multiply the electron orbitals by a spin-1/2 eigenfunction $\chi_{1/2}$, thus forming the spinorbitals

$$\varphi_i(\mathbf{q}; t) = u_i(\mathbf{x}; t) \chi_{1/2}, \quad (3.5)$$

which each may be orthonormalized,

$$\langle \varphi_i | \varphi_j \rangle = \delta_{ij}. \quad (3.6)$$

An appropriate ansatz for equ. (3.3) is then constructed by the so called *Slater determinant*

$$\Psi(\mathbf{q}_1, \dots, \mathbf{q}_f; t) = \frac{1}{\sqrt{f!}} \begin{vmatrix} \varphi_1(\mathbf{q}_1; t) & \cdots & \varphi_f(\mathbf{q}_1; t) \\ \vdots & \ddots & \vdots \\ \varphi_1(\mathbf{q}_f; t) & \cdots & \varphi_f(\mathbf{q}_f; t) \end{vmatrix}. \quad (3.7)$$

This so constructed wavefunction is fully antisymmetric and obeys the Pauli principle. The normalization factor $(f!)^{-1/2}$ arises from the fact that there are $f!$ permutations of the electron coordinates $\mathbf{q}_1, \mathbf{q}_1, \dots, \mathbf{q}_f$. The Slater determinant (wavefunction) Ψ can also be written in the form

$$\Psi(\mathbf{q}_1, \dots, \mathbf{q}_f; t) = \frac{1}{\sqrt{f!}} \sum_{\mathcal{P}} (-1)^{\mathcal{P}} \mathcal{P} \varphi_1(\mathbf{q}_1; t) \dots \varphi_f(\mathbf{q}_f; t), \quad (3.8)$$

with \mathcal{P} the permutation operator. The symbol $(-1)^{\mathcal{P}}$ is equal $+1$, when \mathcal{P} is an even permutation and equal to -1 for an odd permutation. The Hartree-Fock method uses an ansatz of the form of equ. (3.8) to solve the Schrödinger equation. The spinorbitals $\varphi_i(\mathbf{q})$ that give the 'best' f -electron wavefunction are found by using variation theory, which involves minimizing the Rayleigh ratio [29, 31]. This leads to the *Hartree-Fock equations*. Originally the Hartree-Fock (HF) equations are time-independent, but there are methods to extend them to time-dependent problems [107, 60, 61].

Because the potential felt by each electron depends on all the other electrons the time-independent Hartree-Fock equations must be solved iteratively. The iteration is carried out until the solution is self-consistent, hence Hartree-Fock falls into a class of methods called *self-consistent field* (SCF) methods. Time-dependent Hartree-Fock can be formulated such that the equations can be solved by standard propagation methods like Runge-Kutta. Basically there are two different types of HF-calculations, restricted and unrestricted. In restricted HF calculations, which can be applied for closed-shell problems (for which the number of electrons, f , is always even), it is supposed that the spatial components of the spinorbitals are identical for each member of a pair of electrons. Then there are $f/2$ spatial orbitals. In unrestricted HF-calculations this constraint is not present.

As mentioned above, the Hartree-Fock method relies on averages. It does not consider the instantaneous electrostatic interactions between electrons and the effect of the $(f - 1)$ -electron cloud on an electron of interest is treated in an average way. These deficiencies are commonly summarized by saying that Hartree-Fock ignores *electron correlation*. If one compares the ground state energy calculated with HF with the exact ground state energy then the difference is called *correlation energy*. In terms of Slater determinants the exact wavefunction can be written as a linear combination of all possible f -electron Slater determinants arising from a complete set of spinorbitals [108]. These other Slater determinants are different from the one representing the ground state. Of course, a complete basis set of spinorbitals is computationally impossible, one always has to use a finite basis set. Nevertheless, to account for correlation an ansatz Ψ_a for solving the Schrödinger equation with several Slater determinants can be made. This ansatz is of the form

$$\Psi_a(\mathbf{q}_1, \dots, \mathbf{q}_f) = \sum_{J=1}^L A_J \Phi_J(\mathbf{q}_{j_1}, \dots, \mathbf{q}_{j_f}), \quad (3.9)$$

where L is the number of Slater determinants, A_J is the weight for the J -th Slater determinant and Φ_J is a Slater determinant of the form equ. (3.7). If the basis

functions of the Slater determinants are fixed one arrives at *configuration interaction* (CI). This method uses sophisticated basis sets and quite high numbers of Slater determinants are usual. Very common are gaussian basis functions [109]. To calculate the wavefunction Ψ_a the expansion coefficients A_J are optimized. Further improved methods also optimize the spinorbitals. Such methods are called *multi-configurational methods* and are common for molecular structure calculations, which are time-independent problems. However, there is currently, to the best of my knowledge, no method available for time-dependent problems capable of taking into account electron correlation¹. Such a method, called Multi-configuration Time-dependent Hartree-Fock (MCTDHF), will be introduced² in the next section.

3.2 Multi-configuration Time-dependent Hartree-Fock (MCTDHF)

As stated in section 3.1, multiconfigurational methods make an ansatz Ψ_a for solving the Schrödinger equation (3.3) similar to the one used in CI calculations, equ. (3.9). The difference to CI is that also the spinorbitals are optimized which decreases the necessary number of Slater determinants to approximate the exact wavefunction considerably. In laser-matter interaction the wavefunction additionally has to be dependent on time and the ansatz takes the form

$$\Psi_a(\mathbf{q}_1, \dots, \mathbf{q}_f; t) = \sum_{J=1}^L A_J(t) \Phi_J(\mathbf{q}_{j_1}, \dots, \mathbf{q}_{j_f}; t), \quad (3.10)$$

where the same notation as in equ. (3.9) was used. Note, that here A_J as well as Φ_J depend on time in contrast to existing methods used in quantum chemistry, where both of them are independent of time. The index J is an abbreviation for the complete multi-index $J = j_1, j_2, \dots, j_f$. With that the L Slater determinants take the form

$$\Phi_{j_1, \dots, j_f}(\mathbf{q}_{j_1}, \dots, \mathbf{q}_{j_f}; t) = \frac{1}{\sqrt{J!}} \sum_{\mathcal{P}} (-1)^{\mathcal{P}} \mathcal{P} \varphi_{j_1}(\mathbf{q}_{j_1}; t) \dots \varphi_{j_f}(\mathbf{q}_{j_f}; t). \quad (3.11)$$

Such an ansatz means that the antisymmetry of the wavefunction, according to the Pauli principle, is accounted for by the Slater determinant. It is possible, though, to construct an antisymmetric wavefunction even for a not antisymmetrized product of the expansion functions taking the simple form

$$\Phi_J = \varphi_{j_1} \dots \varphi_{j_f}. \quad (3.12)$$

¹There do exist, though, approaches applying Time-dependent Density Functional Theory (TDFT). But as already mentioned above, they still do not perform well [59]. Furthermore there exists a time-dependent multiconfigurational method for molecular quantum dynamics [67, 68, 110, 69, 70]. Thus, this method, called Multiconfiguration Time-dependent Hartree (MCTDH) deals with bosons, which do not have an antisymmetric wavefunction.

²The method was developed together with Armin Scrinzi and Jürgen Zanghellini [72].

In this case the weights $A_J(t)$ must be antisymmetric with respect to the exchange of any two indices,

$$A_{j_1, \dots, j_m, \dots, j_n, \dots, j_f} = -A_{j_1, \dots, j_n, \dots, j_m, \dots, j_f}. \quad (3.13)$$

As it turns out such an ansatz is much easier to treat when inserting into the Schrödinger equation than an ansatz where the expansion functions are antisymmetrized. The ansatz-wavefunction equ. (3.10), when writing the multi-sum, inherent to the notation of the multi-index J , explicitly, reads

$$\Psi_a(\mathbf{q}_1, \dots, \mathbf{q}_f; t) = \sum_{j_1=1}^n \cdots \sum_{j_f=1}^n A_{j_1, \dots, j_f}(t) \varphi_{j_1}(\mathbf{q}_1; t) \cdots \varphi_{j_f}(\mathbf{q}_f; t). \quad (3.14)$$

The sums are carried out over all expansion functions n . Note, that $n = f$ for the Hartree-Fock case (no "multi"), which results in only a single Slater determinant. In the above multi-sum equ. (3.14) the Slater determinants add up 'automatically' since the absolute value of the A 's is the same for every fixed combination of the multi-index j_1, \dots, j_f , only the sign changes with respect to the permutation of its values. For example, the multi-index 1, 3, 4, 2 gives the same value for A as 2, 3, 4, 1, but only the sign changes from "+" to "-". Then the value of A can be singled out of the sum. What then remains is exactly a Slater determinant. This procedure leads, for n expansion functions per spinorbital and f electrons (degrees of freedom), naturally, to a number L of Slater determined by $\binom{n}{f}$. This is clear, since this is nothing but the problem to choose f items out of n .

The ansatz Ψ_a , as outlined above, shall fulfill the time dependent Schrödinger equation (TDSE) for f electrons in a molecular potential (Born-Oppenheimer approximation) and in an electric field. In order to derive the determining equations for $A_J(t)$ and for the expansion functions $\varphi_i(\mathbf{q}; t)$ we apply a variational principle. This will lead to nonlinear, first-order differential equations for both $A_J(t)$ and $\varphi_i(\mathbf{q}; t)$, called *the working equations*. Propagating these working equations starting from a certain initial state, e.g. the ground state, yields the wavefunction under the influence of the electric field and thus allows to investigate the dynamics of the multi-electron cloud under laser impact.

We now turn to the derivation of the working equations and restrict ourselves, in order to keep the numerical effort for the time-propagation tractable, to 1 spatial dimension. Considering one dimensional problems is common in the literature [111] and gives reasonable results for systems which have a favoured spatial extension and if one does not want to investigate problems where angular moments are of importance, such as aligning molecules in laser fields or angular resolved photoelectron spectra [112, 113]. Moreover, in linearly polarized fields the favoured spatial extension is given almost naturally by the polarization direction.

In our derivation we will use a Hamiltonian independent of the spin. Thus, the spin of the spinorbitals does not change during propagation and can be considered

as a parameter for each of the spinorbitals, which can be either present ("up") or not present ("down"). Therefore it is possible to only consider the spatial part of the spinorbitals in the derivation of the working equations. The only point, where the spin comes into play is when matrix elements, for example of the form $\langle \varphi_i | \varphi_j \rangle$, are considered.

Another important remark concerns the time dependency of the A 's and the φ 's in our ansatz. Because both of them depend on time our ansatz is not unique. The orbital functions and the expansion coefficients can still be linearly transformed while representing the same wavefunction, which prohibits singularity-free, well defined working equations. Uniquely defined propagation is obtained by imposing constraints on the orbital functions. The constraints are chosen to be [67]

$$\langle \varphi_i(x; 0) | \varphi_j(x; 0) \rangle = \delta_{ij}, \quad (3.15a)$$

$$\langle \varphi_i(x; t) | \dot{\varphi}_j(x; t) \rangle = 0. \quad (3.15b)$$

3.2.1 Derivation of the Working Equations

We start out from the time-dependent Schrödinger equation for f electrons in 1 spatial dimension,

$$i\dot{\Psi}(x_1, \dots, x_f; t) = H(x_1, \dots, x_f; t)\Psi(x_1, \dots, x_f; t), \quad (3.16)$$

with a Hamiltonian in dipole approximation and in velocity gauge of the form

$$H(x_1, \dots, x_f; t) = \sum_{m=1}^f \left[\frac{1}{2} \left(-i\frac{\partial}{\partial x_m} - \frac{1}{c}A_L(t) \right)^2 + U(x_m) + \sum_{n>m}^f V(x_m - x_n) \right]. \quad (3.17)$$

In this Hamiltonian A_L is the vector potential³ of the laserfield, c is the velocity of light and $U(x_m)$ and $V(x_m - x_n)$ are the nuclear potential for the m^{th} -coordinate and the electron-electron potential for coordinates m and n , respectively. The latter one shall be a smoothed Coulomb potential [111]

$$V(x_m - x_n) = \frac{1}{\sqrt{(x_m - x_n)^2 + a^2}}, \quad (3.18)$$

where a is the smoothing parameter. In principle this potential could be of any form but the form given here makes the "most" physical sense. Also the nuclear potential

³To avoid confusions of the vector potential A_L with the weights A_J from the ansatz, the index L for Laser is used. Moreover, if the letter A is used below, always the weights are meant. This is because the vector potential will not be used in the derivation of the working equations.

can be of arbitrary form. Equation (3.16) is solved by the MCTDHF-ansatz, as explained above,

$$\begin{aligned}\Psi(x_1, \dots, x_f; t) &= \\ &= \frac{1}{\sqrt{f!}} \sum_{j_1=1}^n \dots \sum_{j_f=1}^n A_{j_1 \dots j_f}(t) \times \varphi_{j_1}(x_1; t) \varphi_{j_2}(x_2; t) \dots \varphi_{j_f}(x_f; t) \\ &= \frac{1}{\sqrt{f!}} \sum_J A_J \Phi_J.\end{aligned}\quad (3.19)$$

Note that the ansatz equ. (3.19) is complete in the limit $n \rightarrow \infty$. The greater the number n of expansion functions, and thus, the greater the number $\binom{n}{f}$ of Slater determinants, the better can be accounted for electron correlation. Realistic quantum mechanical problems are not so highly correlated, that $n \rightarrow \infty$ is required to describe the problem. Thanks to the variational principle, which will be applied below, the wavefunction equ. (3.19) is optimal in the sense, that it is the best approximation for a given n . Very recently it was shown for 2 laser-driven electrons in a harmonic potential, that already with the very low number of $n = 6$ (15 Slater determinants) the overlap $|\langle \Psi_{15} | \Psi_e \rangle|^2$ between the approximated wavefunction Ψ_{15} and the exact wavefunction Ψ_e is already 99.939 % [71].

The evolution equations for Ψ are obtained by demanding

$$\langle \delta\Psi | i\partial_t - H | \Psi \rangle = \langle \delta\Psi | i\partial_t | \Psi \rangle - \langle \delta\Psi | H | \Psi \rangle = 0. \quad (3.20)$$

Introducing our ansatz equ. (3.19) into equ. (3.20) leads to the expression

$$\begin{aligned}\langle \delta\Psi | H | \Psi \rangle - i \frac{1}{\sqrt{f!}} \langle \delta\Psi | \sum_J \dot{A}_J \Phi_J + \\ \sum_J A_J \sum_{i=1}^f \dot{\varphi}_{j_i}(x_i; t) \varphi_{j_1}(x_1; t) \dots \varphi_{j_{i-1}}(x_{i-1}; t) \varphi_{j_{i+1}}(x_{i+1}; t) \dots \varphi_{j_f}(x_f; t) \rangle = 0\end{aligned}\quad (3.21)$$

We permit only variations $\delta\Psi$ which remain within the general ansatz

$$\delta\Psi = \frac{1}{\sqrt{f!}} \sum_J (A_J + \delta A_J) (\varphi_{j_1} + \delta\varphi_{j_1}) \dots (\varphi_{j_f} + \delta\varphi_{j_f}), \quad (3.22)$$

which consists of small variations around the exact solution of equ. (3.16). Carrying out the multiplications and neglecting terms of $\mathcal{O}(\delta^2)$ we arrive at

$$\delta\Psi = (f+1)\Psi + \frac{1}{\sqrt{f!}} \sum_J \delta A_J \Phi_J + \frac{1}{\sqrt{f!}} \sum_J A_J \sum_{i=1}^f \varphi_{j_1} \dots \delta\varphi_{j_i} \dots \varphi_{j_f} \quad (3.23)$$

For the coefficients A_J and the function Φ_J in the ansatz equ. (3.19) the variational principle reads

$$\delta\Psi = \frac{\delta\Psi}{\delta\tilde{A}_J} \delta\tilde{A}_J + \frac{\delta\Psi}{\delta\varphi_l} \delta\varphi_l, \quad (3.24)$$

where $\tilde{A}_J = \frac{1}{\sqrt{f!}} A_J$.

The below derivation closely follows the description of the multi-configuration time-dependent Hartree method outlined in ref. [67]. There the position within the multi-index is important when carrying out derivations. In our case here we want to include the antisymmetrization due to the Pauli principle. This allows us to rearrange the multi-indices when applying operations like a derivation and to take care of the position the operation was meant to act on only with the sign of the permutation. Therefore we end up with f equal expressions for every operation. Carrying out the variations yields

$$\frac{\delta\Psi}{\delta\tilde{A}_J} = \varphi_{j_1} \cdots \varphi_{j_f} = \Phi_J \quad (3.25)$$

$$\frac{\delta\Psi}{\delta\varphi_l} = \sum_{j_2 \cdots j_f} \tilde{A}_{lj_2 \cdots j_f} \varphi_{j_2} \cdots \varphi_{j_f}. \quad (3.26)$$

Equ. (3.26) is called the *single hole function* and is denoted by $\Psi^{(l)}$, if l is the index of the "hole". Introducing the variational function of equ. (3.24) together with equations (3.25) and (3.26) into equ. (3.21) leads to expressions for the single hole function and the functions Φ_J , which have to be satisfied in order to cause the wavefunction Ψ to be a solution of the Schrödinger equation. These expressions read

$$\langle \Psi^{(k)} | H | \Psi \rangle = i \langle \Psi^{(k)} | \partial_t | \Psi \rangle \quad (3.27a)$$

$$\langle \Phi_J | H | \Psi \rangle = i \langle \Phi_J | \partial_t | \Psi \rangle. \quad (3.27b)$$

Now the derivative of the wavefunction Ψ from the ansatz with respect to time has to be carried out. The right hand side of equ. (3.27b) reads

$$i \langle \Phi_J | \partial_t | \Psi \rangle = i \langle \Phi_J | \dot{\Psi} \rangle = i \dot{\tilde{A}}_J, \quad (3.28)$$

where use of the constraint equ. (3.15a) has been made. The right hand side of equ. (3.27a), after carrying out the time derivative and some rearrangements, can be written as

$$i \langle \Psi^{(k)} | \dot{\Psi} \rangle = i \sum_l \varphi_l \sum_{j_2, \dots, j_f} \tilde{A}_{k, j_2, \dots, j_f}^* \dot{\tilde{A}}_{l, j_2, \dots, j_f} + i \sum_l \dot{\varphi}_l \rho_{kl}, \quad (3.29)$$

with

$$\rho_{kl} = \sum_{j_2}^n \cdots \sum_{j_f}^n \tilde{A}_{k, j_2, \dots, j_f}^* \tilde{A}_{l, j_2, \dots, j_f}. \quad (3.30)$$

If we introduce the relation equ. (3.28) for the derivative of \tilde{A}_J into equ. (3.29) we

obtain

$$\begin{aligned}
i \langle \Psi^{(k)} | \dot{\Psi} \rangle &= i \sum_l |\varphi_l\rangle \sum_{j_2, \dots, j_f} \tilde{A}_{k, j_2, \dots, j_f}^* (-i) \langle \Phi_{l, j_2, \dots, j_f} | H | \Psi \rangle + i \sum_l \dot{\varphi}_l \rho_{kl} \\
&= \sum_{j_2, \dots, j_f} \tilde{A}_{k, j_2, \dots, j_f}^* \sum_l |\varphi_l\rangle \langle \varphi_l \varphi_{j_2} \dots \varphi_{j_f} | H | \Psi \rangle + i \sum_l \dot{\varphi}_l \rho_{kl} \\
&= \mathcal{P} \langle \Psi^{(k)} | H | \Psi \rangle + i \sum_l \dot{\varphi}_l \rho_{kl},
\end{aligned} \tag{3.31}$$

where we have introduced the projector

$$\mathcal{P} = \sum_{l=1}^n |\varphi_l\rangle \langle \varphi_l|. \tag{3.32}$$

Because equ. (3.31) must be equal to the left hand side of equ. (3.27a) we arrive at

$$\langle \Psi^{(k)} | H | \Psi \rangle = \mathcal{P} \langle \Psi^{(k)} | H | \Psi \rangle + i \sum_l \dot{\varphi}_l \rho_{kl}, \tag{3.33}$$

or, equally,

$$i \sum_l \dot{\varphi}_l \rho_{kl} = (1 - \mathcal{P}) \langle \Psi^{(k)} | H | \Psi \rangle. \tag{3.34}$$

The expression $\langle \Psi^{(k)} | H | \Psi \rangle$ can also be written in the following way

$$\langle \Psi^{(k)} | H | \Psi \rangle = \sum_j \langle \Psi^{(k)} | H | \Psi^{(j)} \rangle \varphi_j = \sum_j \langle H \rangle_{kj} \varphi_j, \tag{3.35}$$

where we have introduced the *mean-field operator*

$$\langle H \rangle_{kj} = \langle \Psi^{(k)} | H | \Psi^{(j)} \rangle. \tag{3.36}$$

Now we introduce the mean-field operator into equ. (3.34). This yields the first working equation for the expansion functions $\varphi_{j_1} \dots \varphi_{j_f}$,

$$i \sum_l \rho_{kl} \dot{\varphi}_l = (1 - \mathcal{P}) \sum_j \langle H \rangle_{kj} \varphi_j. \tag{3.37}$$

Replacing the right hand side of equ. (3.27b) with the right hand side of equ. (3.28) yields the second working equation for the weights A_J ,

$$i \dot{\tilde{A}}_J = \langle \Phi_J | H | \Psi \rangle = \sum_L \langle \Phi_J | H | \Phi_L \rangle \tilde{A}_L, \tag{3.38}$$

where the normalization factor $(f!)^{-1/2}$, which manifests itself in the presence of the tilde, cancels out. Equation (3.37) can be written in a much more convenient form with the help of a matrix formalism. If we define the vector

$$\boldsymbol{\varphi} = (\varphi_{j_1}, \dots, \varphi_{j_f})^T \tag{3.39}$$

and the density matrix

$$\boldsymbol{\rho} = \begin{pmatrix} \rho_{11} & \cdots & \rho_{1f} \\ \vdots & \ddots & \vdots \\ \rho_{f1} & \cdots & \rho_{ff} \end{pmatrix}, \quad (3.40)$$

as well as the matrix of the mean field operator

$$\langle \mathbf{H} \rangle = \begin{pmatrix} \langle H \rangle_{11} & \cdots & \langle H \rangle_{1f} \\ \vdots & \ddots & \vdots \\ \langle H \rangle_{f1} & \cdots & \langle H \rangle_{ff} \end{pmatrix}, \quad (3.41)$$

and consider that the operator ρ_{kl} commutes with the projector \mathcal{P} , the working equations can be written in the final form

$$i\dot{A}_J = \sum_L \langle \Phi_J | H | \Phi_L \rangle A_L \quad (3.42a)$$

$$i\dot{\boldsymbol{\varphi}} = (1 - \mathcal{P})\boldsymbol{\rho}^{-1}\langle \mathbf{H} \rangle\boldsymbol{\varphi}. \quad (3.42b)$$

The working equations are, as announced, nonlinearly-coupled and of first order in time. The non-linearity is brought about, since \dot{A}_J depends quadratically on the φ_j and $\dot{\boldsymbol{\varphi}}$ depends quadratically and in the third power on the φ_j and quadratically on the A 's. The equations can be solved by any numerical propagation method, e.g. by a Runge-Kutta method, provided an initial state is given. For the ground state this initial state can be easily found by an imaginary time propagation, starting from reasonable initial values for $\boldsymbol{\varphi}$ and A_J . For excited states different methods have to be used.

3.2.2 Computational Details

The working equations, equ. (3.42a) and equ. (3.42b), determine the time evolution of the system starting from a certain initial state. They turn the actual values of A_L and $\boldsymbol{\varphi}$ into their derivatives. This is done by the operators $\sum_L \langle \Phi_J | H | \Phi_L \rangle$ and $(1 - \mathcal{P})\boldsymbol{\rho}^{-1}\langle \mathbf{H} \rangle$. These operators contain a lot of multi-sums which have to be implemented efficiently in order to make computation of the time-evolution of systems with up to 10 electrons possible. It is indispensable to use all of the operators properties to ones advantage and not to calculate unnecessary sums. In the following we want to review some of the most important points of the computation of the working equations.

The Matrix Elements

We split the Hamiltonian equ. (3.17) into single particle and two-particle parts

$$H = H_1 + H_2, \quad (3.43)$$

with

$$H_1 = \sum_{m=1}^f H(x_m; t) = \sum_{m=1}^f \left[\frac{1}{2} \left(-i \frac{\partial}{\partial x_m} - \frac{1}{c} A_L(t) \right)^2 + U(x_m) \right] \quad (3.44)$$

and

$$H_2 = \sum_{m=1}^f \sum_{m < k} V(x_m - x_k). \quad (3.45)$$

Further on we define

$$H_{mk} := \langle \varphi_m | H_1 | \varphi_k \rangle. \quad (3.46)$$

With that the one-electron part of the operator $\sum_L \langle \Phi_J | H | \Phi_L \rangle$ from the first working equation (3.42a) can be written as

$$\begin{aligned} \sum_L \langle \Phi_J | H_1 | \Phi_L \rangle A_L = \\ \sum_{l=1}^n [H_{j_1 l} A_{l j_2 \dots j_f} + H_{j_2 l} A_{j_1 l j_3 \dots j_f} + \dots + H_{j_f l} A_{j_1 \dots j_{f-1} l}]. \end{aligned} \quad (3.47)$$

The two-electron part, when treated in the same manner, yields

$$\begin{aligned} \sum_L \langle \Phi_J | H_2 | \Phi_L \rangle A_L = \\ = \sum_m \sum_{m < k} \sum_{l_1=1}^n \dots \sum_{l_f=1}^n \langle \varphi_{j_1} \dots \varphi_{j_f} | V(x_m - x_k) | \varphi_{l_1} \dots \varphi_{l_f} \rangle A_{l_1, \dots, l_f} \\ = \sum_{k=1}^n \sum_{l=1}^n \\ [\langle \varphi_{j_1} \varphi_{j_2} | V | \varphi_k \varphi_l \rangle A_{k l j_3 \dots j_f} + \langle \varphi_{j_1} \varphi_{j_3} | V | \varphi_k \varphi_l \rangle A_{k j_2 l \dots j_f} \dots \\ + \langle \varphi_{j_1} \varphi_{j_f} | V | \varphi_k \varphi_l \rangle A_{k j_2 \dots l} \\ + \langle \varphi_{j_2} \varphi_{j_3} | V | \varphi_k \varphi_l \rangle A_{j_1 k l \dots j_f} \dots + \langle \varphi_{j_2} \varphi_{j_f} | V | \varphi_k \varphi_l \rangle A_{j_1 k \dots l} \\ \vdots \\ + \langle \varphi_{j_{f-1}} \varphi_{j_f} | V | \varphi_k \varphi_l \rangle A_{j_1 \dots k l}]. \end{aligned} \quad (3.48)$$

For the operator $(1 - \mathcal{P})\boldsymbol{\rho}^{-1}\langle \mathbf{H} \rangle$ from the second working equation (3.42b) we only need to treat the mean-field operator $\langle H \rangle_{jl}$ because computing the matrix $\boldsymbol{\rho}$ is trivial via equ. (3.30). However, inversion of this matrix is crucial for the initial state.

The mean-field operator $\langle H \rangle_{jl} = \langle \Psi^{(j)} | H | \Psi^{(l)} \rangle = \langle \Psi^{(j)} | H_1 + H_2 | \Psi^{(l)} \rangle$ can be split into two parts $\langle H_1 \rangle_{jl} + \langle H_2 \rangle_{jl}$. The first part can be expressed as

$$\langle H_1 \rangle_{jl} = \sum_{j_2}^n \dots \sum_{j_f}^n \sum_{l_2}^n \dots \sum_{l_f}^n A_{j j_2 \dots j_f}^* A_{l l_2 \dots l_f} \langle \varphi_{j_1} \dots \varphi_{j_f} | H_1 | \varphi_{l_1} \dots \varphi_{l_f} \rangle. \quad (3.49)$$

The sum over terms of H_1 must now be split distinguishing two cases depending on the electron coordinate. For the first coordinate, x_1 , the sum can be written as

$$\langle H_1 \rangle_{jl}(x_1) = \sum_{j_2}^n \cdots \sum_{j_f}^n A_{jj_2 \dots j_f}^* A_{lj_2 \dots j_f} H(x_1) = \rho_{jl} H(x_1), \quad (3.50)$$

and for the other coordinates, $x_m, m > 1$, the sum yields

$$\begin{aligned} \langle H_1 \rangle_{jl}(x_m) = & \quad (3.51) \\ & \sum_{m=2}^f \sum_{j_2}^n \cdots \sum_{j_f}^n \sum_{l_2}^n \cdots \sum_{l_f}^n A_{jj_2 \dots j_f}^* A_{ll_2 \dots l_f} \langle \varphi_{j_1} \cdots \varphi_{j_f} | H(x_m) | \varphi_{l_1} \cdots \varphi_{l_f} \rangle. \end{aligned}$$

If we now renumber the j_2, \dots, j_f and (simultaneously) the l_2, \dots, l_f such that $m = 2$ in all sums in this expression we arrive at

$$\langle H_1 \rangle_{jl}(x_2) = (f-1) \times \sum_{l_2}^N \sum_{j_2}^N \cdots \sum_{j_f}^N A_{jj_2 j_3 \dots j_f}^* A_{ll_2 j_3 \dots l_f} \langle \varphi_{j_2} | H(x_2) | \varphi_{l_2} \rangle. \quad (3.52)$$

For the two-electron part of the mean-field operator, $\langle H_2 \rangle_{jl} = \langle \Psi^{(j)} | H_2 | \Psi^{(l)} \rangle$, the full sum,

$$\begin{aligned} \langle H_2 \rangle_{jl} = & \quad (3.53) \\ & \sum_{j_2}^n \cdots \sum_{j_f}^n \sum_{l_2}^n \cdots \sum_{l_f}^n \\ & A_{jj_2 \dots j_f}^* A_{ll_2 \dots l_f} \langle \varphi_{j_1} \cdots \varphi_{j_f} | \sum_{m < k} V(x_m - x_k) | \varphi_{l_1} \cdots \varphi_{l_f} \rangle, \end{aligned}$$

must again be calculated differently for two separate cases. The first case is $m = 1, k > 1$. There the sums are the same for all k and carrying out the summation over k gives $(f-1)$ equal terms. If we renumber the indices j_2, \dots, j_f and l_2, \dots, l_f in each multi-sum for fixed $m = 1$ such that $k = 2$, we arrive at

$$\begin{aligned} \langle H_2 \rangle_{jl}(x_1) = & \quad (3.54) \\ & (f-1) \times \\ & \sum_{l_2=1}^n \sum_{j_2=1}^n \cdots \sum_{j_f}^n A_{jj_2 j_3 \dots j_f}^* A_{ll_2 j_3 \dots j_f} \langle \varphi_{j_2} | V(x_1 - x_2) | \varphi_{l_2} \rangle. \end{aligned}$$

The second case concerns $m > 1, k > 2$. Here the sums are the same for all m, k . There are $(f-1)(f-2)/2$ terms in the sum over k . Renumbering the indices j_1, \dots, j_f and l_1, \dots, l_f in each multi-sum for fixed m, k such that $m = 2, k = 3$ leads to

$$\begin{aligned} \langle H_2 \rangle_{jl}(x_2, x_3) = & \quad (3.55) \\ & \frac{(f-1)(f-2)}{2} \times \\ & \sum_{l_2=1}^n \sum_{l_3=1}^n \sum_{j_2=1}^n \cdots \sum_{j_f}^n A_{jj_2 j_3 \dots j_f}^* A_{ll_2 j_3 \dots j_f} \langle \varphi_{j_2} \varphi_{j_3} | V(x_2 - x_3) | \varphi_{l_2} \varphi_{l_3} \rangle. \end{aligned}$$

Summing up equations (3.47) and (3.48) yields the operator for the first working equation, which provides the time-derivative of the expansion weights A_J . The main part of the second working equation, the mean-field operator $\langle \mathbf{H} \rangle$, is obtained by summing up equations (3.50) with (3.52) and equations (3.54) with (3.55).

The MCTDHF Package

The computation of the second working equation (3.42b) is a lot simplified by the fact that some parts of the mean field operator $\langle H \rangle_{jl}$ do not need to be calculated. This concerns the parts

$$\langle H_1 \rangle_{jl}(x_2) \propto \langle \varphi_{j_2} | H(x_2) | \varphi_{l_2} \rangle$$

and

$$\langle H_2 \rangle_{jl}(x_2, x_3) \propto \langle \varphi_{j_2} \varphi_{j_3} | V(x_2 - x_3) | \varphi_{l_2} \varphi_{l_3} \rangle,$$

which are nothing but imaginary figures rather than functions and can therefore be considered as part of a linear transformation, which can be written in the form of a matrix, denoted by \mathbf{M} in the following. With that the second working equation for the i -th expansion function reads

$$i\dot{\varphi}_i(x; t) = (1 - \mathcal{P}) \sum_j (M_{ij} + \mathcal{R}_{ij}(x; t)) \varphi_j(x; t), \quad (3.56)$$

where the operator $\mathcal{R}_{ij}(x)$ contains all the remaining parts of the working equation which are not part of the matrix \mathbf{M} . Taking into account that the matrix \mathbf{M} commutes with the projector, the working equation can be written as

$$i\dot{\varphi}_i(x; t) = \sum_j M_{ij} \left(1 - \sum_{l=1}^n |\varphi_l\rangle \langle \varphi_l| \varphi_j \right) + (1 - \mathcal{P}) \sum_j \mathcal{R}_{ij}(x; t) \varphi_j(x; t). \quad (3.57)$$

The expression in the bracket of the first term on the right hand side yields zero and does therefore not contribute to the derivative of the spinorbital on the left hand side. Taking into account this result, the working equations (3.42a) and (3.42b) were programmed using the multi-sums of the previous subsection. The whole MCTDHF program package consists of several routines to compute, handle, display and transform time-propagated wavefunctions, as well as of routines for extracting important information out of the wavefunction, altogether some 28000 lines of code. At the moment the program is capable of handling up to roughly 6 electrons. This limitation mainly arises from the fact, that the program is not parallelized yet. It is believed that the number of possible electrons will be increased to about 10-15 in a parallelized version, which is being worked on at the moment. Furthermore there will be a 3D-version available in the future.

The Electron-Electron Potential

Except for questions of the expansion size, the most crucial problem in any multi-electron calculation is an efficient description of the electron-electron interaction. In general, for each update of the working equations, the “direct” and “exchange” potentials, which in the present case take the form

$$V_{jl}(x) = \sum_{l_2=1}^n \sum_{j_2=1}^n \sum_{j_3=1}^n \cdots \sum_{j_f=1}^n A_{jj_2j_3\dots j_f}^* A_{ll_2j_3\dots j_f} \langle \varphi_{j_2}(y) | V(x-y) | \varphi_{l_2}(y) \rangle, \quad (3.58)$$

must be computed. As we have seen in the previous subsection the matrix elements of the form

$$\langle \varphi_{j_2} \varphi_{j_3} | V(x-y) | \varphi_{l_2} \varphi_{l_3} \rangle \quad (3.59)$$

do not need to be considered. On the other hand, even when the calculations of the needed matrix elements $\langle \varphi_j(y) | V(x-y) | \varphi_l(y) \rangle$ are performed with high efficiency, the rapidly growing number of integrations in the sum of equ. (3.58) limits the number of expansion functions, n , to smaller than ~ 20 . The evaluation of equ. (3.58) can be greatly accelerated by approximating the potential as

$$V(x-y) \approx V_{\text{app}}(x,y) = \sum_{m=1}^M v_m W_m(x) W_m(y) \quad (3.60)$$

where M is a number much smaller than the number of discretization points for the expansion functions $\varphi(x)$. When V is understood as a (real, symmetric) matrix with indices x and y , then W_m are the eigenvectors of V corresponding to the M most important eigenvalues v_m . This procedure is called *Schmidt approximation* [114]. By giving certain regions of space, e.g. small $|x|$, more weight one can control for which values of x and y the $V_{\text{app}}(x,y)$ is most accurate. This procedure generalizes the multipole expansion that is usually employed to approximate the integrals when one coordinate is small to the case when both, $|x|$ and $|y|$, can be comparable in size.

With only 50 functions $W_m(x)$ on a 1000×1000 grid one obtains relative accuracies of $< 1\%$ in a cross-shaped region that well exceeds the size of the region important for electron correlation. The approximation fails in the far region for double-ionization, where $|x|$ and $|y|$ are large at the same time. This means that post-ionization electron momentum distributions for (non-sequential) double ionization are incorrect, but, e.g., total double-ionization can still be reproduced correctly.

3.2.3 The Single-Electron Case

Because we will (mis)use the above presented method in the next chapter to calculate the dynamics of a single electron in a potential well, we will give here the formulation of the working equations (3.42a) and (3.42b) for 1 electron. In this case the usage

of only one expansion function $\varphi(x)$ and one weight A gives a complete basis set ($n = f = 1$). Therefore the full wavefunction is $\Psi(x; t) = A(t) \varphi(x; t)$ and the working equations read

$$i\dot{A} = \langle \varphi | H | \varphi \rangle A \quad (3.61a)$$

$$i\dot{\varphi} = (1 - \mathcal{P})\rho^{-1}\langle H \rangle \varphi. \quad (3.61b)$$

The projector simply is $\mathcal{P} = |\varphi\rangle\langle\varphi|$, the density matrix $\rho = A^*A$, and the mean-field operator $\langle H \rangle = \langle A | H | A \rangle = A^*AH$. Therefore the working equations "implode" to

$$i\dot{A} = \langle \varphi | H | \varphi \rangle A \quad (3.62a)$$

$$i\dot{\varphi} = H\varphi - \varphi \langle \varphi | H | \varphi \rangle. \quad (3.62b)$$

In these equations the part $i\dot{\varphi} = H\varphi$ is nothing but the Schrödinger equation for the function $\varphi(x; t)$. The additional existence of the first equation reflects the fact that there are two time-dependent functions in the ansatz, $A(t)$ and $\varphi(x; t)$. If we apply a simple phase transformation of the form

$$\varphi = \exp\left(i \int_{-\infty}^t B(t') dt'\right) \chi(x; t),$$

with an arbitrary, time-dependent function $B(t)$ and insert this ansatz into the second working equation (3.62b) we end up with a Schrödinger equation for χ ,

$$i\dot{\chi}(x; t) = H\chi(x; t), \quad (3.63)$$

provided the function $B(t)$ satisfies the relation $B(t) = \langle \varphi | H | \varphi \rangle$. The two working equations (3.62a) and (3.62b) are coupled exactly by this term. Formally inserting equ. (3.62a) into equ. (3.62b) leads to the expression

$$i\dot{\varphi} = H\varphi - i\frac{\dot{A}}{A}\varphi = \left(H - i\frac{\dot{A}}{A}\right)\varphi.$$

This equation can again be transformed into the Schrödinger equation by a phase transformation of the same form as above, if the function $B'(t)$ in the exponent of the transformation satisfies the relation $B'(t) = i\frac{\dot{A}}{A}$. The first working equation (3.62a) provides the link between $B(t)$ and $B'(t)$: $B'(t) = B(t)$. This result means, that the phase of the function $\varphi(x; t)$ is time-dependent and the phase is determined by an additional equation. Descriptively one could say that due to the over-complete ansatz $\Psi(x; t) = A(t) \varphi(x; t)$ the wavefunction's phase is generated by one equation (e.g. by the one for $A(t)$) and destroyed by the other equation. Anyway, this additional phase does not influence the probability density $|\Psi(x; t)|^2 = |A(t)|^2 |\varphi(x; t)|^2$, which can be seen by solving the first working equation,

$$A(t) = \exp\left(-i \int_{-\infty}^t \langle \varphi(x; t') | H | \varphi(x; t') \rangle dt'\right).$$

This means that merely the phase of $A(t)$ depends on time, the absolute value stays constant. The probability density function $|\Psi(x; t)|^2$ can then be expressed as

$$|\Psi(x; t)|^2 = |\chi(x; t)|^2, \quad (3.64)$$

and is determined by the Schrödinger equation (3.63).

Chapter 4

Elimination of Tunneling and Classical Ionization

Almost all of the highly interesting phenomena in laser-atom interaction, such as high harmonic generation (HHG) [73, 8], non-sequential ionization [5, 6, 7], multiple ionization [4], above barrier ionization (ABI) [45] and even above threshold ionization (ATI) [40] take place in the parameter regime, where the Keldysh parameter yields values smaller than unity. This is the regime of strong field ionization or tunneling ionization, see section 1.1 on page 2. Tunneling is well understood for atoms, also in terms of theoretical descriptions [2, 48, 37, 46, 47, 52]. However, understanding how more complex systems, such as molecules, ionize in the tunneling regime, remains a challenge. Currently an increasing number of experimental work is dedicated to the investigation of ionization in multi-electron systems of different size, like (organic) molecules [23, 25, 24, 22] and clusters of metal atoms [53] or clusters of novel gas atoms [54]. Unfortunately theoretical descriptions of effects observed in these experiments are very few at the moment [26, 25, 107, 115, 116]. Most of the theoretical work is dedicated to the description of non-adiabatic effects which involve population of excited states. Currently, there does not exist a theory for the description of strong field ionization for spatially extended systems. Additionally, if the system size increases, as it is the case in bulks of metals or semiconductors or also in structures in semiconductors like quantum dots [117], there are still unresolved issues when it comes to the question, whether ionization happens through a multi-photon process or via tunneling [87, 88, 89].

The MCTDHF-method developed in chapter 3 enables one to study multi-electron dynamics in arbitrary systems. In this chapter we will systematically investigate how the system size and various laser parameters, like pulse intensity or pulse duration, influence ionization and give an explanation how "large" systems ionized. We will describe a new effect, thus far, to the best of my knowledge, not observed experimentally and as well not described theoretically, therefore, not reported in the literature yet. This effect is a completely new kind of ionization, different from

both tunnel- and multiphoton-ionization. A simple picture will emerge, which distinguishes between the parameter regime, where the laser photon energy is smaller than some characteristic frequency¹ of the system and the one, where it is bigger. The latter one is normally not observed in nature since almost all of the commonly considered systems (atoms and molecules) have characteristic frequencies which are larger than the photon energy of lasers in the infrared. But as the system size increases, the characteristic frequency decreases and for sizes in excess some critical length the photon energy is larger than the characteristic frequency. I will refer to this parameter regime as the *overresonant regime*.

As is known, in classical systems of second order the output signal experiences a phase shift of π with respect to the input, when the system is excited with a harmonic oscillation with a frequency higher than the resonance frequency of the system. Our calculations show that completely the analog happens in quantum systems: In the overresonant regime the wavefunction does not follow the field-tilted nuclear potential but propagates in the counterdirection, carrying a phase shift of π to a wavepacket driven by the same laser pulse in an *underresonant system*². As a consequence of this "odd" dynamics the wavepacket is pulled away from the lowered potential barrier and tunneling is suppressed completely. Moreover, we show that in a certain parameter range this overresonant dynamics leads to the suppression of quantum mechanical effects and the electron dynamics can be described by classical mechanics. In this regime ionization occurs through a classical dephasing mechanism. We called this effect *Tunneling Suppression*.

4.1 One Electron in an Overresonant Well Potential

I start by discussing the behaviour of one electron in a smoothed well potential. This simple problem captures a lot of the physics to be discussed later on when we return to the multi-electron behaviour in overresonant potentials. The well potential shall be of the form

$$U(x) = -D \exp(-(2x/L)^b), \quad (4.1)$$

with depth D , length L and the power b of the exponent which determines the steepness of the well's potential barriers. In order to achieve "nice", smoothed well potentials we set $b = 10$ for the rest of the chapter. The model potential does not have a molecular long range behaviour of the form $-f/|x|$, but it is an excellent model for artificially manufactured potentials in semiconductors like quantum dots [117] and it might also be a suitable description of potential discontinuities like vacuum barriers in metals and semiconductors without doping structures. Furthermore, as it will turn out, it is also a valid model for very large molecules with small electron density, like highly charged ions of molecules, because the dynamics there

¹The term 'characteristic frequency' will be specified below.

²We stipulate to use this term for a configuration, where the photon frequency is smaller than the characteristic frequency of the system, thus, being 'underresonant'.

is not governed by the form of the barrier but mainly by its size and density of electrons. Note, additionally, that using smoothed well potentials for investigating molecular dynamics is common in the literature [25, 107].

4.1.1 Ionization Probability over Well Length

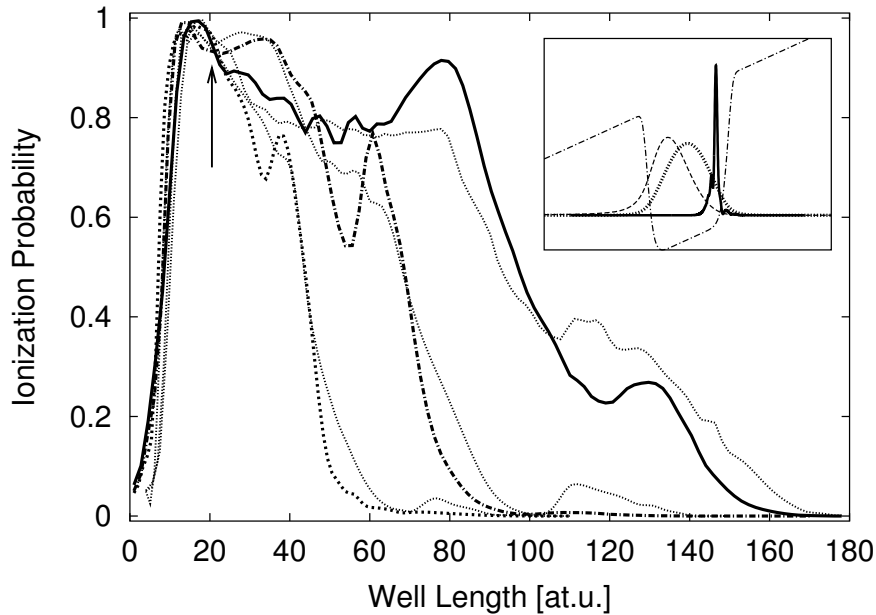


Figure 4.1: Quantum mechanical ionization probability over potential length length of one electron in a smoothed well potential under laser impact for 3 different wavelengths: 600 nm (dotted line), 800 nm (dotted dashed line) and 1200 nm (full line). The thin lines nearest to each of the three thicker lines depict the ionization probability calculated by classical mechanics. The arrow marks the length where the 1200 nm photons are resonant. For parameters of the laser, the form of the potential or the calculation method for the classical results see the text. The inset shows the wavefunction for two different well lengths. As a reference the ground state is also included (dotted line). The full line corresponds to a well of $L = 112$, the dashed line to a well of $L = 3$. The wavefunctions were normalized to unity in width and both (dashed and full) are taken at the same field strength corresponding to the tilt of the potential (dotted dashed line). For the $L = 112$ (overresonant) case the wavefunction is pulled away from the lowered potential barrier (to the right in the inset), in the $L = 3$ (underresonant) case it is pushed to the barrier (to the left).

Fig. 4.1 shows the ionization probability of one electron as a function of the well length L . The depth D of the potential, see equ. (4.1), was adjusted for each L such that the ionization potential was $I_P = 0.44$. The thick lines (full, dashed, dotted) in fig. 4.1 are solutions of the Schrödinger equation (3.16) together with the expression

for the Hamiltonian equ. (3.17) in the velocity gauge, that is

$$i\partial_t \Psi_v(x_1, \dots, x_f; t) = \sum_{m=1}^f \left[\frac{1}{2} \left(-i \frac{\partial}{\partial x_m} - \frac{1}{c} A_L(t) \right)^2 + U(x_m) + \sum_{n>m}^f V(x_m - x_n) \right] \Psi_v(x_1, \dots, x_f; t), \quad (4.2)$$

for $f = 1$:

$$i\partial_t \Psi_v(x; t) = \left[\frac{1}{2} \left(-i \frac{\partial}{\partial x} - \frac{1}{c} A_L(t) \right)^2 + U(x) \right] \Psi_v(x; t). \quad (4.3)$$

This equation is easier to write in the length gauge,

$$i\partial_t \Psi_l(x; t) = \left(-\frac{1}{2} \frac{\partial^2}{\partial x^2} - x \cdot E_L(t) + U(x) \right) \Psi_l(x; t), \quad (4.4)$$

but for numerical reasons the velocity gauge was actually used. However, a solution of the Schrödinger equation (4.3) in the velocity gauge, Ψ_v , can be transformed into a solution Ψ_l of the Schrödinger equation in the length gauge, equ. (4.4), by a phase transformation

$$\Psi_l(x; t) = \Psi_v(x; t) \exp \left(-i \frac{1}{c} A_L(t) x \right) \quad (4.5)$$

together with the relation

$$E_L(t) = -\frac{1}{c} \frac{d}{dt} A_L(t) \quad (4.6)$$

between the laser electric field and the laser vector potential. In the above equations c denotes the speed of light. Equ. (4.5) means that the probability density function is the same for the length gauge and the velocity gauge, $|\Psi_l|^2 = |\Psi_v|^2$, only the phases of the wavefunctions differ. The two gauges are therefore interchangeable with respect to the probability density function.

The ionization probability W is calculated by projection of the wavefunction on the bound states and subtracting the result from 1:

$$W(t) = 1 - \sum_{n=1}^k |\langle \Phi_n(x) | \Psi(x; t) \rangle|^2. \quad (4.7)$$

Φ_n in equ. (4.7) denotes the n -th bound state, k is the total number of bound states and the normalization condition $\langle \Psi(x; -\infty) | \Psi(x; -\infty) \rangle = 1$ justifies the subtraction from 1. In order to calculate the total ionization probability after the laser pulse, $W(t \rightarrow +\infty)$, must be taken. In the following this value, $W(t \rightarrow +\infty) = W_\infty$, is referred to simply as the *ionization probability*.

The three curves in fig. 4.1 correspond to 3 different wavelengths 600 nm, 800 nm and 1200 nm (photon energies of 0.076/0.057/0.038), respectively. The laser vector potential, $A_L(t)$, was of the form

$$A_L(t) = -\frac{\hat{E}_L}{\omega_L} h(t) \sin(\omega_L t + \varphi), \quad (4.8)$$

where ω_L is the laser frequency, $h(t)$ (maximum value 1) is the pulse envelope, \hat{E}_L the maximum field strength and φ the carrier-envelope phase, which was set to 0 in all calculations. The electric field is derived from the vector potential by the relation equ. (4.6). The nuclear potential, $U(x)$, was of the form equ. (4.1). The laser peak intensity was $3 \cdot 10^{14}$ W/cm² for all data points, the pulse envelope $h(t)$ was gaussian and the pulse duration was slightly greater than one cycle per FWHM, that is 2.3/3/4.2 fs for 600/800/1200 nm. The reason for these (unnaturally) short laser pulses is only a desired short computing time. We repeated our calculations with 10 fs and 20 fs for parts of the curves in fig. 4.1 and all of the explanations and conclusions given below stay equally valid. This is due to the fact that it is rather the electric field than the pulse duration, which is responsible for the process to be investigated here, which we will see later on. The actual values of the ionization probability do increase, though, when increasing pulse duration and/or intensity for a certain well length L , but this is merely caused by the greater number of laser cycles for longer pulses or by the bigger excursion amplitude for higher intensities. But for now we return to the interpretation of fig. 4.1. When increasing L from $L = 0$ to $L = 180$ all 3 curves in this figure reveal a rise of the ionization probability up to the saturation value 1 at approximately $L = 17$ then a more or less pronounced plateau and a plunge to 0 at different L 's depending on the wavelength. The energy levels of the potential are further apart than the photon energies for small potential lengths, become resonant around $L = 17 - 20$, where the ionization saturates, and are closer for all $L > 21$. The drop in the ionization probability scales roughly with the electron excursion amplitude $2E_L/\omega_L^2$ of a classical particle in an oscillating electric field which is 32.1/57.1/128.4 for 600/800/1200 nm at the given intensity. These data may suggest a classically governed behaviour of the electron dynamics in potentials for which the energy levels are more closely spaced than the photon energy. If we increase the length L more and more, the levels get closer and closer. For the infinitely long well the energy levels would be infinitely small spaced like for a free electron in the continuum. There, classical mechanics is known to be a suitable description. Furthermore, a classical mechanism would also explain the drop of the ionization probability for lengths much greater than the classical excursion amplitude since the electron just oscillates in the field and never touches the potential barrier. Thus, the electron has no chance to absorb energy from the field which is not possible for a free electron. Energy can be absorbed only when the electron is dephased from its free oscillations. This might be the case for potential lengths smaller than the electron excursion amplitude. Fig. 4.1 shows that there is significant ionization probability in this region.

4.1.2 Ionization through Classical Mechanics

In order to test our hypothesis of the classically governed electron dynamics we compare our quantum calculations with solutions of Newton's equation,

$$\ddot{x}(t) = E(t) - \frac{d}{dt}U(x), \quad (4.9)$$

for a number of trajectories.

Classical Initial Conditions

The crucial point when comparing quantum calculations with classical mechanics are the initial conditions for the starting point x_0 and initial velocity v_0 of each trajectory. There are several methods to determine them. One is to place the trajectories equally apart and weigh each trajectory according to the full quantum mechanical ground state which we know from the solution of equ. (4.4) without the laser field. The ionization probability is then given as the sum of all probabilities represented by those trajectories which have positive energy after propagation in the laserfield. The easiest way to determine the initial velocity for a trajectory placed at x_0 is

$$v_0(x_0) = \pm \sqrt{2(E_g - U(x_0))}.$$

Here, E_g is the quantum mechanical ground state energy. The sign gives the direction into which the velocity points. Note, that the velocity becomes imaginary at the points where $E_g - U(x_0) < 0$. These regions are classically forbidden. Due to the \pm in the relation for $v_0(x_0)$ the number of trajectories is doubled taking both the $+v_0(x_0)$ and $-v_0(x_0)$ trajectory with the same probability, $|\Psi(x_0; -\infty)|^2$, tacitly assuming an equal distribution for both directions. The total probability of all trajectories must be normalized to 1 before time propagation.

Already this simple model for the initial conditions gives reasonable agreement with the quantum mechanical results. But occasionally the classical results under- or overestimate the quantum curve, which leads to a function with some spread values around the quantum mechanical result. Only the tendency of the classical ionization probability over L resembles the quantum mechanical result. Therefore, there is still motivation to improve the calculation of initial conditions. The correct way to get classical initial conditions from quantum mechanical wavefunctions is to use a Husimi distribution [118, 119]

$$q_{H,\lambda}(v_0, x_0) = \frac{1}{\pi} \int dv \int dx q_W(v, x) \exp \left[-(\lambda(x - x_0)^2 + \frac{(v - v_0)^2}{\lambda}) \right], \quad (4.10)$$

where $q_W(v, x)$ is the Wigner function

$$q_W(v, x) = \int d\eta \langle x - \eta/2 | \Psi \rangle \langle \Psi | x + \eta/2 \rangle e^{i v \eta} \quad (4.11)$$

with $|\Psi\rangle$ the (ground) state the initial conditions should be derived from. Unfortunately the Husimi distribution contains a parameter λ which makes the initial

conditions not unique. This parameter determines the form of the Husimi distribution in the (v, x) space, more clearly the ratio of the width in x - and v -direction, respectively. We used this λ as a fitting parameter to our quantum results and found best agreement for a relatively small value of $\lambda = 0.02$ (see fig. 4.1, calculated for 250 trajectories in x -direction and 57 trajectories in v -direction, leading to 14250 trajectories). This value of λ corresponds to a narrow distribution in the velocity. The agreement between the classical results and the full quantum mechanical curves in fig. 4.1 is excellent revealing that quantum interference and quantum mechanical wave packet spreading, which are not included in the classical treatment, are not of importance for the electron dynamics in systems where the photon energy is bigger than the level spacing. But as can be seen in fig. 4.1 the classical treatment gives also good agreement for $4 < L < 20$, where the levels are further apart than the photon energy, meaning that the electron can gain energy in a non-adiabatic manner through its motion in the field also in (short) molecular potentials. This behaviour was not further investigated since the focus of the present work lies on the overresonant case $L > 21$. But there are already hints about this mechanism in refs. [25, 26, 107].

Classical Ionization Mechanism

In the classical description an electron can only pick up energy through its motion in the well when it is dephased from the laser field by hitting the potential barrier. This energy, $W(t)$, is given by

$$W(t) = - \int_{-\infty}^t \frac{dx(t')}{dt'} E_L(t') dt'. \quad (4.12)$$

As long as $E_L(t)$ and $v(t) = dx(t)/dt$ are out of phase by $\pi/2$, as it is the case for the free electron, no energy can be gained. This behaviour, that no “real” power is accumulated although an electron moves in a field is the equivalent to *reactive power* in electrical engineering. But since there is significant ionization and therefore energy consumption visible in fig. 4.1, dephasing must occur.

This is just another hint that electron wave packet dynamics is not negligible even for small potentials like molecular potentials, as has been proven in the previous section. For $L < 20$ (underresonant case) the electron moves according to the laser tilted nuclear potential; to the right, when the laser electric field is positive and vice versa. As we will see, this is not the case for the overresonant case. Equ. (4.12), which is the basis of our classical data in fig. 4.1, only accounts for the classical dephasing mechanism. Tunneling ionization is not included in equ. (4.12) and, hence, also not in fig. 4.1. Therefore, the classical curves in this picture underestimate the quantum mechanical results. For very narrow potentials ($L < 4$) tunneling is the primary method of ionization and the results can be reproduced by the ADK-theory [37, 48] very nicely. Note, however, that ADK gives wrong results when L is increased. At the same time the classical treatment reproduces the quantum result better and better.

Further Remarks on Classical Ionization

The unsatisfying fact that the Husimi distribution contains a parameter, which has to be adjusted to reproduce the quantum results with classical mechanics, can be avoided by directly transforming the quantum ground state $\Psi(x) = \langle x|\Psi\rangle$ into Fourier space, $\tilde{\Psi}(v) = \langle v|\Psi\rangle$. Then the distribution $P(x, v) = |\tilde{\Psi}(v)|^2 |\Psi(x)|^2$ can be taken as the probability of a trajectory with velocity v placed at space coordinate x . Descretizing the probability function P in x - as well as in v -space and propagating all those trajectories leads numerically to the same results in fig. 4.1 as with the Husimi distribution for $\lambda = 0.02$. However, this method to determine the initial conditions cannot be derived from quantum mechanics as thoroughly as the Husimi distribution but avoids the fitting parameter.

Not only did we compare the quantum mechanical and classical ionization probability as a function of the system's length but also as a function of the pulse duration and the pulse intensity. We calculated the ionization probability for two different system lengths (50 and 70) and increased the pulse duration from 3 fs to 20 fs (800 nm, $3 \times 10^{14} \text{W/cm}^2$) leading to increasing ionization probability with the pulse duration. For the dependence of the ionization on the laser intensity systems with lengths 50, 70 and 120 were exposed to 800 nm-pulses with durations 3 fs, 10 fs and 20 fs with increasing intensity from $3 \times 10^{12} \text{W/cm}^2$ to $8 \times 10^{16} \text{W/cm}^2$. In every case a similar agreement between the quantum and the classical results as the one shown in fig. 4.1 could be obtained by either the Husimi based initial conditions or the Fourier-method. It is worth mentioning that the ionization probability does neither increase steadily with the pulse duration nor with the pulse intensity. For certain duration- or intensity-ranges the ionization probability goes rather down than up for increasing duration or intensity. Generally this would be a hint of a destructive quantum interference mechanism. Nevertheless, the quantum results could be reproduced (within the mentioned accuracy) with classical mechanics. This shows that it cannot be an interference mechanism since wave packet interference is not included in the classical analysis. Therefore, this effect must be of pure classical nature and must be caused by the electron's dynamics.

Tunneling Suppression through Counterdirective Electron Dynamics

The possibility to describe quantum effects classically suggests that the quantum effects usually governing ionization (Tunneling, Multiphoton absorption, Above Barrier Ionization) must be suppressed. For the parameters of fig. 4.1 the Keldysh parameter yields $\gamma = 0.770/0.578/0.385$ for a wavelength of 600/800/1200 nm. This places us into the dominant tunneling regime, which means that multiphoton ionization is negligible in our quantum calculations. Then, there must be an effect which suppresses tunneling in large systems. Otherwise the quantum results could not be described by classical mechanics. In fact, when looking at the electron wavefunction in our simulations, in the overresonant regime the electron's probability density

function $|\Psi(x;t)|^2$ moves exactly in counterdirection to the laser tilted potential; to the left when the potential is tilted to the right and vice versa. This motion pulls the wavefunction's tail out of the lowered potential barrier and thus suppresses tunneling, see inset of fig. 4.1 for an illustration of this effect. Hence, we called this effect *tunneling suppression*. This dynamically induced effect is not a consequence of the parameters used here but one of general validity. Even when solving such a simple system as the harmonic oscillator, which can be done partly analytically, the electron motion changes its sign as the photon energy becomes larger than the level spacing [120]. This is also valid for 2 electrons [120], suggesting that tunneling suppression might also occur in multi-electron systems. Tunneling suppression, to my knowledge, has neither been observed nor calculated or reported so far.

4.2 Multi-electron Dynamics in Overresonant Systems

Thus far we have discussed the behaviour of one electron in large systems. The question is, whether tunneling suppression is also observable in multi-electron systems. To this end equ. (4.2) was solved for $f = 4$ electrons. We used $n = 8$ (70 Slater determinants; the Hartree-Fock case would be 1 determinant, $n = f = 4$) in the ansatz for Ψ , equ. (3.19). As it was proven recently, 15 determinants are enough to fully include correlation effects for 2 electrons [71]. To decide, whether the number of Slater determinants is big enough and correlation effects are fully included, either (i) a comparison with exact calculations has to be done, which is not possible in the here considered 4-electron case, since an exact treatment of the time-dependent 4-electron case is not feasible at the moment, or (ii) the number of Slater determinants in the MCTDHF-ansatz equ. (3.19) has to be increased until there is no change in the result any more. An increase from 15 determinants — $n = 6$ expansion functions — to 70 Slater determinants ($n = 8$) resulted only in a change of a few percent ($< 0.02 - 0.03$) of ionization probability. A calculation carried out for the next possible value of 210 determinants ($n = 10$) for 1 data point resulted in a difference of not even 0.01. Thus, the uncertainty of the ionization probability is smaller than ± 0.01 as compared to the "exact" value including full correlation. Unfortunately, due to limitations of the computational resources, it was not possible to calculate every data point with $n = 10$. However, as a first remark, an uncertainty of < 0.01 is better than accuracies of even the best high-resolution measurements. Second, this uncertainty lies within the Runge-Kutta propagation accuracy and could therefore also arise from the propagation and not from an insufficient number of determinants. And finally, the calculations cannot be compared to experimentally gathered data, anyway, because they are carried out for 1D-model-potentials. Therefore, the absolute value of the computed ionization probability is not very crucial, as long as all computed data to be compared with each other are calculated for the same n and the same grid. Note, however, that these results are the first multiconfigurational, time-dependent calculations for more than 2 electrons, where correlation was included. Thus far correlation has never been

considered, except for Time-Dependent Density Functional Theory calculations in metal bulks (not molecular or atomic potentials!) [89].

The calculation range in our simulations was $-150 \dots +150$ with absorbing boundary conditions at the ends. The nuclear potential was again a smoothed well potential of the same form as in the one-electron calculations above, and the electron-electron potential was a smoothed coulomb potential [111],

$$V(x_m - x_n) = \frac{1}{\sqrt{(x_m - x_n)^2 + a^2}}, \quad (4.13)$$

where a is the smoothing parameter. For 1D-calculations the electron-electron smoothing parameter a in equ. (4.13) must be chosen carefully in order to simulate the 3D-behaviour correctly. A large a gives “soft” electrons whereas small a ’s lead to very “hard” electrons. Softening the electrons in 1D-calculations is necessary since it brings some 3D-behaviour into the simulations. This is, because it is energetically easier for the electrons to pass each other (as is the case in 3D) in softened electron-electron potentials than in infinitely repulsive potentials. On the other hand it is not quite clear how the 3D-nature of real systems can be passed on to 1D-calculations and whether softening of the electrons in our simulations captures the 3D-behaviour correctly. However, $a = 1$ is very common in the literature [25, 111, 62, 107] and this value was chosen for the calculations. Once a is fixed, the ionization potential I_P , which is greatly influenced by a , must be adjusted with free parameters of the nuclear potential, in our case this is the depth D of the well.

Once the number of electrons, f , the nuclear potential, $U(x_m)$, and the electron-electron potential, $V(x_m - x_n)$, are chosen, the energy level structure of the (unperturbed) system is fully determined. To observe tunneling suppression (counter-directive wavepacket dynamics!), the characteristic frequency of the system must be smaller than ω_L . In the one-electron case this frequency was determined by the energy gap between the ground and the first excited state, $E_1 - E_g$. For molecules the according energy gap would then be the HOMO-LUMO gap. This means the energy difference between the Highest Occupied Molecular Orbital and the Lowest Unoccupied Molecular Orbital. Usually this gap is much larger than the photon energy of commonly used lasers in the infrared. The Ti:Sapphire laser radiates at $\lambda \approx 800$ nm, hence $\omega_L = 0.057$ or roughly 1.55 eV, whilst HOMO-LUMO in organic molecules is of the order of a few electron volt and therefore larger than the photon energy, a situation which would not support counterdirective electron dynamics. However, the energy level structure in molecules when excited with strong fields is blurred and energy bands are formed. Moreover, HOMO-LUMO is the energy gap relevant for the excitation of a single electron in the multi-electron ensemble [31]. The energy gap responsible for the excitation of the whole multi-electron cloud is rather the plasma frequency than the HOMO-LUMO gap [25, 31]. The plasma frequency reads (atomic units!)

$$\omega_p = \sqrt{4\pi N}, \quad (4.14)$$

where N is the density of electrons per unit volume. In order to observe tunneling suppression and counterdirective electron dynamics, the laser photon energy, ω_L , must be larger than ω_p . A simple estimate tells us that this cannot be the case in molecules, not even in large organic ones: Those molecules studied in refs. [24, 25] are up to approximately 35 at.u. long and have several active electrons. Decatetraene for example can be treated as a potential well of length 13.2 Å or roughly 25 at.u. with 8 active π -electrons [25, 107]. The σ -electrons have a much smaller movability and are therefore neglected. Calculating the plasma frequency for decatetraene yields $\omega_p \approx 0.642$, where the volume which is available to the electrons motion is calculated assuming an interatomic distance of $25/8 = 3.125$. Then the volume is estimated as $3.125^2 \times 8 \times 3.125 = 244.14$, leading to $N = 8/244.14 = 0.0328$ and hence via the relation equ. (4.14) for the plasma frequency to the above given value $\omega_p \approx 0.642 \gg \omega_L$. As a consequence the electron-dynamics is underresonant, which is also confirmed by a TDHF-study carried out in ref. [107], where the non-adiabatic dynamics reported in refs. [24, 25] was investigated. Therefore there is no hope to observe tunneling suppression due to counterdirective electron dynamics in molecules, not even in very large ones. However, it might be, that because of the smaller electron density in ions of such molecules tunneling suppression could be observed, provided the ions stay stable and do not fragment during ionization. These considerations above lead us to the conclusion that multi-electron tunneling suppression is not to be observed easily in "natural" systems like molecules. However, the prerequisite $\omega_p < \omega_L$ is met in large, artificially produced systems like structures in semi-conductors, e.g. quantum dots [117], or any other system with small electron density N . It will be proven in the next subsection that tunneling suppression does occur even for unexpectedly small quantum dots.

4.2.1 MCTDHF Simulations

In order to investigate if tunneling suppression also happens in multi-electron systems, the electron dynamics in a 100 at.u. long, smoothed potential well was studied as a function of the laser intensity and the photon energy. The ionisation potential of our 4 electron-system was $I_P = 0.448$, defined by

$$I_P = E_{g,f} - E_{g,f-1}, \quad (4.15)$$

the difference of the ground state energy of the f -electron system minus the ground state energy of the $(f - 1)$ -electron system. The plasma frequency in this system can be estimated similiar as outlined above. Each electron occupies a length of $100/4 = 25$ at.u., which can be considered as an equivalent interatomic distance. If it is assumed that this length defines a cube of free space for every electron than the density of electrons per unit volume, N , can be calculated according to $N = 4/(25^2 \times 100) = 25^{-3} = 6.4 \times 10^{-5}$, leading to a plasma frequency of $\omega_p = 0.0284$, which supports overresonant electron dynamics for wavelengths $\lambda \lesssim 1600$ nm, for which the photon energy is $\omega_L = 0.0285$. Note, that $L = 100$ at.u. is very small for

artificially produced systems. Bigger systems will support $\omega_p < \omega_L$ for even higher numbers of electrons.

When studying the time evolution of the wavefunction, which is not directly possible since the wavefunction is 8-dimensional (4 spatial- and 4 spin-coordinates), but what can be done conveniently with the help of a one-dimensional function, the so called *electron probability density*, (see appendix B on page 78 for a derivation) it can be seen that the electrons do not spread over the potential length when excited by the laser electric field. They stay confined to a narrow bunch and this bunch's motion in the field beautifully exhibits a phase shift of $\propto \pi$ to the laser field, as observed in the one-electron case and as used to from classical overresonantly excited systems, see top panel of fig. 4.2. Therefore, tunneling dynamics might again be captured by classical mechanics as predicted. To investigate this dynamics and the agreement of classical mechanics with our quantum results we solve the f coupled Newton's equations for $f = 4$ electrons and model the quantum mechanical ground state distribution by a bunch of trajectories similar to the one-electron case.

4.2.2 Initial Conditions and Classical Wavepacket Propagation in the Multi-Electron Case

In order to calculate the initial conditions for our classical simulations we opted for the simplest model, as described for the one electron case, since the Husimi distribution in the multi-electron case is a very demanding task to compute. Therefore, we should bear in mind that the agreement of our classical simulations with the quantum results is the worst we can get. Every other method of calculating the initial conditions would improve the agreement. In detail the initial conditions are calculated as follows. We use an equidistant spatial grid and place our trajectories at positions $x_{i,1} \dots x_{i,f}$ such that $x_{i,1} < x_{i,2} \dots < x_{i,f}$. The subscript i denotes that the trajectories are part of the i -th trajectory combination $\zeta_i = \{x_{i,1}, \dots, x_{i,f}\}$. The condition $x_{i,1} < x_{i,2} \dots < x_{i,f}$ ensures that no unnecessary combinations are calculated since the ground state wavefunction is f -dimensional symmetric due to the exchange symmetry. The probability every trajectory combination ζ_i represents is given by the quantum mechanical ground state probability density $|\Psi(x_{i,1}, \dots, x_{i,f}; -\infty)|^2$. Then the classical energy $E_{c,i}$ of the trajectory combination ζ_i is calculated according to

$$E_{c,i} = \sum_{m=1}^f U(x_{i,m}) + \sum_{m<n}^f V(x_{i,m} - x_{i,n}). \quad (4.16)$$

If this energy is higher or equal than the ground state energy $E_{g,f}$, ζ_i is taken as a classically allowed trajectory combination. The initial velocities of the trajectories belonging to ζ_i are then calculated as $v_i = \pm \frac{1}{f} \sqrt{2(E_{c,i} - E_{g,f})}$, meaning that the total positive energy of the combination ζ_i is equally distributed among all the f trajectories representing the electrons. A more sophisticated distribution function might give better results, but already with this simple model reasonable results are

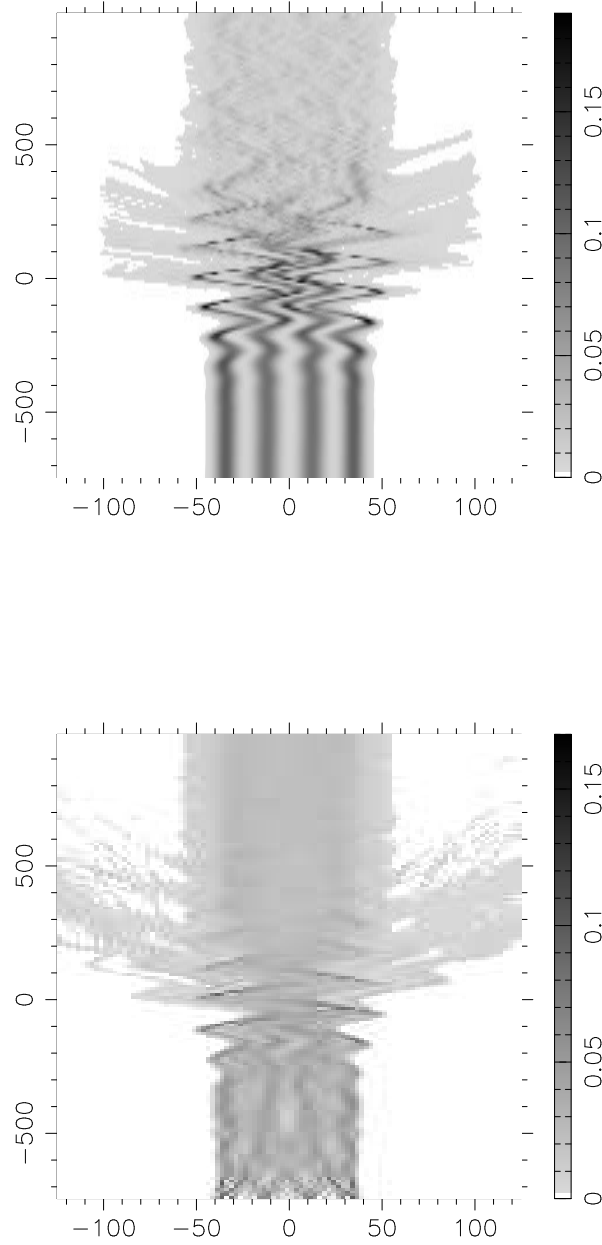


Figure 4.2: Time evolution of the electron density calculated by quantum mechanics via equ. (B.2) (top panel) and by classical mechanics (lower panel) for 4 electrons. The vertical axes are time, the horizontal ones space. Potential length $L = 100$, $I_P = 0.448$, laser intensity $I_L = 8 \times 10^{13}$ W/cm², laser pulse duration 6 fs FWHM, wavelength 800 nm. The here presented data is marked by an arrow in fig. 4.3.

achieved. Moreover it is assumed that the + and the - sign in the equation for the velocity v_i are equally probable. This leads to 2^f different combinations of + and - for every ζ_i . If we discretize the space within the potential $U(x)$ with N base points then there are, because the initial x -values are ordered for every trajectory combination, $\binom{N}{f}$ trajectory combinations ζ_i . Not all of them fulfill the requirement $E_{c,i} - E_{g,f} > 0$. Let us denote the number of them, which do fulfill this condition, with k . Hence, because of the 2^f equally probable combinations due to the velocity permutations, this leads to $k 2^f$ trajectory combinations. After having gone through all ζ_i the total probability of all the trajectory combinations $k 2^f$ must be normalized to 1. This leads to a normalization condition for the probability $P(\zeta_i)$ of the i -th trajectory combination of the form

$$P(\zeta_i) = \frac{|\Psi(x_{i,1}, \dots, x_{i,f}; -\infty)|^2}{\sum_{m=1}^{k 2^f} |\Psi(x_{m,1}, \dots, x_{m,f}; -\infty)|^2}. \quad (4.17)$$

Each of these combinations is taken as an initial condition for the f coupled Newton's equations

$$\begin{aligned} \ddot{x}_{i,1}(t) &= E(t) - \frac{d}{dx}U(x) \Big|_{x=x_{i,1}} - \frac{1}{2} \sum_{n=1, n \neq 1}^f \frac{d}{dx}V(x - x_{i,n}) \Big|_{x=x_{i,1}} \\ \ddot{x}_{i,2}(t) &= E(t) - \frac{d}{dx}U(x) \Big|_{x=x_{i,2}} - \frac{1}{2} \sum_{n=1, n \neq 2}^f \frac{d}{dx}V(x - x_{i,n}) \Big|_{x=x_{i,2}} \\ &\vdots \\ \ddot{x}_{i,f}(t) &= E(t) - \frac{d}{dx}U(x) \Big|_{x=x_{i,f}} - \frac{1}{2} \sum_{n=1, n \neq f}^f \frac{d}{dx}V(x - x_{i,n}) \Big|_{x=x_{i,f}} \end{aligned}$$

which are propagated using a Runge-Kutta method for the same laser pulse and the same potentials as in the quantum calculations. In classical mechanics it is possible to define an energy for each of the f electrons in a trajectory combination. Therefore, it is easy to determine the probability of one-, two-, ... f -electron ionization³. The ionization probability $W_{\infty, M}$ for ionization of M electrons is defined as the sum of all probability of trajectory combinations where M electrons have an energy greater than 0 after the laser pulse. The energy of the j -th electron of ζ_i is calculated by

$$E_{i,j} = U(x_{i,j}) + \frac{1}{2} \sum_{\substack{m=1 \\ m \neq j}}^f V(x_{i,j} - x_{i,m}) + \frac{1}{2} \ddot{x}_{i,j}^2. \quad (4.18)$$

Then the number of ionized electrons of trajectory combination ζ_i , denoted by M_i , is given by

$$M_i = \sum_{j=1}^f \begin{cases} 1 & \text{if } E_{i,j} > 0 \\ 0 & \text{else} \end{cases}. \quad (4.19)$$

With that the probability for the ionization of exactly M electrons is given by

$$W_{\infty, M} = \sum_{i=1}^{k 2^f} \begin{cases} P(\zeta_i) & \text{if } M_i = M \\ 0 & \text{else} \end{cases}. \quad (4.20)$$

³ M -electron ionization means, exactly M electrons are ionized, $(f - M)$ electrons remain bound.

For comparisons with the quantum mechanical ionization probability given by equ. (A.4) the sum $W_\infty = \sum_{M=1}^f W_{\infty, M}$ must be taken. This is the probability of finding at least one electron ionized.

Classical Ionization vs. Quantum Mechanics

Fig. 4.2 shows the ionization dynamics calculated by quantum mechanics (top panel) and classical mechanics (lower panel). For the classical calculations $k = 3296$ trajectory combinations in space were used. This gives a total number of 52736 trajectory combinations, due to the $2^4 = 16$ velocity combinations per trajectory combination in space ($3296 \times 2^4 = 52736$). The vertical axes shows time and the horizontal axes space. The pictures show the evolution of the electron density defined by equ. (B.2) in appendix B. The classical electron density is defined accordingly. Technically, for the lower panel in fig. 4.2, the probability of finding at least an electron in a space region Δx was summed up. The potential length L in fig. 4.2 was 100, thus the potential spans from approximately -50 to $+50$, cf. fig. 4.2. For approximately $t < -300$ the laserfield is not strong enough to induce noticeable motion. Thus, the wavefunction stays mainly in the ground state (upper panel). For the classical case there is, of course, no eigenstate. Therefore the electron density in the lower panel of fig. 4.2 does not exhibit a stationary structure like the quantum mechanical electron density in the upper panel but an all over the potential spread density also for $t < -300$. This is only the result of the initial velocities of the electrons. Then the laserfield sets in, inducing dynamics in both the quantum and classical case. When the laserfield is strong enough such that the electrons (wavefunction) hit the potential barrier they can absorb energy (dephasing mechanism). Eventually, when their energy becomes positive, they will ionize which can be seen in fig. 4.2 by the probability clouds leaving the range $-50 \dots +50$. Tunneling suppression can be seen clearly in fig. 4.2: For our hamiltonian of equ. (3.17) the well's potential barrier is tilted to the right ($U(x > 0) < U(x < 0)$) for positive laser field strengths. Thus, if the electrons would minimize their energy by following the potential, they would sit at positive x -values at the time $t = 0$, where the laserfield has the maximum positive value. But instead the electron cloud sits at $x < 0$ clearly revealing the movement in counterdirection, thus, suppressing tunneling. The shielding factor a (see equ. (4.13)) was $a = 1$ (as stated above) yielding relatively "hard electrons". This can be seen in the upper panel of fig. 4.2 by the fact, that the electron density clearly exhibits 4 pronounced maxima up to $t \approx 0$, where ionization sets in and blurs this structure. The 4 electrons move in the laserfield forming sort of a chain. No electron can pass the other since that is energetically very unlikely. "Softer electrons" would stick together more closely (due to energetic reasons). The electron density would merge, forming a bunch. This means that softer electrons allow for even more pronounced tunneling suppression. This makes our result independent of a .

To test the agreement between classical mechanics and quantum mechanics also

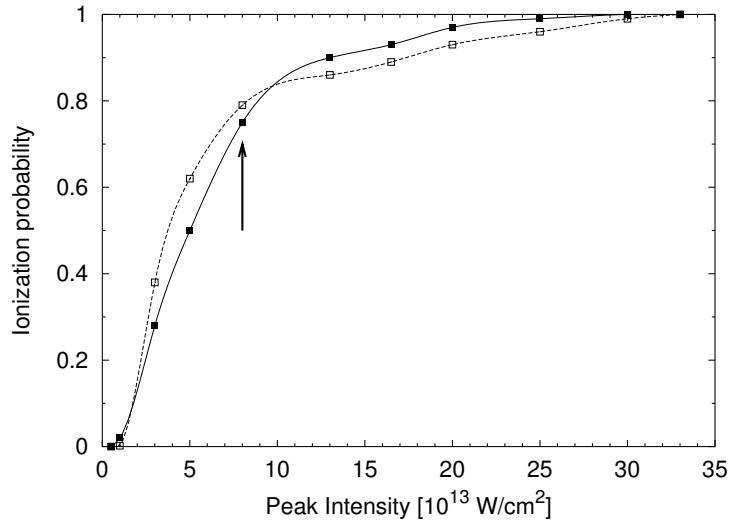


Figure 4.3: Quantum mechanical (filled squares) and classical (open squares) ionization probability as a function of the laser intensity for a wavelength of $\lambda = 800$ nm. The lines are only to guide the eye and the arrow indicates the data points displayed in fig. 4.2. The laser pulse was gaussian with a duration of 6 fs FWHM (2.25 full cycles), $I_P = 0.448$, $a = 1$, $L = 100$.

quantitatively the ionization probability as a function of the laser peak intensity was calculated, see fig. 4.3. The same potential as in fig. 4.2 was used. The filled squares in fig. 4.3 correspond to the solution of the full Schrödinger equation and the open squares depict the solutions of Newton’s equations (4.18). All the parameters are indicated in the figure caption and correspond to those of fig. 4.2. The arrow marks the data displayed in fig. 4.2. As can be seen in fig. 4.3 the agreement between classical and quantum mechanics is excellent also in a quantitative manner.

Limits of the Classical Description

It is important to identify parameter ranges where the quantum dynamics can be quantitatively described by classical mechanics. Basically, for fixed shielding a , the agreement between classical mechanics and quantum mechanics depends on 4 parameters: the well length L , the ionization potential I_P , the laser peak intensity I_L and the laser wavelength λ , which is proportional to the photon energy ω_L .

We have compared the ionization probability as a function of the laser intensity calculated by quantum mechanics and classical mechanics for various limiting cases. The parameters considered were: 4 electrons, laser wavelengths $\lambda = 400, 800, 1200$ nm, well lengths $L = 50, 100$ and ionization potentials $I_P = 0.322, 0.448, 0.451, 0.586$. The calculations revealed, that classical mechanics failed for 400 nm in all cases. The agreement was better for higher intensities than for lower ones. $I_P = 0.586$ did not give satisfying results for any of the wavelengths,

whereas the other I_P 's led to good agreement for 800 nm and 1200 nm. For $L = 100$ the agreement was always better than for $L = 50$, which is not surprising since the plasma frequency for $L = 50$ is $\omega_p = 0.04$, which is not much smaller than the photon energy of 0.057 for 800 nm and even bigger than 0.038, the photon energy for $\lambda = 1200$ nm. Therefore $L = 50$ is too small to support overresonant electron dynamics for 1200 nm.

By carefully comparing all the results it was concluded that an important parameter to decide, whether a classical description of the electron dynamics is acceptable, is U_p/ω_L , with U_p the average (ponderomotive) energy of an electron in a laserfield, $U_p = E_L^2/(4\omega_L^2)$. The ratio U_p/ω_L is a measure of an electrons classical energy (U_p) as compared to its energy of quantum mechanical origin (wave picture, ω_L). In quantum mechanics an electron can only pick up energy in multiples of the photon energy, it gains energy stepwise. If the photon energy is large, the function 'gained energy over time' of the electron cannot be approximated by a smoothed curve anymore. Therefore, the classical energy consumption mechanism proposed in equ. (4.12) will fail. This is confirmed by the fact, that the calculations with 400 nm could not be approximated by classical mechanics. Further on the ionization potential is of importance. High I_P 's result in Keldysh parameters greater than unity and, thus, leading to multi-photon ionization, which is not suppressed by the counterdirective, overresonant electron dynamics. Only tunnel ionization is suppressed by this mechanism. In the calculations $I_P = 0.586$ did not lead to satisfying agreements which is consistent with the required small I_P 's. Finally, as a precondition, the photon energy ω_L must be bigger than the plasma frequency in order to achieve tunneling suppression. Therefore, summarizing, the classical description will only lead to quantitative agreement with quantum mechanics in a parameter range limited by the introduced parameter U_p/ω_L and by the I_P , leading to three conditions: (i) "high" values of U_p/ω_L , (ii) I_P not too large to support tunnel ionization and (iii) overresonant dynamics through $\omega_L > \omega_p$.

Concluding it can be said that tunneling suppression does exist in multi-electron systems. For quantitative agreement of ionization probabilities calculated by quantum and classical mechanics there are restrictions on the system size, the ionization potential and the laser wavelength. Note, however, that our classical calculations used a very crude model for the initial conditions. Nevertheless the results obtained with them match the quantum results very well, see fig. 4.2 and fig. 4.3. The concordance might be even better with more sophisticated initial conditions.

Chapter 5

Tunneling Suppression through Laser Induced Polarization

In the previous chapter 4 the electron dynamics of big systems with few electrons was investigated. We found that for such systems the laser induced motion of the wavepacket is in the opposite direction as compared to dense systems like atoms and smaller molecules. The reason is that in few-electron systems the plasma frequency can be smaller than the photon frequency of common infrared lasers. This overresonant excitation leads to the described wavepacket dynamics, tunneling is suppressed and ionization happens via a classical mechanism, which is determined by a deceleration of the electrons when they hit the potential barriers. Because of this deceleration the electrons are dephased to the driving laser electric field and are enabled to pick up energy from the field. Atomic and molecular systems usually have densities of electrons and energy level structures exhibiting plasma frequencies bigger than the photon energy. Therefore the laser induced wavepacket dynamics follows the tilted nuclear potential and tunneling is no longer suppressed. Recently a lot of experimental work was done on strong field ionization of complex multi-electron systems like molecules [22, 23, 24, 25] and metal clusters [53]. It was found that the wavelength dependency of the *saturation intensity*¹ in organic molecules, like e.g. all-trans decatetraene, is such that for a laser wavelength of $\lambda \lesssim 1\mu\text{m}$ the saturation intensity can be described [25] by a length corrected molecular single active electron model (MSAE) [121, 116, 115] which is based on the ADK theory but takes into account the actual molecule potential structure which is not included in the ADK theory. As the wavelength increases the saturation intensity increases, too, and saturates for wavelengths $\lambda \gtrsim 1.4\mu\text{m}$. In this (long wavelength) limit the electron dynamics is quasistatic and the ADK theory should apply. But as the experiments show, the saturation intensity is by about a factor of 5-10 higher than the ADK

¹This is the laser peak intensity where the ionization probability exceeds a certain probability. The saturation intensity can be determined experimentally with high precision [23]. In numerical calculations usually the intensity corresponding to an ionization probability of 0.9 or 0.95 is taken.

value [24, 25, 23]. This increased saturation intensity is also detectable in metal clusters [53]. This result could not be explained but it was speculated that some multi-electron effects like correlation could be responsible for this result [26, 25]. To further investigate these supposed multi-electron effects strong field ionization experiments in a very big molecular system, the C60 molecule [22], and in very small multi-electron systems, metal clusters [53], were carried out. The results of the C60-experiments carried out for $\lambda = 1.2 - 2.2\mu\text{m}$ suggested that this increase might be explained by a field induced polarization which raises the effective tunneling barrier. Applying the *above barrier model* of ionization [122], which relates the saturation intensity of molecules to the intensity where the Coulomb barrier is suppressed below the ionization potential, and including the potential obtained when modelling C60 as a conductive sphere, it was possible to quantitatively describe the actual experimentally obtained saturation intensity [22]. However, as it turned out, it is not possible to explain the data of the experiments for all measured metal clusters with this approach [53]. This might be attributed to the fact that metal clusters are much smaller than C60 and therefore cannot be described as a conducting sphere, which is a pure classical model. This motivates a quantum mechanical investigation of the ionization process in molecules and metal clusters in the quasistatic tunneling limit (long wavelength limit). The aim of this chapter is to explain the discrepancies between the saturation intensity calculated by the ADK theory and the experimentally obtained value. Although it is very difficult to develop a tunneling theory for molecules, considering their complex level structures, let alone multi-electron influences of the remaining electron cloud on the tunneling electron, the applicability of the ADK tunneling theory for molecules shall be questioned and an extended model shall be given.

5.1 The Quasistatic Limit

As a first point we want to determine the wavelength required to be in the quasistatic regime. Taking the Keldysh parameter as a measure, as it can be done for atoms, is not possible for molecules. The Keldysh parameter γ loses its meaning for molecules and it was shown that $\gamma < 1$ does not necessarily mean that ionization takes place quasistatically [25, 121, 116, 115]. Therefore, in order to determine the minimum wavelength for being in the quasistatic limit, we solve the Schrödinger equation (4.2) for 4 electrons in a nuclear potential of the form equ. (4.1),

$$U(x) = -D e^{-(2x/L)^{10}}, \quad (5.1)$$

which is a smoothed well potential. The length L of the potential was chosen to be $L = 18$ and D was adjusted to obtain an ionization potential of $I_P = 0.2$, which is defined, as stated above, by

$$I_P = E_{g,f} - E_{g,f-1}, \quad (5.2)$$

the difference of the ground state energies of the f -electron system minus the $(f-1)$ -electron system. We used, as in the previous chapter, $n = 8$ expansion functions

(70 Slater determinants). The Hartree-Fock case would be $n = f = 4$ (1 Slater determinant). The electron-electron potential was chosen as in equ. (4.13), that is

$$V(x_m - x_n) = \frac{1}{\sqrt{(x_m - x_n)^2 + a^2}}, \quad (5.3)$$

and the shielding parameter a was 1.4. Smoothed well potentials do not have a Coulombic long range behaviour as it is the case for molecular and atomic systems. However, they are very common in the literature [25, 107]. This is mainly due to the fact that Coulomb potentials extend very widely and therefore call for big calculation boxes which is numerically very demanding. In order to investigate the influence of the laser induced polarization on the tunneling barrier we will get back to Coulomb shaped potentials. Equ. (4.2) was solved on a grid with a spacing of $\Delta x < 0.15$. For the smoothed well potentials the calculation range was $-150 \dots + 150$. For the Coulomb potentials the calculation range must be chosen much bigger. The maximum possible calculation range for our computers was $-420 \dots + 420$, due to limitations of the main memory. At the ends of the calculation range absorbing boundary conditions were applied. The simulations were carried out on a 1.8 GHz Desktop PC and each simulation took typically 20-40 hours, depending on the calculation range and the electron-electron potential expansion accuracy.

We used two different wavelengths, $\lambda = 800$ nm and $\lambda = 1500$ nm, in our simulations and the pulse form was chosen to be gaussian. The simulations revealed that the saturation intensity for 1500 nm is by about a factor of 3 higher than the one for 800 nm, in accordance with the experiments [53, 25]. This may be attributed to the fact that for 800 nm non-adiabatic transitions greatly influence the ionization dynamics [25] and add to the ionization probability, thus, decreasing the saturation intensity. Here, we want to exclude such effects, since we want to investigate “pure” quasistatic tunneling, which accordingly will give the highest saturation intensity. In ref. [25] it is shown that the saturation intensity for all-trans decatetraene is independent of the wavelength for $\lambda \gtrsim 1.4 \mu\text{m}$ (quasistatic limit) and that it does not increase any more when the wavelength is increased further. This means that even if we are not fully in the quasistatic limit when using $\lambda = 1500$ nm, we are on the save side since further increasement of the wavelength would just increase the saturation intensity. Therefore, the discrepancy obtained between ADK and our numerical calculations is just a *lower* value.

5.2 The Effective One-Electron Potential

Now, that we have established that using a wavelength of $\lambda = 1.5 \mu\text{m}$ gives a suitable (lower) boundary for comparisons with the quasistatic ADK ionization probability we return to the problem of the influence of the laser induced polarization on tunneling. We now use Coulomb shaped nuclear potentials, which in the case of an even

number f of nuclei take the form

$$U(x) = - \sum_{m=0}^{f-1} \frac{1}{\sqrt{(x + \frac{f-1}{2} \delta - m \delta)^2 + b^2}}, \quad (5.4)$$

with b a smoothing parameter and δ the internuclear distance. Such a potential form basically models a molecule consisting of f ‘‘Hydrogen’’ atoms. In considering the influence of the field-induced polarization on tunneling we will use the density matrices of the first, $\rho(x;t)$, and the second order, $\gamma(x_1, x_2;t)$. They are derived in appendix B on page 78. With the help of $\gamma(x_1, x_2;t)$ we analyze the influence of the $(f - 1)$ remaining electrons on the tunneling electron. To do so, we calculate the expectation value of the potential, which the electron cloud executes on an electron situated at R , taken at an instant t . We denote this potential with $\varphi(R;t)$ and the expectation value, which is derived from the Hamiltonian given by equ. (3.17), with $\langle \varphi(R;t) \rangle$. This expectation value is given by

$$\langle \varphi(R;t) \rangle = \sum_{m=1}^f \langle R, x_2, \dots, x_f | U(x_m) + \sum_{m < n}^f V(x_m - x_n) | R, x_2, \dots, x_f \rangle, \quad (5.5)$$

where, for the sake of simplicity, we have suppressed the spin coordinates although the integration is meant to be carried out over them. Expression (5.5) can be written as

$$\begin{aligned} \langle \varphi(R;t) \rangle &= \quad (5.6) \\ &\sum_{m=1}^f \int \Psi^*(R, x_2, \dots, x_f; t) U(x_m) \Psi(R, x_2, \dots, x_f; t) (d\tilde{x}_1) + \\ &f \sum_{m=2}^f \int \Psi^*(R, x_2, \dots, x_m, \dots, x_f; t) V(R - x_m) \\ &\quad \times \Psi(R, x_2, \dots, x_m, \dots, x_f; t) (d\tilde{x}_1) \\ &= U(R) f \int \Psi^*(R, x_2, \dots, x_f; t) \Psi(R, x_2, \dots, x_f; t) (d\tilde{x}_1) + \\ &f(f-1) \int \Psi^*(R, x, x_3, \dots, x_f; t) V(R - x) \\ &\quad \times \Psi(R, x, x_3, \dots, x_f; t) (d\tilde{x}_1), \end{aligned}$$

where the notation of appendix B was used. Inserting the definitions of the electron densities from appendix B leads to

$$\langle \varphi(R;t) \rangle = U(R) \rho(R;t) + 2 \int V(R - x) \gamma(x, R; t) dx.$$

To obtain the potential $\varphi(R; t)$ instead of the expectation value $\langle \varphi(R; t) \rangle$, the electron density function $\rho(R; t)$ must be singled out of this equation. This leads to

$$\begin{aligned} \varphi(R; t) &= \frac{\langle \varphi(R; t) \rangle}{\rho(R; t)} = \\ &= U(R) + \frac{2}{\rho(R; t)} \int V(R-x) \gamma(x, R; t) dx, \\ &= U(R) + \pi(R; t), \end{aligned} \tag{5.7}$$

where $\pi(R; t)$ denotes the potential produced by the $(f-1)$ -electron cloud taken at a position R . The integral in $\pi(R; t)$ is a Green's integral for our electron-electron potential $V(R-x)$ and the first term, $U(R)$, is just the nuclear potential.

In deriving equ. (5.7) we have integrated over the positions and spins of the remaining $(f-1)$ electrons. Thus the influence of these remaining electrons is only considered in average just like in Hartree-Fock only the integral influence of all other electrons on one electron is taken into account. By calculating $\varphi(R; t)$ effects of correlation and antisymmetry are neglected. Indeed, when calculating the ground state energy for a one-electron system with a binding potential $\varphi(R; t \rightarrow -\infty)$ derived from the f -electron ground state wavefunction of the system to be considered in the next sections this one-electron ground state energy deviated by roughly 20% from the actual I_P of the f -electron system. However, $\varphi(R; t)$ is the best approximation for a single active electron potential for the tunneling electron one can derive from the full f -electron wavefunction. For values of R within the $(f-1)$ -electron cloud $\varphi(R; t)$ does not represent the actual potential felt by the weakest bound electron (due to the above mentioned reasons). But $\varphi(R; t)$ is expected to give a reasonable approximation for situations where one electron is sufficiently far away from the $(f-1)$ -electron cloud. This is because for such situations the weakest bound electron (the tunneling electron) does not feel each of the other electrons separately but only the integral influence of the whole cloud. Therefore $\varphi(R; t)$ can be considered as an approximation for an effective potential for the tunneling electron. It consists of the nuclear potential, $U(R)$, and *additionally* of the potential $\pi(R; t)$ caused by the integral influence of all other electrons corresponding to their positions at the considered instant t . We will refer to $\varphi(R; t)$ defined by equ. (5.7) as *the effective one-electron potential* in the following but have to bear in mind that it is only a good approximation for a single electron sufficiently far away from the other electrons, e.g. for a tunneling electron.

5.3 Tunneling Dynamics

We now turn to the investigation of the tunneling process. As explained in appendix B, the diagonal elements of $\gamma(x, R, x, R; t) = \gamma(x, R; t)$ have the following meaning: $\gamma(x, R; t) dx dR$ is the probability of finding one electron with arbitrary spin within dx around the point x and another electron with arbitrary spin within dR around the

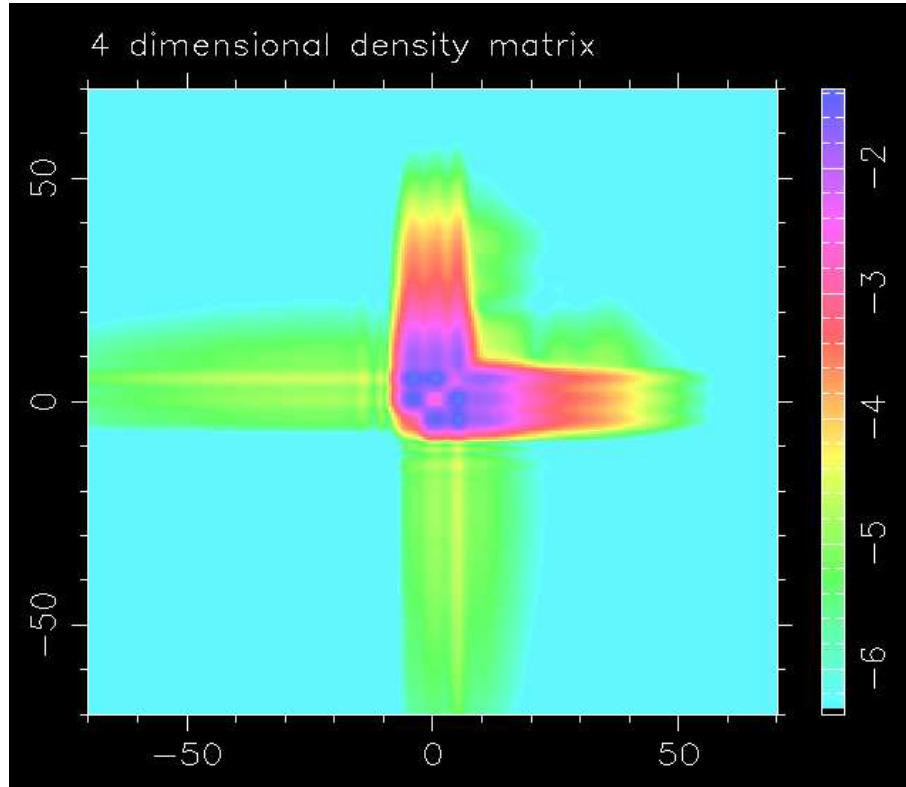


Figure 5.1: Tunneling dynamics of one electron in the effective potential caused by the influence of all other electrons depicted by the electron density function of second order $\gamma(x, R, x, R; t) = \gamma(x, R; t)$, defined by equ. (B.1), in logarithmic scale, exactly one laser cycle before the laser pulse peak, that is at $t = -186.04$. Note that $\gamma(x, R; t) = \gamma(R, x; t)$ and that the horizontal axis and the vertical axis are interchangeable. Probabilities within the bands $-15 < x < 15$ and $-15 < R < 15$ correspond to the ionization of one electron while the other electrons remain bound. The shift of the probability to values $R > 0$ for a certain $x > 0$ during tunneling is caused by the motion of the remaining electron cloud after the tunneling electron. This excursion of the cloud is responsible for a polarization of the molecule. The effective potential caused by the shifted electrons can be evaluated by equ. (5.7).

point R , all other electrons having arbitrary positions and spins. Therefore plotting the matrix $\gamma(x, R; t)$ visualizes the probability of the tunneling electron under the influence of all other electrons. To study the tunneling process we propagated the ground state wave function of a molecule consisting of four electrons and nuclei ($f = 4$). The nuclear potential was of the form equ. (5.4) with $\delta = 3.5$ and $b = 1.5$. The smoothing parameters of the electron-electron potential was $a = 0.9$. This resulted in an ionization potential of $I_P = 0.261$, defined by equ. (5.2), and a ground state energy of $E_g = -2.972$. Note, that $I_P = 0.261$ is a very common value for metal clusters and (organic) molecules. The wavelength of the laser light was $\lambda = 1500$ nm, the laser peak intensity $I_L = 5 \times 10^{13}$ W/cm² and the pulse duration was 10 fs (FWHM).

Fig. 5.1 shows $\gamma(x, R; t)$ at the time $t = -186.04$, which is exactly one laser-cycle before the laser pulse peak situated at $t = 0$. The actual field strength at this time is $E(t = -186.04) \approx 0.0247$, corresponding to an intensity of roughly 2.14×10^{13} W/cm². Note, that $\gamma(x, R; t) = \gamma(R, x; t)$ which can also be seen from equ. (B.1). The potential barrier is tilted to the right (into the positive R or x direction) and consequently the probability of finding an electron at a certain x (or R) is higher for positive x or R than for negative ones, since we are in the underresonant parameter regime and the electrons follow the tilted nuclear potential. According to the above explanations, the probability of finding the other electrons, when one electron is situated at $R = R_0$ is given by $\gamma(x, R_0; t = -186.04)dx dR$. Thus, the bands $-15 < R < 15$ (and $-15 < x < 15$) in fig. 5.1 show tunneling of one electron when all the other $(f - 1)$ -electrons stay in the potential. Significant probability values outside this area would correspond to multi-electron ionization. As can be seen, there is nearly no multi-electron ionization in fig. 5.1. The most striking feature of fig. 5.1 is, that for a certain $R = R_0 > 0$ the probability for finding the other electrons is not centered around $x = 0$ but is shifted to values $x > 0$. This means, that during the tunneling process the remaining $(f - 1)$ -electrons move after the tunneling electron. This displacement of the electrons corresponds to a laser-induced polarization. The effects of the asymmetric electron distribution within the molecule can be calculated from the wavefunction with the help of equ. (5.7). The next section is dedicated to the investigation of the consequences of this behaviour of the remaining electron cloud.

5.4 The Effects of the Laser-Induced Polarization

In order to quantitatively estimate the influence of the induced polarization on the tunneling electron we calculate the potential caused by the $(f - 1)$ -electron cloud according to $\pi(R; t)$ of equ. (5.7). The full line in the upper panel of fig. 5.2 on the following page shows the potential $\pi(R; t)$ for the situation depicted in fig. 5.1, that is at $t = -186.04$. The dotted line in the upper panel shows the electron density $\rho(R; t)$. The tunneling process can be seen by the hump of $\rho(R; t)$ for $R \approx 12 - 16$. That the $(f - 1)$ remaining electrons in the nuclear potential follow the tunneling

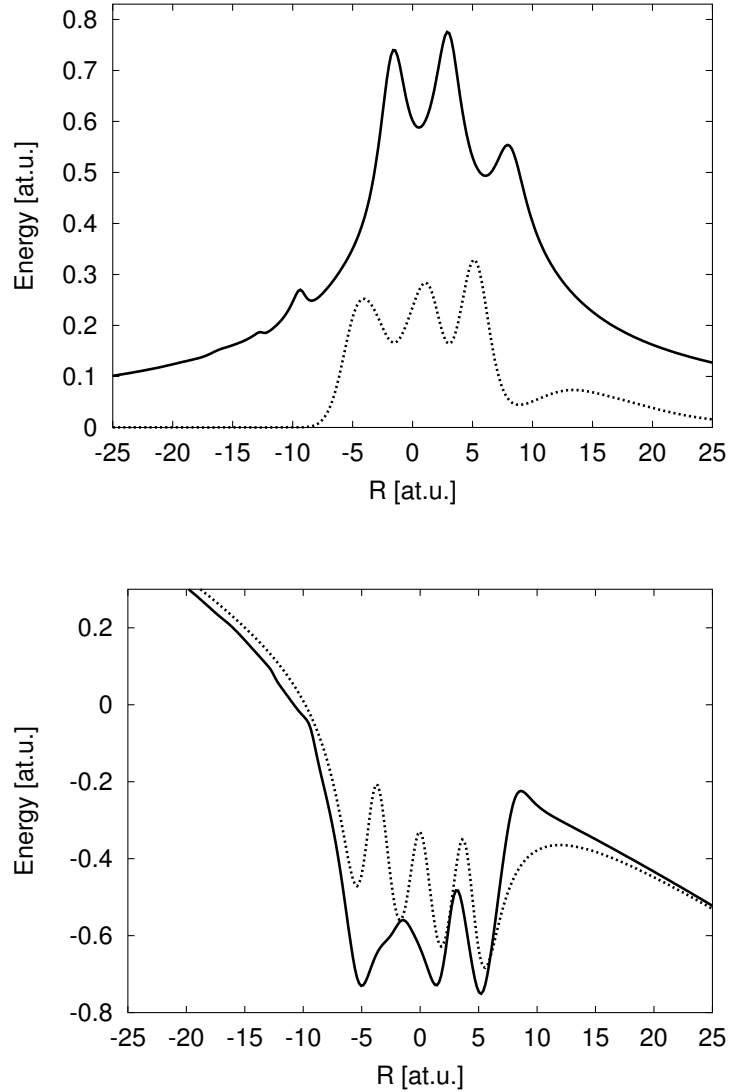


Figure 5.2: The upper panel shows the potential $\pi(R; t)$ (full line) and the electron density (dotted line) for the density matrix of fig. 5.1 at $t = -186.04$. The full line of the lower panel shows the effective one-electron potential $\varphi(R; t) = U(R) + \pi(R; t)$ with $\pi(R; t)$ of the upper panel in comparison to the effective one-electron potential taken at an instant before the laser pulse, denoted by the dotted line, which was tilted taking the same electric field strength as the one which causes the tilt of the full line. At times before the laser pulse the system is in the ground state and no laser-induced polarization is present. Therefore the influence of the laser-induced polarization can be seen by the boosted potential barrier (full line) as compared to the unaffected potential (dotted line).

electron, as was explained in the previous section, can be seen in the electron density by the fact that $\rho(R; t)$ is asymmetric with respect to $R = 0$ and exhibits larger values for $R > 0$. This subsequently leads to an asymmetric potential $\pi(R; t)$, see full line in the upper panel of fig. 5.2.

The lower panel of fig. 5.2 depicts the effective one-electron potential in the laser field corresponding to the situation of the upper panel and fig. 5.1, as well as for the ground state. This effective potential can be formally written as

$$\varphi(R; t) = U(R) + \pi(R; t) + R \times E(t).$$

The dotted line in the lower panel shows the effective potential for times before the laserpulse, $\varphi(R; t \rightarrow -\infty)$, when the system is still in the ground state. Then the $(f-1)$ electrons are not shifted, neither to $R > 0$ nor to $R < 0$, their influence, $\pi(R; t \rightarrow -\infty)$, is symmetric with respect to $R = 0$. To make this potential comparable to the one corresponding to $\pi(R; t = -186.04)$ of the upper panel, it is tilted by the same field strength at this instant, that is $E(t = -186.04) = 0.0247$. This potential acts as a reference in the sense, that no influence of any shifted electrons is included. The full line, however, depicts $\varphi(R; t = -186.04)$, with $\pi(R; t)$ from the upper panel. As can be seen, the effective potential is boosted for $R \approx 18 - 15$ as compared to the reference potential, which does not contain effects of the laser induced shift of the electron cloud. The increase of the barrier is approximately 0.14 at.u. This increased potential barrier makes it harder for the outermost electron to tunnel into the continuum and higher intensities to compensate for the decreased tunneling probability are needed to free the electron. This might explain, why the saturation intensities in molecules are higher than expected. In refs. [24, 25, 23] experimental results are compared with results obtained by the ADK tunneling theory. In the next section we will do the equivalent with numerically obtained results: MCTDHF-solutions of the full, time-dependent Schrödinger equation will be compared with ADK tunneling formulas in 1D.

5.5 Comparison with ADK

As was shown in the previous section, due to the laser induced polarization (the shift of the electron cloud), the tunneling barrier is increased. Now we want to estimate the influence of the barrier boost on the saturation intensity. In order to do so we compare numerical results for 4 electrons in a molecular potential with numerical results obtained for an atom and with analytical results calculated by the ADK theory [37, 48]. As mentioned, the experimentally obtained saturation intensities are by about a factor of 5-10 higher [22, 23, 24, 25, 53] than the saturation intensities given by ADK and the length corrected molecular single active electron model (MSAE) [121, 116, 115]. We calculated the probability for the ionization of at least one electron as a function of the laser peak intensity for the molecule already used in figs. 5.1 and 5.2. The same measure was calculated for an atom-like

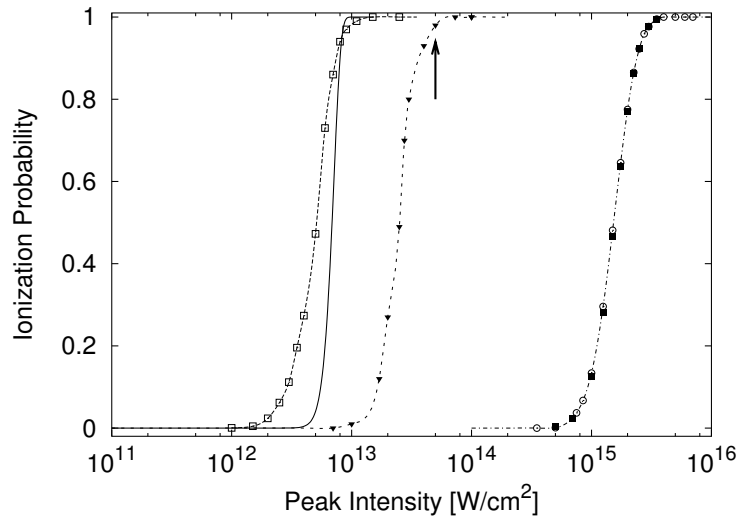


Figure 5.3: Ionization probabilities for the ionization of at least one electron over laser peak intensity. Full numerical calculations for Helium (filled squares) and for an equivalent one-electron atom with same I_P (open circles). The filled triangles depict results obtained for the molecule explained earlier, and the open squares are obtained for a one-electron system equivalent to the effective potential, $\varphi(R; t \rightarrow -\infty)$, of the molecule. The full line shows the result obtained with ADK theory for this equivalent system and the arrow indicates the data point used for figs. 5.1 and 5.2.

potential, also of the form equ. (5.4). The parameters of this atom were: 2 electrons and nuclei ($f = 2$), $\delta = 0$ (2 nuclei at the same place; “Helium”) and $a = b = 0.7408$. These parameters led to an $I_P = 0.978$ and a ground state energy $E_g = -2.902$ and are commonly used in the literature as a 1D-model of the Helium atom [62, 123]. The wavelength of the laser light was again $\lambda = 1500$ nm and the pulse duration was 10 fs (FWHM) for both cases. The numerical ionization probabilities are depicted in fig. 5.3, see figure caption for a mapping between the used symbols and the systems.

In addition to Helium and the 4-electron molecule, values calculated for a one-electron atomic system ($\delta = 0$) with the shielding parameter b adjusted such, that it has the same ionization potential as the Helium atom, are shown in fig. 5.3 (open circles). Because this atom has only one electron it is impossible that the barrier is boosted up by a shift of the remaining electron cloud, since there is no remaining cloud. This comparison reveals that for Helium (and therefore also for other noble gas atoms, for which ADK suits best) no influence of any barrier boost is detectable: the values of the one-electron atom and the Helium atom are identical, see fig. 5.3. This proves that the SAEA is justified and only the weakest bound electron tunnels through the barrier, whilst the stronger bound electron does not influence the ionization behaviour of the atom. Therefore the assumptions of the ADK theory are met.

In order to compare the numerical results for Helium with the ADK theory we

derive the quasistatic tunneling probability in 1D. This formula is calculated for a delta potential as a binding potential and corrected for the Coulombic longrange behaviour of the potential barriers. This is the standard procedure for the derivation of ADK-formulas also applied in the original work [48, 37]. The ADK theory foosts on the quasiclassical WKB approximation. In principle it is possible to derive the tunneling probability also with a different approach – the one applied by Keldysh and which the KFR theory relies on. The KFR approach is very similar to the one outlined in chapter 2 for the derivation of equ. (2.5). The crucial point in the KFR theory is the dipole matrix element $\langle 0|x|p\rangle$ of the transition from the bound state into the continuum. It is not always possible to calculate this matrix element and in such cases WKB has to be used [124]. Nevertheless, both ADK and KFR lead to the same form of the tunneling probability as a function of time, that is

$$w(t) = \hat{d} \times e^{-\frac{2\kappa^3}{3E(t)}}, \quad (5.8)$$

with the characteristic tunneling coefficient $\exp(-\frac{2\kappa^3}{3E(t)})$, where $E(t)$ denotes the electric field at time t and $\kappa = \sqrt{2I_P}$. The preexponential factor \hat{d} depends on the actual form of the potential and on the electric field and does also contain the Coulomb-correction. As we will prove below, it is not sufficient to only calculate the ionization probability with exponential accuracy and forget about the preexponential factor, as often done. In fact, it is the preexponential factor which causes the difference between experiment and the ADK-theory.

For 1D-atoms (delta potential plus Coulomb correction) the preexponential factor \hat{d} reads

$$\hat{d} = \frac{\kappa^3}{4\pi} \left(\frac{4e\kappa^4}{E(t)} \right)^{2/\kappa}. \quad (5.9)$$

The ionization probability at time t is calculated from the tunneling probability by assuming that the number of atoms in the ground state of the atomic ensemble under consideration, denoted by n , decreases proportional to the tunneling probability,

$$\frac{dn(t)}{dt} = -n(t) w(t). \quad (5.10)$$

Equ. (5.10) is solved by the function

$$n(t) = n_0 \exp \left(- \int_{-\infty}^t w(t') dt' \right), \quad (5.11)$$

where $n_0 = n(t \rightarrow -\infty)$ is the total number of atoms in the ensemble. Since tunneling is a process from the ground state directly into the continuum (no population of higher bound states), the diminution of $n(t)$ is inverse to the increase of ionized atoms. Therefore the expression

$$W(t) = 1 - \frac{n(t)}{n_0} \quad (5.12)$$

is nothing but the probability of ionizing the fraction $n(t)/n_0$ of the ensemble up to the time t . As explained before, $W(t)$ must be taken at times after the laser pulse for comparison with experimental results and the ionization probability can be written as

$$W(t \rightarrow +\infty) = W_\infty = 1 - \exp\left(-\int_{-\infty}^{+\infty} w(t') dt'\right). \quad (5.13)$$

W_∞ of equ. (5.13) was calculated as a function of the laser peak intensity for the Helium atom of fig. 5.3. This function was in good agreement with the numerical values – an expected result, since ionization probabilities obtained with the ADK formula of ref. [37] usually predict the experimentally obtained values very well. What we are especially interested in here is to investigate how the shift of the remaining electron cloud in a laser-driven multi-electron system influences the saturation intensity. To this end W_∞ was calculated with the atomic preexponential factor of equ. (5.9) as a function of the laser peak intensity for $\kappa = \sqrt{2 \times 0.261}$, the value of the 4-electron molecule. This yielded a saturation intensity which is even slightly higher (!) than the numerically obtained one, in contradiction to the experimentally found statement "molecules are harder to ionize than atoms" [23]. This finding, that a one-dimensional spatially extended multi-electron system yields lower saturation intensities than a 1D one-electron system with the same I_P , was recently confirmed [72]. The reason for this inconsistency is yet to be explained. We want to concentrate here, however, on the influence of the remaining electrons on the ionization probability (and, hence, on the saturation intensity). As was shown above, the laser induced shift of the $(f - 1)$ -electron cloud produces a potential which boosts up the Coulomb barrier and makes it more difficult for the outermost electron to tunnel through this barrier. Therefore, in order to make the influence of this boost visible, the multi-electron system has to be compared with an equivalent system with no influence of any remaining electrons, that is a one-electron system of the same form as the effective one-electron potential and with the same I_P as the molecule. By comparing these two systems we will prove, that the barrier boost causes indeed a factor of 5-10 difference in saturation intensities, as observed in the experiments. Furthermore we will show below, that it is the preexponential factor in the ADK tunneling rate, which is responsible for the lower saturation intensities yielded by the ADK theory as compared to experimental results.

The equivalent one-electron model-system, which approximates the effective one-electron potential $\varphi(R; t \rightarrow -\infty) = U(R) + \pi(R; t \rightarrow -\infty)$ of the molecule, is given by a nuclear potential, $\tilde{U}(x)$, of the form

$$\tilde{U}(x) = \begin{cases} \frac{-1}{\sqrt{(x-4.3)^2 + \left(\frac{1}{0.2775}\right)^2}} & \text{for } x > 4.3 \\ \frac{-1}{\sqrt{(x+4.3)^2 + \left(\frac{1}{0.2775}\right)^2}} & \text{for } x < 4.3 \\ -0.2775 & \text{else} \end{cases} \quad (5.14)$$

This model-potential has the form of a well potential with Coulomb shaped barriers

and differs from the form of $\varphi(R; t \rightarrow -\infty)$ of the molecule only by a flat ground, cf. dotted line in the lower panel of fig. 5.2. The depth -0.2775 in the above equation was adjusted in order to obtain the same $I_P = 0.261$ as the 4-electron system. Analytically calculating the ADK tunneling rate for this system yields a Coulomb corrected preexponential factor

$$\hat{d} = \frac{\kappa^2 \cos^2(kd) e^{2\kappa d}}{\cos^2(kd) + \kappa d + \frac{\kappa}{2k} \sin(2kd)} \left(\frac{2\kappa^3}{E(t)} \right)^{2/\kappa}, \quad (5.15)$$

with d half the length of the potential well (without Coulomb barrier) and $k = \sqrt{2\hat{V} - \kappa^2}$, where \hat{V} is the absolute value of the depth of the well. The values are $d = 4.3$ and $\hat{V} = 0.2775$. Note, that the laser induced motion of the electron in the spatially extended potential $\tilde{U}(x)$ is not considered in this formula. Hence, any possible polarization effects are excluded from this tunneling probability. The difference between \hat{d} of equ. (5.15) for the well as compared to \hat{d} of equ. (5.9) for the atom only arises from the spatially extended ground state in the well.

First we want to compare numerical results obtained for this one-electron system (no influence of any remaining electrons!) with the 4-electron system system. This yields the influence of the excursion of the remaining electron cloud. According to the results of the experiments the multi-electron system (the molecule) should be harder to ionize than the one-electron system (the atom) and thus lead to an approximately 5-10 times higher saturation intensity for the molecule as compared to the atom. The empty squares in fig. 5.3 depict the numerical results obtained for the atom, whilst the filled triangles are the results obtained for the molecule. Clearly, the molecule yields a saturation intensity 6 times higher than the atom, in accordance with the experiments and the boost of the Coulomb barrier calculated in section 5.4, revealing that this boost is capable of explaining the increased saturation intensities observed in the experiments. The values W_∞ calculated with the preexponential factor \hat{d} of equ. (5.15) for the one-electron model-atom yield a dependency on the laser peak intensity as depicted by the full line in fig. 5.3: The numerical curve and the analytical curve agree very well and give the same saturation intensity of roughly 5×10^{13} W/cm², 6 times smaller than the one of the corresponding 4-electron molecule (filled triangles).

Contrariwise, the by a factor of 6 smaller saturation intensity of the one-electron model potential can $\tilde{U}(x)$ can be re-increased to the value of the molecule by an effectively increased ionization potential in eqs. (5.15) and (5.8). This means, that the boost of the barrier due to the motion of the remaining electron cloud can be modelled by a higher ionization potential in the ADK formula. As was shown in section 5.4, the boost of the barrier at time $t = -186.04$ is about 0.14. Of course, because the boost depends on the excursion of the $(f-1)$ -electron cloud, it basically depends on the electric field strength. The higher, the more boost (as long as there is no multi-electron ionization and the electron cloud follows the tilted potential adiabatically). Thus, the influence of the induced potential $\pi(R; t)$ varies within the laser pulse and also with the laser peak intensity. The displayed case in fig. 5.2,

marked by an arrow in fig. 5.3, corresponds to an ionization probability of 0.98 and is therefore representative when contemplating the increase of the saturation intensity, since the saturation intensity is defined for an ionization probability of $W_\infty = 0.95$. The field strength at the time point $t = -186.04$ displayed in fig. 5.2 is also intermediate within the pulse and therefore we expect the displayed boost of 0.14 to be representative for the whole pulse. Taking an I_P in eqs. (5.15) and (5.8) which is by 0.14 higher than the actual one of 0.261, we arrive at a saturation intensity which is roughly a factor of 6 higher than the one obtained both numerically (open squares) and analytically (full line) of the one-electron system with $I_P = 0.261$, confirming the above statement that the barrier boost effectively leads to a dynamically increased ionization potential.

5.6 Interpretations

The results of the above considerations and calculations can be summarized and interpreted as follows. First, numerical results obtained for Helium and a one-electron atom with the same ionization potential as the Helium atom yield the same dependence of the ionization probability on the laser peak intensity. This demonstrates, that in atoms there is no influence of any polarization, produced by the remaining electrons, recognizable. The single active electron approximation (SAEA) is justified and the numerical results can be reproduced by the ADK theory, that means by a tunneling coefficient of the form $\exp(-\frac{2\kappa^3}{3E(t)})$ together with a preexponential factor \hat{d} which in our case takes the form of eq. (5.9).

When looking at the motion of the $(f-1)$ -electron cloud in a f -electron molecule during tunneling of the outermost electron it can be realized that the cloud moves after the tunneling electron, cf. fig. 5.1. This excursion from the equilibrium polarizes the molecule and the potential corresponding to this electron configuration boosts up the Coulomb barrier, cf. fig. 5.2, and decreases the tunneling probability. The boost can also be seen as if the ionization potential was increased.

When comparing the ionization probability as a function of the laser peak intensity of a molecule with that of an atom with the same I_P the resulting saturation intensity of the atom is even higher or comparable to the one of the molecule. This behaviour was confirmed by independent calculations in 1D [72] and is in contradiction to the experiments [22, 23, 24, 25, 53], where a saturation intensity, which is a factor of 5-10 higher than the one given by the ADK theory [37], was identified. The preexponential factor taken in those experiments was the one corresponding to Xenon but with the I_P of the molecule. Experimentally obtained results for Xenon are known to match the theoretical predictions of the ADK formula very well and Xenon is commonly taken as a reference target to calibrate laser intensities. The reason why the numerical comparison of atoms with molecules does not lead to the behaviour observed in the experiments is yet to be explained.

However, the influence of the remaining electron cloud on the ionization probability can be investigated with the help of a model-system consisting of only one electron with a nuclear potential which has the form of the effective one-electron potential of the molecule. Comparing the saturation intensities obtained for the multi-electron system with the one of the equivalent one-electron system yields the experimentally observed differences, in the above case a factor of 6. The ionization probability as a function of the laser peak intensity for the one-electron case can be modelled analytically by a quasistatic tunneling formula. This ADK-formula does not contain the motion of the electron in the spatially extended potential and therefore no polarization effects either. Nevertheless does this formula reproduce the numerical values for this one-electron model potential very well. Consequently, there cannot be any influence of polarization present in the numerical values (open squares in fig. 5.3). Therefore the difference in the saturation intensity between the multi-electron system and the one-electron system must arise from the boost of the barrier only. This proves that in multi-electron systems the motion of the remaining electron cloud must be accounted for by any theory describing ionization in molecules or other spatially extended multi-electron systems having delocalized electrons. This applies in the quasistatic tunneling limit. For shorter wavelengths non-adiabatic transitions, which we have excluded here by using $\lambda = 1500$ nm, have to be taken into account [25, 26].

As for the question, why in refs. [22, 23, 24, 25, 53] a comparison of the ADK tunneling probability for Xenon with the experimental values led to increased saturation intensities of the molecules, we would like to point out, that the difference between all quasistatic tunneling theories lies alone in the preexponential factor. The exponential tunneling coefficient, $\exp(-\frac{2\kappa^3}{3E(t)})$, is the same for *all* systems. In the above described comparisons the preexponential factor of the atomic potential led to a higher saturation intensity than stated by the full numerical calculations for the 4-electron molecule. On the other hand the preexponential factor of the model-potential determined by equ. (5.14) yielded a 6 times lower saturation intensity than the numerical calculations. This lets us conclude, that the preexponential factor is crucial and, furthermore, that the outcome of comparisons of experimental results with analytical theories, e.g. the ADK theory, is greatly influenced by the analytical form of this factor. Most important, however, is the fact that the laser induced polarization of the remaining electron cloud boosts up the barrier and as a consequence the saturation intensity is increased *as compared to a one-electron system*, where this polarization is not present. This proves the fact that the SAEA cannot be applied for molecules.

Conclusion and Outlook

Conclusion

The results presented in this thesis add to the understanding for processes taking place in atoms and molecules when irradiated by ultrashort laser pulses with peak intensities in the range of $10^{12} - 10^{16}$ W/cm² and wavelengths in the xuv and infrared regime. There are four main results presented in this thesis: (i) a measurement method for xuv-pulses in the attosecond (10^{-18} s) regime based on the energy shift which the xuv-photoelectron spectrum experiences in the field of a strong infrared laserpulse; (ii) a method for the numerical investigation of the multi-electron response of arbitrary systems to a strong laser pulse, which is capable of fully taking into account electron-correlation; (iii) the investigation of a new effect, unobserved so far, taking place in spatially far extended systems which manifests itself in a classically governed electron dynamics leading to an ionization mechanism analogous to the energy-pick-up of a free, classical particle; and (iv) a proof and first quantum mechanical demonstration that in the quasistatic tunneling regime the remaining electron cloud influences the tunneling electron such, that the effective potential barrier is boosted up by the laser induced polarization, rendering it more difficult for the outermost electron to tunnel through this barrier as compared to systems, where the remaining electron cloud does not move and consequently no polarization is evoked.

Outlook

Future advancements in experimental techniques, such as attosecond pump-probe spectroscopy, and ever more available computational power will further increase the understanding of light-matter interaction. Until very recently mainly the interaction of laserlight with atoms was investigated. This has led to several extremely valueable results as stated in the introduction, section 1. The response of atoms to laserlight is quite well understood in general.

In the last decade increasing work was done on the interaction of lasers with more complex matter, especially molecules and plasmas, but also with clusters of atoms,

with metals and dielectrics and other solids. Very few works were done with biological targets like tissue and cells but this kind of matter will become increasingly relevant due to important applications in medicine and biology.

Because dealing with many-body problems in a non-perturbative way is one of the most demanding tasks in physics, severe difficulties arise if one wants to study the interaction of light with solids on a microscopic level as was done with atoms. Therefore, knowledge about such targets is poor at the moment. With the availability of more and more computer power and increasingly sophisticated numerical techniques it will be possible to gain understanding of the complicated physics taking place in these targets.

High power laser pulses directed into plasmas have led to the discovery of Coulomb explosion [16] in clusters, neutron production [17] and laser wake field acceleration of electrons [125], which has led to relativistic electrons, see e.g. ref. [126]. Exposing metal bulks to such pulses has led to the production of hard x-rays [127, 128]. Still stronger pulses, with intensities in excess of 10^{20} W/cm², may lead to the discovery of interesting effects unknown so far. Simulations predict the generation of superhot electrons in the GeV regime [129], when such intense pulses interact with highly charged ions. It is interesting to investigate how more complex matter reacts to such high power laser pulses.

Laser machining in solids is another very hot topic [130, 131, 132] of the future and may open the way to major applications like laser-produced integrated optical circuits and waveguides in dielectrics [133] or even to integrated lasers. Laser-control of chemical processes [19, 20, 21] seems to be another promising avenue of future research.

It will be a great challenge to fully understand the processes taking place in the above outlined cases. But dragging the comprehension of the interaction of atoms with laser pulses to the next levels of more complicated matter like molecules and clusters, or even further to solids, will open the way to applications at least that fascinating as they were discovered in atoms. Increasing computer power and ever more advanced numerical- and experimental techniques, in special cases even analytical approaches, will path these routes.

Appendix A

Derivation of the Multi-Electron Ionization Probability

In the framework of the MCTDHF method introduced in chapter 3 the probability for ionizing (at least) one electron is calculated as follows. Let the symbol

$$(dx) = dx_1 dx_2 \dots dx_f \quad (\text{A.1})$$

indicate integration over all spatial coordinates and

$$(ds) = ds_1 ds_2 \dots ds_f \quad (\text{A.2})$$

integration over all spin coordinates. With that, normalization of the wavefunction before the laser pulse can be expressed as

$$\int (dx) \int (ds) |\Psi(x_1, s_1, \dots, x_f, s_f; -\infty)|^2 = 1. \quad (\text{A.3})$$

Then the probability for ionizing at least one electron within the time span $\{-\infty \dots t\}$ can be calculated by integrating over the whole f -dimensional probability density function within a range $-x_b \dots x_b$, where x_b must be much greater than the potential range, and subtracting this value from 1:

$$W(t) = 1 - \int_{-x_b}^{x_b} (dx) \int (ds) |\Psi(x_1, s_1, \dots, x_f, s_f; t)|^2. \quad (\text{A.4})$$

For comparison with experiments $W(t)$ must be taken at a time $t \rightarrow \infty$ (long after the laser pulse), in order to collect every ionized wave packet which will eventually drift out of the box $-x_b \dots x_b$.

Appendix B

Derivation of Electron Densities

In accordance with eqs. (A.1) and (A.2) defined in appendix A on the preceding page we define the symbol $(d\tilde{x}_i)$, which denotes integration over all spatial coordinates except for x_i and $(d\tilde{x}_i\tilde{x}_j)$, which consequently means integration over all spatial coordinates except for x_i and x_j . With these definitions the 4 dimensional density matrix can be defined as [134, 56]

$$\begin{aligned} \gamma(x_1, x_2, x'_1, x'_2; t) &= \binom{f}{2} \times \\ &\int \Psi^*(x_1, s_1, x_2, s_2, x_3, s_3, \dots, x_f, s_f; t) \times \\ &\Psi(x'_1, s_1, x'_2, s_2, x_3, s_3, \dots, x_f, s_f; t) (d\tilde{x}_1\tilde{x}_2)(ds). \end{aligned} \quad (\text{B.1})$$

The 2 dimensional density matrix is then defined as

$$\begin{aligned} \rho(x, x'; t) &= f \int \Psi^*(x, s_1, x_2, s_2, \dots, x_f, s_f; t) \\ &\times \Psi(x', s_1, x_2, s_2, \dots, x_f, s_f; t) (d\tilde{x}) (ds). \end{aligned} \quad (\text{B.2})$$

The diagonal elements $\rho(x, x; t) = \rho(x; t)$ have the following physical meaning: $\rho(x; t) dx$ is the probability of finding an electron of arbitrary spin in the space-region dx around x multiplied by the number of electrons. The diagonal elements of γ can be similarly interpreted: $\gamma(x_1, x_2, x_1, x_2; t) dx_1 dx_2 = \gamma(x_1, x_2; t) dx_1 dx_2$ is the probability of finding one electron with arbitrary spin within dx_1 around the point x_1 and another electron with arbitrary spin within dx_2 around the point x_2 , all other electrons having arbitrary positions and spins. The relation between $\rho(x; t)$ and $\gamma(x_1, x_2; t)$ is

$$\rho(x; t) = \frac{2}{f-1} \int \gamma(x, x_2; t) dx_2. \quad (\text{B.3})$$

Appendix C

Conversion between Atomic Units and SI

Atomic units are used for convenience in quantum mechanics [29, 135], as by setting the fundamental constants $\hbar = m = e^2 = 1$ calculations are simplified substantially. In the following conversion factors between atomic units and SI units are given

- 1 atomic charge unit = charge of the electron = $1.602 \times 10^{-19} \text{C}$
- 1 atomic mass unit = mass of the electron = $9.109 \times 10^{-31} \text{kg}$
- 1 atomic length unit = radius of the first Bohr orbit = $5.2917 \times 10^{-11} \text{m}$
- 1 atomic velocity unit = electron velocity in the first Bohr orbit = $2.1877 \times 10^6 \text{m/s}$
- 1 atomic momentum unit = electron momentum in the first Bohr orbit = $1.9926 \times 10^{-24} \text{kg m/s}$
- 1 atomic energy unit = twice the ionization potential of hydrogen = $4.359 \times 10^{-18} \text{J}$
- 1 atomic time unit = $2.4189 \times 10^{-17} \text{s}$
- 1 atomic frequency unit = $4.1341 \times 10^{16} \text{s}^{-1}$
- 1 atomic unit of electric potential = 27.210V
- 1 atomic unit of electric field strength = $5.142 \times 10^{11} \text{V/m}$.

Appendix D

Common Abbreviations

| | |
|--------|-------------------------------------------------------------------|
| ABI | Above Barrier Ionization |
| ADK | Tunneling Theory named after Ammosov-Delone-Krainov |
| ATI | Above Threshold Ionization |
| CI | Configuration Interaction |
| DFT | Density Functional Theory |
| HF | Hartree-Fock |
| HHG | High Harmonic Generation |
| I_P | Ionization Potential |
| KFR | Tunneling Theory named after Keldysh-Faisal-Reiss |
| MCTDH | Multi-configuration Time-dependent Hartree |
| MCTDHF | Multi-configuration Time-dependent Hartree-Fock |
| MPI | Multi-Photon Ionization |
| MSAE | Molecular Single Active Electron |
| PIC | Particle in Cell |
| SAEA | Single Active Electron |
| SFA | Strong Field Approximation |
| SCF | Self-consistent Field |
| TDFT | Time-dependent Density Functional Theory |
| TDHF | Time-dependent Hartree-Fock |
| TDSE | Time-dependent Schrödinger Equation |
| U_p | Ponderomotive Potential |
| WKB | Quasiclassical Approximation named after Wentzel-Kramer-Brillouin |

List of Figures

| | | |
|-----|------------------------------------------------------------------------------------------------------------------------------------------------------|----|
| 1.1 | Schematic illustration of the continuum evolution of an electron in a strong laser field. | 6 |
| 1.2 | Schematic illustration of the elementary processes responsible for high harmonic generation. | 8 |
| 1.3 | Regimes of atomic ionization. | 10 |
| 2.1 | Rms width of the electron spectrum for a hydrogen (1s) ground state as a function of delay time, t_d , between laser and xuv-pulse. | 22 |
| 2.2 | Photo electron spectrum for the parameters of fig. 2.1 and delay $t_d = 0$ | 23 |
| 2.3 | Schematic of the optimized experimental setup. | 24 |
| 2.4 | Signature of two attosecond pulses with delay times $t_d = \pm 1/4$ laser optical cycles compared to a single pulse with delay $t_d = 1/4$ | 25 |
| 4.1 | Quantum mechanical ionization probability over potential length length of one electron in a smoothed well potential. | 45 |
| 4.2 | Time evolution of the electron density for 4 electrons calculated by quantum mechanics and by classical mechanics. | 55 |
| 4.3 | Quantum mechanical and classical ionization probability as a function of the laser intensity. | 58 |
| 5.1 | Tunneling dynamics of one electron in the effective potential caused by the influence of all other electrons. | 65 |
| 5.2 | Electron density and effective one-electron potential for the situation depicted in fig. 5.1. | 67 |
| 5.3 | Ionization probabilities over laser peak intensity for Helium and for a 4-electron model-molecule. | 69 |

Bibliography

- [1] A. L. Schawlow and C. H. Townes. Infrared and optical masers. *Phys. Rev.*, 112:1940–1949, 1958.
- [2] L. V. Keldysh. Ionization in the field of a strong electromagnetic wave. *Sov. Phys. JETP*, 20:1307–1314, 1965.
- [3] P. Agostini, F. Fabre, G. Mainfray, and G. Petite. *Phys. Rev. Lett.*, 42:1127, 1979.
- [4] L. J. Fasinski, K. Codling, P. A. Hatherly, J. Barr, I. N. Ross, and W. T. Toner. *Phys. Rev. Lett.*, 58:2424, 1987.
- [5] A. L’Huillier, L. A. Lompré, , G. Mainfray, and C. Manus. *J. Phys. B*, 16:1363, 1983.
- [6] D. N. Fittinghoff, P. R. Bolton, B. Chang, and K. C. Kulander. *Phys. Rev. Lett.*, 69:2642, 1992.
- [7] B. Walker, B. Sheehy, L. F. DiMauro, P. Agostini, K. J. Schafer, and K. C. Kulander. *Phys. Rev. Lett.*, 73:1227, 1994.
- [8] P. B. Corkum. *Phys. Rev. Lett.*, 71:1994, 1993.
- [9] K. C. Kulander, K . J. Schafer, and J. L. Krause. Super-intense laser-atom physics. In B. Piraux, A. L. L’Huillier, and K. Rzazewski, editors, *NATO Advanced Study Institute; Series B: Physics*, volume 316, page 93. Plenum, New York, 1993.
- [10] G. L. Yudin and M. Yu. Ivanov. *Phys. Rev. A*, 63(033404), 2001.
- [11] Markus Drescher, Michael Hentschel, Reinhard Kienberger, Gabriel Tempea, Christian Spielmann, Georg A. Reider Paul B. Corkum, , and Ferenc Krausz. X-ray pulses approaching the attosecond frontier. *Science*, 291:1923–1927, 2001.
- [12] M. Hentschel, R. Kienberger, Ch. Spielmann, G. A. Reider, N. Milosevic, T. Brabec, P. Corkum, U. Heinzmann, M. Drescher, and F. Krausz. Attosecond metrology. *Nature*, 414:509–513, 2001.

- [13] R. Kienberger, M. Hentschel, M. Uiberacker, Ch. Spielmann, M. Kitzler, A. Scrinzi, M. Wieland, Th. Westerwalbesloh, U. Kleineberg, U. Heinzmann, M. Drescher, and F. Krausz. Steering attosecond electron wave packets with light. *Science*, 297:1144–1148, 2002.
- [14] M. Drescher, M. Hentschel, R. Kienberger, M. Uiberacker, V. Yakovlev, A. Scrinzi, Th. Westerwalbesloh, U. Kleineberg, U. Heinzmann, and F. Krausz. Time-resolved atomic inner-shell spectroscopy. *Nature*, 419:803–807, 2002.
- [15] A. Baltuska, Th. Udem, M. Uiberacker, M. Hentschel, E. Goulielmakis, Ch. Gohle, R. Holzwarth, V. S. Yakovlev, A. Scrinzi, T. W. Hänsch, and F. Krausz. Attosecond control of electronic processes by intense light fields. *Nature*, 421:611–615, 2003.
- [16] J. Purnell et al. *Chem. Phys. Lett.*, 229:333, 1994.
- [17] T. Ditmire et al. *Nature*, 398:489, 1999.
- [18] S. Chelkowski, P. B. Corkum, and A. D. Bandrauk. *Phys. Rev. Lett.*, 82:3416, 1999.
- [19] A. Assion, T. Baumert, M. Bergt, T. Brixner, B. Kiefer, V. Seyfried, M. Strehle, and G. Gerber. *Science*, 282:919, 1998.
- [20] B. Sheehy and L. F. DiMauro. *Annu. Rev. Phys. Chem.*, 47:463, 1996.
- [21] T. C. Wehnacht, J. L. White, and P. H. Bucksbaum. *J. Chem. A*, 103:10166, 1999.
- [22] V. R. Bhardwaj, P. B. Corkum, and D. M. Rayner. Internal laser-induced dipole forces at work in a large molecule, c_{60} . *Phys. Rev. Lett.*, 2003. submitted.
- [23] S. M. Hankin, D. M. Villeneuve, P. B. Corkum, and D. M. Rayner. *Phys. Rev. Lett.*, 84(22), 2000.
- [24] M. Lezius, V. Blanchet, D. M. Rayner, D. M. Villeneuve, A. Stolow, and M. Yu. Ivanov. *Phys. Rev. Lett.*, 86(51), 2001.
- [25] M. Lezius, V. Blanchet, M. Yu. Ivanov, and A. Stolow. *J. Chem. Phys.*, 117(4), 2002.
- [26] A. N. Markevitch, S. M. Smith, D. A. Romanov, H. B. Schlegel, M. Yu. Ivanov, and R. J. Levis. *Phys. Rev. A*, 68(011402(R)), 2003.
- [27] Thomas Brabec and Ferenc Krausz. Intense few-cycle laser fields: Frontiers of nonlinear optics. *Reviews of Modern Physics*, 72(2), 2000.
- [28] L. D. Landau and E. M. Lifschitz. *Quantum Mechanics*. Pergamon, Oxford, 1977.

- [29] B. H. Bransden and C. J. Joachain. *Physics of Atoms and Molecules*. Addison Wesley Longman Limited, Essex, England, 1997.
- [30] Leonard I. Schiff. *Quantum Mechanics*. McGraw-Hill, New York, Toronto, London, 2. edition, 1955.
- [31] P. W. Atkins and R. S. Friedman. *Molecular Quantum Mechanics*. Oxford University Press, Oxford, 3. edition, 1997.
- [32] Robert W. Boyd. *Nonlinear Optics*. Academic Press, Inc., San Diego, 1992.
- [33] Georg A. Reider. *Photonik*. Springer Lehrbuch Technik, Wien, New York, 1997. Eine Einführung in die Grundlagen.
- [34] J. Parker, K. T. Taylor, C. W. Clark, and S. Blodgett-Ford. *J. Phys. B*, 29(L33), 1996.
- [35] A. M. Perelomov, V. S. Popov, and V. P. Krainov. *Sov. Phys. JETP*, 23, 1966.
- [36] V. S. Popov, V. P. Kuznetsov, , and A. M. Perelomov. *Sov. Phys. JETP*, 26, 1968.
- [37] M. V. Ammosov, N. B. Delone, and V. P. Krainov. Tunnel ionization of complex atoms and of atomic ions in an alternating electromagnetic field. *Sov. Phys. JETP*, 64(6), 1986.
- [38] A. Talebpour, S. Larochelle, and S. L. Chin. *J. Phys. B*, 31, 1998.
- [39] K. C. Kulander, K. J. Schafer, and J. L. Krause. In M. Gavrilu, editor, *Atoms in Intense Fields*, page 247. Academic Press, Boston, 1992.
- [40] P. B. Corkum. *Phys. Rev. Lett.*, 62:1259, 1989.
- [41] E. Sarachick and G. Schappert. *Phys. Rev. D*, 1, 1970.
- [42] L. F. DiMauro, R. R. Freeman, and K. C. Kulander, editors. *Multiphoton Processes*, ICOMP VIII, Melville, NY, 2000. American Institute of Physics.
- [43] R. Shakeshaft and coworkers. *Phys. Rev. A*, 42, 1990.
- [44] N. B. Delone and V. P. Krainov. *Multiphoton Processes in Atoms*. Springer Series on Atoms and Plasmas. Springer-Verlag, Berlin, Heidelberg, 1994.
- [45] A. Scrinzi, M. Geissler, and T. Brabec. *Phys. Rev. Lett.*, 83(4), 1999.
- [46] F. H. M. Faisal. *J. Phys. B*, 6(L89), 1973.
- [47] H. R. Reiss. *Phys. Rev. A.*, 22:1786, 1980.
- [48] M. Perelomov, V. S. Popov, and M. V. Terent'ev. *Sov. Phys. JETP*, 23(924), 1965.

- [49] S. Augst, D. Strickland, D. D. Meyerhofer, S. L. Chin, and J. H. Eberly. *Phys. Rev. Lett.*, 63(20), 1989.
- [50] H. G. Muller. *Phys. Rev. A*, 60(2), 1999.
- [51] M. J. Nandor, M. A. Walker, L. d. Van-Woerkom, and H. G. Muller. *Phys. Rev. A*, R1771, 1999.
- [52] Ch. Fabian, M. Kitzler, N. Milosevic, and T. Brabec. Multi-electron strong field theory. *J. Mod. Optics*, 50:589–595, 2003.
- [53] M. Smits et al. *Phys. Rev. Lett.*, 2004. manuscript in preparation.
- [54] V. Kummarappan, M. Krishnamurthy, and D. Mathur. *Phys. Rev. Lett.*, 87(8), 2001.
- [55] Ch. Fabian. *Multi-electron dynamics in matter exposed to strong laser fields*. PhD thesis, TU Wien, 2003.
- [56] Robert G. Parr and Weitao Yang. *Density-Functional Theory of Atoms and Molecules*. Oxford University Press, 1989.
- [57] D. Bauer. *Phys. Rev. A*, 56:3028, 1997.
- [58] E. Runge and E. K. U. Gross. *Phys. Rev. Lett.*, 52:997, 1984.
- [59] V. Véniard, R. Taïeb, and A. Maquet, July 2002. presented at LPhys'02, Bratislava.
- [60] K. C. Kulander. *Phys. Rev. A*, 36(2726), 1987.
- [61] K. C. Kulander. *Phys. Rev. A*, 38(778), 1988.
- [62] M. S. Pindzola, D. C. Griffin, and C. Bottcher. *Phys. Rev. Lett.*, 66:2305, 1991.
- [63] M. S. Pindzola, T. W. Gorczyca, and C. Bottcher. *Phys. Rev. A*, 47(4982), 1993.
- [64] M. S. Pindzola, P. Gavras, and T. W. Gorczyca. *Phys. Rev. A*, 51(3999), 1995.
- [65] M. S. Pindzola, F. Robicheaux, and P. Gavras. *Phys. Rev. A*, 55(1307), 1997.
- [66] Ch. Jungreuthmayer and T. Brabec. *Phys. Rev. Lett.*, 2004. manuscript in preparation.
- [67] M. H. Beck, A. Jäckle, G. A. Worth, and H.-D. Meyer. The multiconfiguration time-dependent Hartree (MCTDH) method: A highly efficient algorithm for propagating wavepackets. *Physics Reports*, 324:1–105, 2000.

- [68] H.-D. Meyer. Multiconfiguration time-dependent Hartree method. In P. v. R. Schleyer, N. L. Allinger, T. Clark, J. Gasteiger, P. A. Kollman, H. F. Schaefer III, and P. R. Schreiner, editors, *The Encyclopedia of Computational Chemistry*, volume 5, pages 3011–3018, Chichester, 1998. John Wiley and Sons.
- [69] H. D. Meyer, U. Manthe, and L. S. Cederbaum. The multi-configurational time-dependent Hartree-approach. *Chem. Phys. Lett.*, 165:73, 1990.
- [70] H. D. Meyer and Graham A. Worth. Quantum molecular dynamics: Propagating wavepackets and density operators using the multi-configuration time-dependent hartree (mctdh). *Theoretical Chemistry Accounts*, 2003. to be published.
- [71] J. Zanghellini, M. Kitzler, T. Brabec, and A. Scrinzi. The harmonic quantum dot: a test for the multi-configuration time-dependent hartree-fock method. *J. Phys. B.*, 2003. submitted.
- [72] J. Zanghellini, M. Kitzler, C. Fabian, T. Brabec, and A. Scrinzi. An mctdhf approach to multielectron dynamics in laser fields. *Laser Physics*, 13(8):1064–1068, 2003.
- [73] A. L’Huillier and P. Balcou. *Phys. Rev. Lett.*, 70:774, 1993.
- [74] McPherson et al. *J. Opt. Soc. Am. B*, 4, 1987.
- [75] J. J. Macklin, J. D. Kmetec, and C. L. Gordon III. *Phys. Rev. Lett.*, 70, 1993.
- [76] Ch. Spielmann et al. *Science*, 278, 1997.
- [77] Ch. Spielmann et al. *IEEE JSTQE*, 4, 1998.
- [78] Z. Chang et al. *Phys. Rev. Lett.*, 79, 1997.
- [79] M. Lewenstein et al. *Phys. Rev. A*, 49, 1994.
- [80] A. Zewail. Femtochemistry: atomic-scale dynamics of the chemical bond. *J. Phys. Chem. A*, 104, 2000. adapted from the Nobel Lecture.
- [81] F. Krausz. From femtochemistry to attophysics. *Physics World*, 14(9):41, 2001.
- [82] Z. Cheng et al. In T. Elsässer, J. G. Fujimoto, D. A. Wiersma, and W. Zinth, editors, *Ultrafast Phenomena XI*, page 8. Springer, Berlin, 1998.
- [83] Gy. Farkas and Cs. Toth. *Phys. Lett. A*, 168, 1992.
- [84] M. Ivanov, P. B. Corkum, T. Zuo, and A. Bandrauk. Routes to control of intense-field atomic polarizability. *Phys. Rev. Lett.*, 74, 1995.

- [85] J. Karczmarek, J. Wright, P. Corkum, and M. Ivanov. *Phys. Rev. Lett.*, 82, 1999.
- [86] H. Niikura et al. *Nature*, 417, 2002.
- [87] B. Witzel et al. *Phys. Rev. A*, 58(5):3836, 1998.
- [88] B. Witzel et al. *Phys. Rev. A*, 60(4):3311, 1999.
- [89] C. Lemell, X.-M. Tong, F. Krausz, and J. Burgdörfer. *Phys. Rev. Lett.*, 90(7), 2003.
- [90] J. M. Schins, P. Breger, and P. Agostini. Observation of laser-assisted auger decay in argon. *Phys. Rev. Lett.*, 73:2180–2183, 1994.
- [91] J. M. Schins, P. Breger, P. Agostini, R. C. Constantinescu, H. G. Muller, A. Bouhal, G. Grillon, A. Antonetti, and A. Mysyrowicz. Cross-correlation measurements of femtosecond extreme-ultraviolet high-order harmonics. *JOSA B*, 13:197–200, 1996.
- [92] T. E. Glover, R. W. Schoenlein, A. H. Chin, , and C. V. Shank. Observation of laser assisted photoelectric effect and femtosecond high order harmonic radiation. *Phys. Rev. Lett.*, 76:2468–2471, 1996.
- [93] A. Bouhal, R. Evans, G. Grillon, A. Mysyrowicz, P. Breger, P. Agostini, R. C. Constantinescu, H. G. Muller, and D. von der Linde. Cross-correlation measurement of femtosecond noncollinear high-order harmonics. *JOSA B*, pages 950–956, 1997.
- [94] J. Itatani, F. Quéré, G. L. Yudin, M. Yu. Ivanov, F. Krausz, and P. B. Corkum. Attosecond streak camera. *Phys. Rev. Lett.*, 88(173903), 2002.
- [95] E. Constant, V. D. Taranukhin, A. Stolow, and P. B. Corkum. Methods for the measurement of the duration of high-harmonic pulses. *Phys. Rev. A*, 56:3870–3878, 1997.
- [96] A. Scrinzi, M. Geissler, and T. Brabec. Attosecond cross correlation technique. *Phys. Rev. Lett.*, 86:412–415, 2001.
- [97] P. M. Paul, E. S. Toma, P. Breger, G. Mullot, F. Augé, Ph. Balcou, H. G. Muller, and P. Agostini. Observation of a train of attosecond pulses from high harmonic generation. *Science*, 292:1689–1692, 2001.
- [98] E. S. Toma, H. G. Muller, P. M. Paul, P. Breger, M. Cheret, P. Agostini, C. Le Blanc, G. Mullot, , and G. Cheriaux. Ponderomotive streaking of the ionization potential as a method for measuring pulse durations in the xuv domain with fs resolution. *Phys. Rev. A*, 62(061801(R)), 2000.
- [99] Valérie Véniard, Richard Taïeb, and Alfred Maquet. Phase dependence of $(n+1)$ -color $(n>1)$ ir-uv photoionization of atoms with higher harmonics. *Phys. Rev. A*, 54:721–728, 1996.

- [100] M. Kitzler, N. Milosevic, A. Scrinzi, F. Krausz, and T. Brabec. Quantum theory of attosecond xuv pulse measurement by laser dressed photoionization. *Phys. Rev. Lett.*, 88(173904), 2002.
- [101] U. Becker and D. A. Shirley. *VUV and soft x-ray photoionization*. Plenum, New York, 1996.
- [102] M. Abramowitz and I. A. Stegun. *Handbook of mathematical functions*. Dover publications, New York, 1973.
- [103] C. M. Bender and S. A. Orszag. *Advanced mathematical methods for scientists and engineers*. Mc Graw Hill, New York, 1978.
- [104] B. Piraux and K. Rzaszewski, editors. *Proceedings of the Workshop on Super-Intense Laser-Atom Physics*. Kluwer Academic Publishers, 2001.
- [105] D.B. Milosevic and F. Ehlotzky. Coulomb and rescattering effects in above-threshold ionization. *Phys. Rev. A*, 58:3124–3127, 1998.
- [106] O. Smirnova, V. Yakovlev, and A. Scrinzi. Quantum model of the time-resolved auger measurement. *Phys. Rev. Lett.*, 2003. manuscript in preparation.
- [107] M. Suzuki and S. Mukamel. *J. Chem. Phys.*, 2003. submitted.
- [108] P.-O. Löwdin. *Adv. Chem. Phys.*, 2:207, 1959.
- [109] M. J. Frisch, G. W. Trucks, et al. GAUSSIAN 95. Technical report, Gaussian, Inc., Pittsburgh, PA, 1995.
- [110] A. Jäckle and H.-D. Meyer. Time-dependent calculation of reactive flux employing complex absorbing potentials: General aspects and application within the multi-configuration time-dependent Hartree approach. *J. Chem. Phys.*, 105:6778–6786, 1996.
- [111] Q. Su and J. H. Eberly. *Phys. Rev A*, 44:5997, 1991.
- [112] Tamar Seideman. *J. Chem. Phys.*, 107(19):7859–7868, 1997.
- [113] Tamar Seideman. *Phys. Rev. A*, 64(042504), 2001.
- [114] E. Schmidt. *Math. Ann.*, 63, 1906.
- [115] Merrick J. DeWitt and Robert J. Levis. *Phys. Rev. Lett.*, 81(23), 1998.
- [116] Merrick J. DeWitt and Robert J. Levis. *J. Chem. Phys.*, 108:7045–7048, 1998.
- [117] L. Jacak, P. Hawrylak, and A. Wojs. *Quantum Dots*. Springer-Verlag, Berlin, 1998.
- [118] A. Sugita and H. Aiba. *Phys. Rev. E*, 65(036205), 2002.
- [119] K. Husimi. *Proc. Phys. Math. Soc. Jpn.*, 22(246), 1940.

- [120] Uwe Schwengelbeck. Analytical solution of the schrödinger equation of a laser driven two-particle system. *Phys. Lett. A*, 253:168–172, 1999.
- [121] B. S. Prall, M. J. DeWitt, and R. J. Levis. *J. Chem. Phys.*, 111:2865–2868, 1999.
- [122] S. Augst, D. D. Meyerhofer, D. Strickland, and S. L. Chin. Laser ionization of noble gases by coulomb-barrier suppression. *JOSA B*, 8:858, 1991.
- [123] R. Grobe and J. H. Eberly. *Phys. Rev. Lett.*, 68:2905, 1992.
- [124] N. Milosevic, V. P. Krainov, and T. Brabec. Relativistic theory of tunnel ionization. *J. Phys. B*, 35:3515, 2002.
- [125] K. Nakajima, D. Fisher, et al. *Phys. Rev. Lett.*, 74:4428–4431, 1995.
- [126] V. Yakimenko, I. V. Pogorelsky, I. V. Pavlishin, I. Ben-Zvi, K. Kusche, Yu. Eidelman, T. Hirose, T. Kumita, Y. Kamiya, J. Urakawa, B. Greenberg, and A. Zigler. *Phys. Rev. Lett.*, 91(014802), 2003.
- [127] B. E. Lemoff, C. P. J. Barty, and Se. E. Harris. *Opt. Lett.*, 19(569), 1994.
- [128] J. D. Kmetec, C. L. Gordon III, J. J. Macklin, B. E. Lemoff, G. S. Brown, and S. E. Harris. *Phys. Rev. Lett.*, 68:1527–1530, 1992.
- [129] S. X. Hu and A. F. Starace. *Phys. Rev. Lett.*, 88(245003), 2002.
- [130] M. Lenzner et al. *Phys. Rev. Lett.*, 80:4076, 1998.
- [131] A. Tien, S. Backus, H. Kapetyn, M. Murnane, and G. Morou. *Phys. Rev. Lett.*, 82:3883, 1999.
- [132] M. Marcinkevicius. *Opt. Lett.*, 26(277), 2001.
- [133] K. Miura et al. *Appl. Phys. Lett.*, 71:3329, 1997.
- [134] Per-Olov Löwdin. *Phys. Rev.*, 97(6), 1955.
- [135] H. A. Bethe and E. E. Salpeter. *Quantum Mechanics of One- and Two-Electron Atoms*. Plenum, New York, 1977.

Curriculum Vitae

Markus Kitzler

August 2003

PERSONAL

| | |
|-----------------|------------------------------------------------------------------------------------------------------------|
| Address | Photonics Institute Vienna University of Technology Gusshausstrasse 27/387 A-1040 Vienna, Austria |
| Tel/Fax | +43 1 58801-38740 / +43 1 585 22 99 |
| Date of Birth | November 14, 1974 |
| Birthplace | Waidhofen/Thaya, Lower Austria |
| Citizenship | Austria |
| Marital Status | married with Ingrid |
| Language Skills | German (mother tongue), English (fluent), Spanish (moderate) |

EDUCATION

| | |
|----------------------|---------------------------------------------------------------------------------------------------------------------------------------------------------------------------------------------------------------------|
| November 2000- | Ph.D. Student at Photonics Institute Vienna University of Technology |
| October 2000 | M.Sc. in Electrical Engineering (with distinction) Vienna University of Technology Topic of Master Thesis: <i>Shielding Currents and Fields in Thin-Film Superconductors under magnetic Levitation</i> |
| Oct. 1995-Sept. 2000 | Study of Electrical Engineering Vienna University of Technology Subject: Automation and Control Techniques Specialization in Biomedical Engineering |
| June 1994 | Matura (with distinction) St. Pölten, Lower Austria |

| | |
|-----------|-----------------------------------------------------------------------------------------------|
| 1989-1994 | Technical High School ("HTL") St. Pölten, Lower Austria Subject: Mechanical Engineering |
| 1985-1989 | Gymnasium in Waidhofen/Thaya, Lower Austria |
| 1981-1985 | Primary School in Dobersberg, Lower Austria |

WORK EXPERIENCE

| | |
|----------------------|--------------------------------------------------------------------------------------------------|
| Aug. 2003- | Photonics Institute, Vienna University of Technology Research Assistant |
| June 2002- Aug. 2003 | Physics Department, University of Ottawa, Canada Research Assistant |
| Oct. 2000-June 2002 | Photonics Institute, Vienna University of Technology Research Assistant |
| 1999 | Siemens Verkehrstechnik, Vienna, (2 months) Design of automated driving systems for subways |
| 1997-1998 | Elin Energieversorgung, Vienna, (3 months) Design of excitation systems for generators |
| 1993-1996 | Schrack Components, Waidhofen/Thaya, Lower Austria, (8 months) Development laboratory |
| 1991-1992 | Pollmann Feinwerktechnik, Karlstein, Lower Austria, (2 months) Manufacturing of prototypes |
| Oct. 1994-June 1995 | Civil Service |

CERTIFICATES

| | |
|-----------|---------------------------------------------------------------------------------------------------------------------------------------------------------|
| Feb. 2003 | Level I High Performance Computing – MPI and Sun Cluster Tools High Performance Computing Virtual Laboratory (HPCVL) Kingston, Ontario, Canada |
| Feb. 1999 | Seminar "Teamentwicklung – Managementtraining" Coverdale Managementberatungs- u. Trainings GesmbH, Vienna |
| Feb. 1999 | Seminar "Sachgerecht verhandeln – erfolgreich abschliessen" Coverdale Managementberatungs- u. Trainings GesmbH, Vienna |
| May 1994 | REFA basic training, Part II Verband für Arbeitsstudien und Betriebsorganisation REFA St. Pölten, Lower Austria |
| Nov. 1993 | Qualitätstechnik II - statistical Methods of Quality Assurance (ÖVQ QII certificate) Österreichische Vereinigung für Qualitätssicherung |

COLLABORATIONS

| | |
|---------------------|--------------------------------------------------------------------------------------------------------------------------------------------------|
| Nov. 1995-Aug. 2003 | Prof. Dr. Thomas Brabec Supervisor of Ph.D. work University of Ottawa, Canada, and Photonics Institute, Vienna University of Technology |
| June 2003 | Prof. Dr. Vladimir P. Krainov Moscow Institute of Physics and Technology, Russia |
| June 2002-Aug. 2003 | Dr. Albert Stolow and Dr. Paul Corkum National Research Council of Canada, Ottawa |
| Jan. 2002-June 2003 | Prof. Dr. Ferenc Krausz Photonics Institute, Vienna University of Technology |
| 2001/2002 | Dr. Armin Scrinzi Photonics Institute, Vienna University of Technology |

LIST OF PUBLICATIONS

-
- M. Kitzler, J. Zanghellini, M. Smits, A. Scrinzi, and T. Brabec
The role of electron mobility in optical field ionization of complex systems
Physical Review Letters, submitted, 2003
- J. Zanghellini, M. Kitzler, T. Brabec and A. Scrinzi
The harmonic quantum dot: a test for the multi-configuration time-dependent Hartree-Fock method
J. Phys. B., submitted, 2003
- J. Zanghellini, M. Kitzler, Ch. Fabian, T. Brabec and A. Scrinzi
An MCTDHF Approach to Multielectron Dynamics in Laser Fields
Laser Physics, **13**(8), 1064-1068, 2003
- Ch. Fabian, M. Kitzler, N. Milosevic and T. Brabec
Multi-electron strong field theory
J. Mod. Optics, **50**, 589-595, 2003
- M. Kitzler, Ch. Fabian, N. Milosevic, A. Scrinzi and T. Brabec
Quantum theory of single subfemtosecond extreme-ultraviolet pulse measurements
JOSA B, **20**, 591, 2003
- R. Kienberger, M. Hentschel, M. Uiberacker, Ch. Spielmann, M. Kitzler,
A. Scrinzi, M. Wieland, Th. Westerwalbesloh, U. Kleineberg,
U. Heinzmann, M. Drescher and F. Krausz
Steering Attosecond Electron Wave Packets with Light
Science, **297**, 1144-1148, 2002

M. Kitzler, N. Milosevic, A. Scrinzi, F. Krausz and T. Brabec
*Quantum Theory of Attosecond XUV Pulse Measurement by
 Laser Dressed Photoionization*
 Physical Review Letters, **88**, 173904, 2002

N. Milosevic, M. Kitzler, A. Scrinzi and T. Brabec
Theory of Attosecond Pulse Characterization
 Laser Physics, **12**(2), 377, 2002

M. Kitzler, A. Scrinzi and T. Brabec
Theory of attosecond cross correlation measurement
 in OSA *Trends in Optics and Photonics (TOPS)*,
 Vol. **65**, Applications of High Field and Short Wavelength Sources IX,
 OSA Technical Digest, Postconference Edition,
 (OSA, Washington DC, 2001), pp. TuC1:1-3

CONTRIBUTIONS TO CONFERENCES

MULTIPHOTON PROCESSES
 Gordon Research Conference
 Poster Presentation
*Quantum Theory of Attosecond XUV Pulse Measurement
 by Laser Dressed Photoionization*
 Tilton, New Hampshire, USA, June 30-July 5, 2002

SEMINAR ON FUNDAMENTALS OF LASER INTERACTIONS III
 Poster Presentation
*Quantum theory of single subfemtosecond extreme-ultraviolet
 pulse measurements*
 Kühtai, Tyrol, Austria, January 13-18, 2002

APPLICATIONS OF HIGH FIELD AND SHORT WAVELENGTH SOURCES IX
 Optical Society of America (OSA)
 Talk
Theory of attosecond cross correlation measurement
 Palm Springs, California, USA, October 21-24, 2001